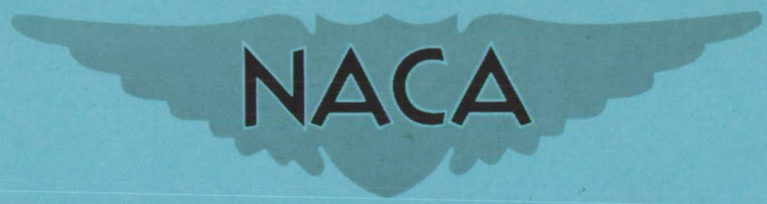


NOV 20 1957

Copy 1
RM A57G01

~~CONFIDENTIAL~~



RESEARCH MEMORANDUM

TRANSONIC WIND-TUNNEL TESTS OF THE LAUNCH, JETTISON,
AND LONGITUDINAL CHARACTERISTICS OF AN AIRPLANE-
AND MISSILE-MODEL COMBINATION

By Joseph W. Cleary, Joseph L. Frank,
and C. Forbes Dewey, Jr.

Ames Aeronautical Laboratory
Moffett Field, Calif.

CLASSIFICATION CHANGE

To Unclassified
By authority of Memo dtd. 4-15-77 b/ by H. Maines
Changed by M. Rusa Date 4-28-77

CLASSIFIED DOCUMENT

This material contains information affecting the National Defense of the United States within the meaning of the espionage laws, Title 18, U.S.C., Secs. 793 and 794, the transmission or revelation of which in any manner to an unauthorized person is prohibited by law.

NATIONAL ADVISORY COMMITTEE FOR AERONAUTICS

WASHINGTON
November 20, 1957

~~CONFIDENTIAL~~

FILE COPY
To be returned to
the files of the National
Advisory Committee
for Aeronautics
Washington, D. C.

NATIONAL ADVISORY COMMITTEE FOR AERONAUTICS

RESEARCH MEMORANDUMTRANSONIC WIND-TUNNEL TESTS OF THE LAUNCH, JETTISON,
AND LONGITUDINAL CHARACTERISTICS OF AN AIRPLANE-
AND MISSILE-MODEL COMBINATION

By Joseph W. Cleary, Joseph L. Frank,
and C. Forbes Dewey, Jr.

SUMMARY

Tests of an airplane model equipped with missiles were made to investigate the capability of this combination to achieve satisfactory launching and jettisoning of the missiles. An evaluation of pylons suitable for supporting the missiles was made from measurements of forces and moments of the airplane and missile models. The tests were made at Mach numbers from 0.80 to 1.20.

Large variations of missile forces and moments were observed for missile positions simulating launch or jettison within the local flow field of the airplane model. At transonic Mach numbers, the influence of the wing leading edge and shocks originating from components of the airplane were dominant factors contributing to the nonuniformity of the missile flow field. A simplified analysis of the data indicated that for a rapidly accelerating missile, however, these large variations in forces and moments would not cause excessive displacements of the missile when launched from the airplane in level unaccelerated flight. Idealized jettison boundaries estimated from the missile jettison data indicate satisfactory jettison would be achieved from the airplane in level flight at sea level but not at 40,000 feet altitude.

Canting or cambering the pylons supporting the missiles generally resulted only in small changes in the longitudinal force and moment characteristics of the airplane model. However, when the missile was pylon mounted, the rolling-moment coefficient was decreased by canting the pylons.

INTRODUCTION

The use of missiles as armament for high-speed airplanes has created new problems that must be considered in integrating the airplane-missile combination into an effective weapon. Satisfactory launching and jettisoning of a missile may not be achieved if the missile is improperly positioned within the nonuniform flow field created by the airplane. Tests at subsonic Mach numbers of a missile near the mid-semispan of a typical swept-wing-body combination (ref. 1) show large changes in aerodynamic forces and moments can be expected on the missile as it moves forward of the wing leading edge. A comprehensive treatment of this and other aspects of the composite missile-airplane problem is given in reference 2. At transonic and supersonic Mach numbers, shocks originating from components of the airplane contribute to the complexity of the problem.

Tests were made in the Ames 14-foot transonic wind tunnel at Mach numbers from 0.80 to 1.20 to gain some insight into the nature of the trajectory of the missile when launched or jettisoned. Measurements of forces and moments of the missile mounted in proximity to the airplane model were made. The effects of canting and cambering the pylons on the airplane and missile forces were also investigated.

COEFFICIENTS AND SYMBOLS

Airplane Model

The coefficients and related aerodynamic parameters are with respect to a moment center on the fuselage reference line at $0.25\bar{c}$.

| | |
|-----------|--|
| C_D | drag coefficient, $\frac{\text{drag}}{q_\infty S}$ |
| C_{D_0} | drag coefficient at zero lift |
| C_L | lift coefficient, $\frac{\text{lift}}{q_\infty S}$ |
| C_m | pitching-moment coefficient, $\frac{\text{pitching moment}}{q_\infty S \bar{c}}$ |
| b | wing span |
| \bar{c} | mean aerodynamic chord, $\frac{\int_0^{b/2} c^2 dy}{\int_0^{b/2} c dy}$ |
| c | local chord |

| | |
|-----------------------------------|----------------------------------|
| $\left(\frac{L}{D}\right)_{\max}$ | maximum lift-drag ratio |
| $\frac{dC_L}{d\alpha}$ | lift-curve slope |
| $\frac{dC_m}{dC_L}$ | longitudinal stability parameter |
| n | load factor |
| S | wing area |
| α | angle of attack |
| α_0 | angle of attack for zero lift |

Missile Model

The force and moment coefficients are presented with respect to the x'y'z' body system of axes fixed to the missile with the origin as the moment center at 0.531 of the missile length (center of gravity of the missile). An exception is the data presented for missile roll angles of 15° and 45°; these data are with respect to axes through the moment center parallel to the xyz system. The direction of positive forces, moments and displacements are as shown in figure 1.

| | |
|-----------|--|
| C_{A_m} | chord-force coefficient, $\frac{\text{chord force}}{q_{\infty} S_m}$ |
| C_{N_m} | normal-force coefficient, $\frac{\text{normal force}}{q_{\infty} S_m}$ |
| C_{Y_m} | side-force coefficient, $\frac{\text{side force}}{q_{\infty} S_m}$ |
| C_{l_m} | rolling-moment coefficient, $\frac{\text{rolling moment}}{q_{\infty} S_m b_m}$ |
| C_{m_m} | pitching-moment coefficient, $\frac{\text{pitching moment}}{q_{\infty} S_m \bar{c}_m}$ |
| C_{n_m} | yawing-moment coefficient, $\frac{\text{yawing moment}}{q_{\infty} S_m b_m}$ |
| b_m | wing span |

| | | |
|---|---|---|
| \bar{c}_m | mean aerodynamic chord of exposed wing, | $\frac{\int_{0.100b_m}^{0.500b_m} c_m^2 dy}{\int_{0.100b_m}^{0.500b_m} c_m dy}$ |
| c_m | local chord | |
| $F_{x,y,z}$ | applied forces | |
| g | acceleration due to gravity | |
| $I_{x',y',z'}$ | moment of inertia | |
| $\left. \begin{array}{l} I_{x'z'} \\ I_{y'z'} \\ I_{x'y'} \end{array} \right\}$ | product of inertia | |
| $K_{x',y',z'}$ | radius of gyration | |
| L | rolling moment | |
| m | mass | |
| M | pitching moment | |
| N | yawing moment | |
| p | rolling velocity | |
| q | pitching velocity | |
| r | yawing velocity | |
| S_m | exposed wing area | |
| t | time | |
| T | thrust | |
| u,v,w | velocity components parallel to the x',y',z' axes | |
| W | weight | |
| x,y,z | reference axes fixed to the airplane | |
| x',y',z' | axes fixed to the missile | |
| Δ | incremental value | |
| θ | angle of pitch | |

| | |
|--------------------|----------------------------------|
| ψ | angle of yaw |
| ϕ | angle of roll |
| μ | $\frac{W/g}{\rho S_m \bar{c}_m}$ |
| ($\bar{\cdot}$) | arithmetic mean value |
| ($\dot{\cdot}$) | $\frac{d(\cdot)}{dt}$ |
| ($\ddot{\cdot}$) | $\frac{d^2(\cdot)}{dt^2}$ |

General

| | |
|------------|------------------------------|
| h | altitude |
| M | Mach number |
| q_∞ | free-stream dynamic pressure |
| R | Reynolds number |
| V | free-stream velocity |
| ρ | free-stream density |

APPARATUS AND METHODS

Wind Tunnel

The tests were conducted in the Ames 14-foot transonic wind tunnel. This tunnel has a square perforated test section and an adjustable nozzle. Details of the test section and nozzle are shown in figure 2. Operation is continuous and Mach number can be varied from 0.30 to 1.20. Detailed longitudinal static-pressure measurements indicate a uniform flow; the variations in local Mach number are less than about ± 0.005 . Stagnation pressure in the test section is approximately atmospheric pressure. Variations in stagnation temperature are tolerated but the variations in Reynolds number that result are small and for this test, fell within the shaded region shown in figure 3.

Investigations of the effects of model blockage and reflected waves in this and related smaller tunnels have shown that for blockage ratios (ratio of maximum model cross-sectional area to test-section area) of less than about 0.5 percent, the effects are generally small. Since the

blockage ratio for this investigation was about 0.1 percent, the results are considered basically free of interference from model blockage and reflected waves.

Models

The airplane and missile models used during this investigation were 0.07-scale models.

Airplane.- The model was constructed from steel, wood, and Duralumin and was equipped with canopy, inlets, control surfaces, etc. All control surfaces were set at 0° . The mass-flow ratio of the air flowing through the inlets was adjusted to a value of about 0.8 to represent a high subsonic cruise condition. A sketch of the model showing the major components is given in figure 4 and additional geometrical details are supplied in table I.

The basic model configuration was equipped with missile pylons having symmetrical airfoil sections. Provisions were made for canting the leading edge of these pylons 3° toward the plane of symmetry (rotation about the z axis). Also furnished were cambered pylons similar in plan form to the symmetrical pylons with maximum camber at the wing-pylon juncture. Details of the symmetrical and cambered pylons are shown in figure 5.

The model was sting supported on approximately the tunnel center line as shown in the photographs of figure 6.

Missiles.- The airplane model was equipped with two missiles mounted on pylons beneath the wing as shown in figures 4, 5, and 6. Only the left missile was instrumented for measuring forces and could be either pylon or sting mounted. Missile position and attitude were varied by mounting the missile on stings of various lengths and angles. The stings were mounted on supports attached to the wing of the model as in a typical setup shown in figures 6(b) and 6(c).

The missiles were built of steel and Duralumin. A sketch of the missile model is presented in figure 7 and additional geometrical details are given in table II. For all phases of the test, the wings and tails were set at 0° incidence.

Measurements and Accuracies

Airplane model.- Model forces were measured with an electrical strain-gage balance mounted within the model. These measured forces were

resolved into lift, drag, and pitching moment about the moment center at $0.25\bar{c}$. The accuracy of the coefficients are believed to be:

$$C_L = \pm 0.010$$

$$C_D = \pm 0.0010$$

$$C_m = \pm 0.002$$

The data have been corrected for an average upflow angle of 0.7° evaluated from tests with the model upright and inverted. Surveys of the test section with probes that detected flow angularity indicated some spanwise variation of upflow angle but the data have not been corrected for this effect.¹ Since the model span was relatively small, the spanwise variations in flow angle are believed unimportant.

The effects of sting interference on the external pressures of the model forward of the duct exit were not evaluated. Experimental transonic research of similarly supported models indicate this effect would be small for this particular installation. However, the drag data have been adjusted to correspond to a base pressure equal to free-stream static pressure.

Corrections for the drag of the internal ducting have been applied to the drag data. These corrections were determined from measurements of total and static pressures within the duct and at the duct exit. Therefore the drag coefficients were based on a summation of the external aerodynamic forces parallel to the relative wind with the static pressure in the plan of the duct exit equal to the free-stream value.

Measurements of the inclination of the model to the horizontal are believed accurate to within $\pm 0.1^\circ$. However, inaccuracies in determining upflow give a probable accuracy of measuring angle of attack within about $\pm 0.2^\circ$.

Missile model.- The forces of the left missile were measured with an internal five-component strain-gage balance. Axial force was not measured, since it was considered irrelevant to the test. Because of the small size of the balance, the precision of measurement of forces and moments was only fair. The data have been corrected for deflections of the balance and the sting supporting the missile.

¹The primary source of the upflow and the spanwise variations have been traced to mixing of the cooling air in the air-exchange tower. Subsequent to these tests, the flow angularity has been reduced to a small value by installing a screen in the low-speed stagnation section of the tunnel circuit.

TESTS

The tests were conducted at Mach numbers from 0.80 to 1.20 and Reynolds number per foot of about 4×10^6 (see fig. 3). Angle of attack was varied from about -3° to 9° but for some parts of the test this range was decreased because of fouling of the missile balance.

Static longitudinal characteristics of the airplane model were measured to evaluate the effects of the pylons and missiles. Tests were made to determine the effect of pylon modifications on the lateral and longitudinal characteristics of the pylon-mounted missile. Tests with the missile at several longitudinal and vertical positions were made to evaluate the forces and moments of the missile at various positions in the airplane flow field.

RESULTS AND DISCUSSION

Pylon Modifications

An investigation was undertaken to determine the effects of pylon canting and pylon camber on the static aerodynamic forces and moments of the airplane and missile models. These tests were directed toward developing a pylon that would induce flows favorable to the reduction of forces of the missile when pylon mounted without adversely affecting the lift, drag, and pitching-moment characteristics of the airplane model. The effects of camber were evaluated from tests of the symmetrical and cambered pylons shown in figure 5. The effects of canting were determined from tests of the symmetrical pylon with the leading edge canted 3° toward the plane of airplane symmetry.

Airplane characteristics.- The effect of the symmetrical pylons and the missiles on the lift, drag, and pitching-moment characteristics of the airplane model are presented in figure 8. Similar data are presented in figures 9 and 10 showing the effects of the canted and cambered pylons, respectively. These data are summarized in figure 11 in a comparison of aerodynamic parameters of the model with missiles installed on each of the three pylons with those of the clean configuration. The comparisons indicate that from the standpoint of best airplane performance, none of the pylons exhibited a clear-cut superiority. In general within the accuracy of the data, the increase in drag coefficient at zero lift and the reduction in maximum lift-drag ratios were about the same for all pylon configurations.

A slight reduction in longitudinal stability $-(dC_m/dC_L)$ was incurred throughout the Mach number range by adding the pylons and missiles.

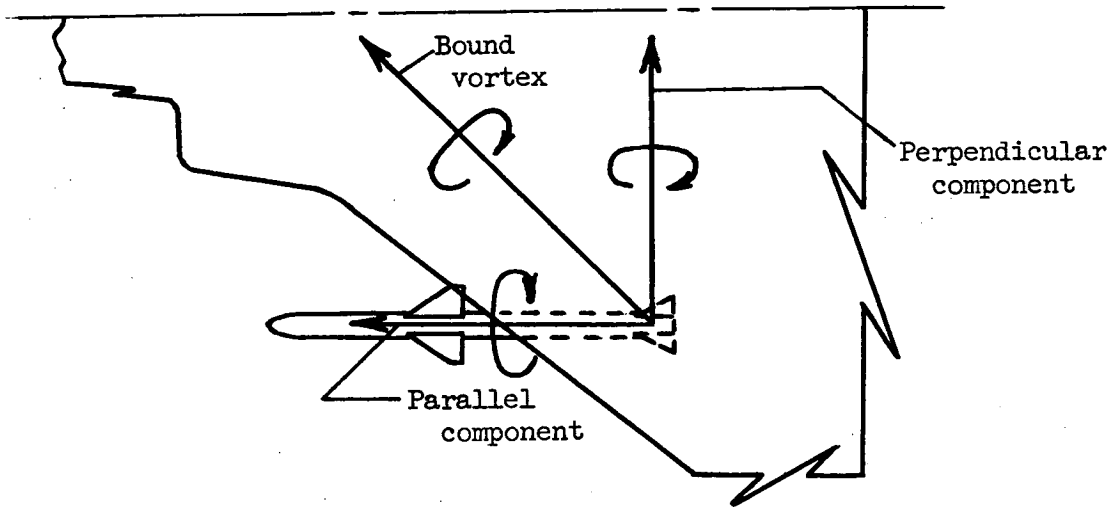
This reduction of stability might be of some concern at Mach numbers near 0.90 where the static margin is small at low lift coefficients.

Missile characteristics.- Static forces and moments of the pylon-mounted missile are presented in figure 12 for the various pylon configurations. The orientation of positive forces, moments, and displacements of the missile are as shown in figure 1 and the discussion and analysis of these and the data that follow apply only to the left missile. The presence of shocks arising from the airplane model, as will be shown later, may have a significant effect on the force and moment characteristics of the missile. Since data were obtained for only a limited number of Mach numbers, namely 0.80, 0.90, 0.92, 0.95, 1.00, 1.10, and 1.20, some caution should be exercised when extracting values from the joined curves at other than the Mach numbers of the test.

An examination of figures 12(a) and 12(b) reveals that canting the pylon and missile effected a negative shift in the rolling-moment coefficient and a positive shift in the side-force coefficient with only minor changes in the other coefficients. In general, the rolling-moment coefficients were decreased about 0.02.

To achieve a successful launch of the missile, considerable importance is attached to the values of moment coefficients in the initial phase of the launch. Depending on the magnitude of the missile acceleration, large moments may cause the missile to rotate sufficiently to strike the pylon or some other component of the airplane. Even relatively small values of rolling-moment coefficient may be of some concern, since for typical missile configurations, the inertial resistance to roll is small compared to that for pitching or yawing motions. It would appear then, that depending on angle of attack, canting the pylon and missile may be useful for reducing the magnitude of the rolling-moment coefficients. Cambering the pylon, on the other hand, was relatively ineffective in modifying the force or moment characteristics as shown by comparing figure 12(c) with 12(a).

Of interest is the large dependence of the force and moment coefficients on angle of attack since this variable determines in large measure the nature of the local flow field. Pertinent observations of the effects of increasing angle of attack made from figure 12 are (1) an increase in normal-force, pitching-moment, and rolling-moment coefficients and (2) a decrease in side-force coefficient with only minor changes in yawing-moment coefficient. While it is evident the local flow field is a complex combination of varying dynamic and static pressure, flow curvature, and flow angularity, the effects observed can be explained in a qualitative fashion by resorting to subsonic wing theory. The wing at angle of attack is replaced by a sweptback bound vortex. The circulation due to this vortex can be resolved into components perpendicular and parallel to the



missile axis as shown in the sketch. For a highly swept wing, the component parallel to the missile axis induces a strong lateral flow beneath the wing toward the tip, causing a decrease in side-force coefficient with increasing angle of attack. Interference of this flow by the pylon induces a vortex about the missile axis causing a rolling-moment coefficient that increases with increasing angle of attack. The component perpendicular to the missile axis induces upwash forward of the leading edge causing large increases in normal-force and pitching-moment coefficient with increasing angle of attack.

Missile in Launch Positions

Force and moment coefficients of the missile at several longitudinal positions forward of the pylon-mounted position and at various attitudes with respect to the launch reference line are given in the following figures:

| x/c | θ | ψ | ϕ | Figure | x/c | θ | ψ | ϕ | Figure |
|-------|----------|--------|--------|--------|-------|----------|--------|--------|--------|
| 0.185 | 0 | 0 | 0 | 13 | 1.108 | -8 | 0 | 0 | 17(b) |
| .369 | 0 | 0 | 0 | 14(a) | | 0 | -3 | 0 | 17(c) |
| | 0 | 0 | 15 | 14(b) | | 0 | -8 | 0 | 17(d) |
| | 3 | 0 | 0 | 14(c) | 1.477 | 0 | 0 | 0 | 18(a) |
| | -3 | 0 | 0 | 14(d) | | 0 | 0 | 45 | 18(b) |
| | 0 | -3 | 0 | 14(e) | | -8 | 0 | 0 | 18(c) |
| .554 | 0 | 0 | 0 | 15(a) | | 0 | -3 | 0 | 18(d) |
| | 0 | 0 | 15 | 15(b) | | 0 | -8 | 0 | 18(e) |
| | 3 | 0 | 0 | 15(c) | 1.846 | 0 | 0 | 0 | 19(a) |
| | -3 | 0 | 0 | 15(d) | | -8 | 0 | 0 | 19(b) |
| | 0 | -3 | 0 | 15(e) | | -16 | 0 | 0 | 19(c) |
| .738 | 0 | 0 | 0 | 16 | | 0 | -3 | 0 | 19(d) |
| 1.108 | 0 | 0 | 0 | 17(a) | | 0 | -8 | 0 | 19(e) |

From these data it can be seen that the local flow fields significantly influence the forces and moments on the missile as it moves forward of the pylon-mounted position. The highly nonuniform flow near the wing leading edge appears to be the governing factor but shocks arising from components of the airplane are important if impinging on the missile.

Effect of airplane-model shocks.- To illustrate how impinging shocks can affect the force and moment coefficients of the missile, figure 20 shows the variation of the coefficients along the launch reference line and the shocks the missile would penetrate. Coefficients are plotted versus position of the missile moment center and the symbols designate the corresponding positions of the wing and tail. The shock fronts depicted were taken from schlieren photographs of the flow of which figure 21 is typical. The data are presented for an angle of attack of 0.7° and are generally typical of level-flight low-altitude conditions.

For Mach numbers greater than 1.00, shocks originating from the fuselage bow, the air inlets, and the wing-fuselage juncture are indicated in the region of interest. The most significant effects of Mach number are observed when one or more shocks cross some part of the missile. Values of normal-force and pitching-moment coefficient obtained from tests of a 0.11-scale model of the missile (ref. 3) in a uniform flow at Mach numbers from 0.8 to 1.30 are shown at the left as a dashed line. With the missile at $x/c = 1.477$, a large increase in yawing moment occurred at a Mach number of 1.20, tending to yaw the missile toward the airplane. This effect is attributed to the increased strength of the bow wave and the attendant abrupt changes in flow direction behind the shock as Mach number increased to 1.20. Increasing Mach number caused a large decrease in normal-force coefficient when the missile is placed at $x/c = 0.738$. This is believed due to the inlet shock crossing the missile between the wing and tail. Corresponding reductions in pitching-moment coefficient are observed. Related smaller effects can be detected on the other force and moment coefficients when one or more of the shocks cross the missile.

Missile Trajectory

It is important to know the missile path in the initial phase of the launch to determine whether the missile will strike some component of the airplane. It is also important to know the missile attitude during the controls-locked phase of the launch, since the target may be lost from the field of view of the missile if large pitching and yawing motions are incurred.

An estimate of missile trajectory and attitude from measurements of static forces and moments requires simplifying assumptions that make the equations of motion amenable to solution. The detailed assumptions and a development of equations relating missile position and attitude to

external forces and moments are given in the appendix. The analysis is based on equations of motion for small disturbances with controls locked and the assumptions neglect aerodynamic damping and forces opposing the missile thrust. It is believed that the results of this analysis are of sufficient accuracy to define problem areas and to assess the probability of a successful launch.

Airplane in unaccelerated flight.- The results of the analysis showing the effect of flight altitude are presented in figure 22. The airplane was assumed in level unaccelerated flight and the angle of attack required is given in figure 27. Computations were based on an airplane wing loading of 40 pounds per square foot and a missile thrust-to-weight ratio of 25. The inertia properties of the missile are given in table III. Except for forward motion, the missile was restrained by the launcher during the initial 3 feet of the launch (to $x/c = 0.185$). Mention should be made that the analysis was hampered by a lack of data giving the complete effect of missile attitude on the aerodynamic coefficients at all longitudinal positions. Where necessary, extrapolations of data have been made.

The results indicate that the vertical and lateral displacements of the missile with respect to the airplane are small and that the missile would not contact the airplane. At any given Mach number, the magnitude of the missile's vertical and lateral displacements decreased with increasing altitude. This generally indicates that the effects of decreasing density of the air overshadowed changes in missile coefficients due to increased angle of attack. Similarly the magnitude of the rotational motions of the missile, in general, decreased with increasing altitude. At transonic Mach numbers the largest angles of pitch and yaw were 16° and -15° , respectively. It is believed these angles are not sufficient for the missile to lose the target during a routine approach. Abrupt changes in missile position and attitude as it traverses the shocks is not predicted by this analysis because of the averaging process over the intervals of the finite step-by-step computing procedure.

To clear the launcher, the missile must travel approximately 10.5 feet and allowable axial rotation before the tail contacts the launcher is approximately 14° . Figure 22 indicates that contact would not occur at transonic Mach numbers but clearance was marginal at a Mach number of 1.00.

Airplane in turning flight.- As an example of the effects of maneuvering the airplane when missile launch occurs, figure 23 shows the relative position and attitude of the missile during a turn to the left at a load factor of 3. The computations were made for flight at 20,000 feet altitude and a Mach number of 1.20. Shown for comparison are the displacements presented in figure 22(c) for these same conditions but at a load factor of unity. In general, missile displacements are increased by this maneuver because of the usually larger aerodynamic forces of the

missile that result from the increased angle of attack. Turning of the airplane compensates in large measure for the linear displacements that occur from increase in angle of attack. Thus, a corresponding turn to the right would result in larger linear displacements of the left missile.

The increase in roll angle due to increasing load factor results in marginal rotational clearance of the missile for a load factor of 3. On the basis that decreasing altitude increases the missile rotations as shown previously for unaccelerated flight, it is probable that the missile would contact the pylon in roll if a load factor of 3 were required at lower altitude.

Missile in Jettison Positions

Force and moment data simulating possible missile jettison positions below the carry position are presented in the following figures:

| z/c | θ | ψ | ϕ | Figure |
|--------|----------|--------|--------|--------|
| 0.0308 | 0 | 0 | 0 | 24(a) |
| | 3 | 0 | 0 | 24(b) |
| | -3 | 0 | 0 | 24(c) |
| .0923 | 0 | 0 | 0 | 25(a) |
| | 8 | 0 | 0 | 25(b) |
| | -8 | 0 | 0 | 25(c) |
| | -16 | 0 | 0 | 25(d) |
| .2051 | 0 | 0 | 0 | 26(a) |
| | 8 | 0 | 0 | 26(b) |
| | -8 | 0 | 0 | 26(c) |
| | -16 | 0 | 0 | 26(d) |

From these data it can be observed, as was the case with simulated launch positions, that the force and moment coefficients are highly dependent on angle of attack, missile position, attitude, and Mach number. However, as might be expected, the influence of angle of attack decreases with missile distance from the pylon-mounted position. In this connection, it can be observed by comparing figure 24(a) with figure 12(a) that a small vertical displacement of the missile reduced the variation in rolling-moment coefficient with angle of attack by about 50 percent. This is believed due primarily to creating an opening between the launcher and missile allowing passage of the lateral component of the flow. Thus, a reduction in rolling-moment coefficient of the missile in the pylon-mounted position might be achieved by strategic openings in the pylon.

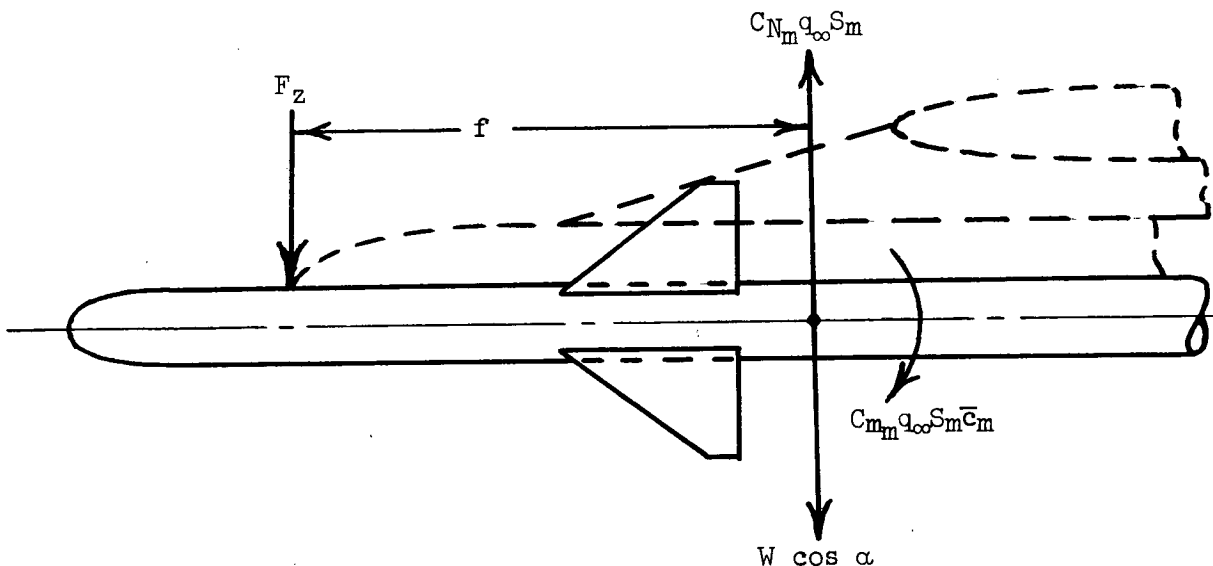
Jettison boundaries.- An idealized analysis of the data was made to estimate the approximate boundaries for satisfactory jettisoning of the missiles. This analysis assumed that jettison was achieved by the

unbalanced force due to gravity without assistance from other devices. Furthermore, because of the limited data, it was assumed that the coefficients in the longitudinal plane were independent of missile attitude and displacement in the lateral direction. However, the boundaries take account of possible lateral motions if it is assumed that the coefficients in the lateral direction are functions only of missile position and attitude in the longitudinal plane. The boundaries do not take into account longitudinal motions due to missile drag.

The results of the analysis are shown in figure 27 for release at altitudes of sea level, 20,000 feet, and 40,000 feet for level unaccelerated flight. The upper boundary shown at sea level and 20,000 feet gives the airplane angle of attack for which the missile would not depart even though jettison was initiated. This boundary is defined by considering the free-body static forces and moments of the missile in the longitudinal plane, the inequality relating C_{N_m} , C_{m_m} , and missile weight being

$$C_{N_m} - C_{m_m} \frac{\bar{c}_m}{f} \geq \frac{W \cos \alpha}{q_\infty S_m}$$

and the dimension, f , as shown in the sketch. Other aerodynamic forces were neglected. Sufficient data were not available to obtain this boundary at 40,000 feet.



The lower of the two boundaries was determined from an analysis of the dynamic motions of the missile and neglects damping. Below this boundary, a region is defined wherein the missile would jettison satisfactorily; that is, at a minimum z/c of 0.205 without contacting the airplane. Primary concern was contact of the missile wings with the pylon due to positive rolling and negative yawing motions. Pitching and lateral motions were generally small at low angles of attack.

The results shown in figure 27 indicate that jettisoning of the missile becomes less satisfactory as the altitude for release increased from sea level to 40,000 feet. At 40,000 feet altitude, jettisoning was unsatisfactory throughout the Mach number range of the test, primarily because of the large rolling moments of the missile induced at high angles of attack.

CONCLUDING REMARKS

Static force and moment measurements at transonic Mach numbers of a missile model showed large variations of forces and moments due to position and attitude within the flow field of the airplane model. The dominant factors contributing to the nonuniformity of the local flow are believed due to the influence of the wing leading edge and shocks originating from components of the airplane model. If launched at Mach numbers greater than 1.00, the missile would traverse shocks from the wing-fuselage juncture, the air inlets, and the fuselage bow. When the missile penetrates the bow wave at a Mach number of 1.20, a yawing moment is incurred tending to yaw the missile toward the airplane. A simplified analysis of the data however, indicates that for a rapidly accelerating missile the large variations in forces and moments would not cause excessive motions of the missile when launched from the airplane in level unaccelerated flight.

Idealized boundaries estimated from the missile jettison data indicate the missile would jettison satisfactorily from the airplane in level flight at sea level but not at 40,000 feet altitude.

An investigation of the effects of cambering and canting the pylons showed canting the pylons decreased the rolling-moment coefficients of the missile in the pylon-mounted position. Cambering the pylons, however, had little effect on the missile loads.

Ames Aeronautical Laboratory
National Advisory Committee for Aeronautics
Moffett Field, Calif., July 1, 1957

APPENDIX

MISSILE LAUNCH EQUATIONS

The equations defining the missile path and attitude with respect to the airplane are developed by relating applied forces and moments to the time rate of change of momentum and moment of momentum, respectively. The development is based on the airplane's being in level unaccelerated flight when launching occurs and therefore the airplane is used as a reference frame for the fixed-axes system. A moving system of body axes is attached to the missile as depicted in figure 1. For these systems of axes the following equations relate the forces and moments applied to the missile to the inertia forces and moments (see, e.g., ref. 4):

Applied forces along fixed axes

$$\Sigma F_x = ma_x = m\ddot{x}$$

$$\Sigma F_y = ma_y = m\ddot{y}$$

$$\Sigma F_z = ma_z = m\ddot{z}$$

By symmetry, the x', y', z' axes define principal axes and therefore

$$I_{x'y'} = I_{x'z'} = I_{z'y'} = 0$$

$$I_{z'} = I_{y'}$$

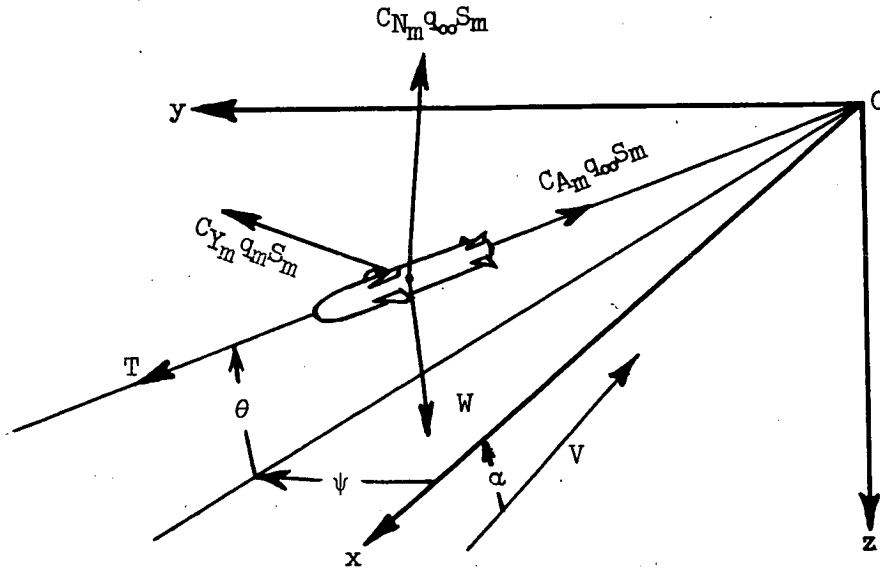
The equations for the applied moments about the body axes are:

$$\Sigma L_{x'} = \dot{p}I_{x'}$$

$$\Sigma M_{y'} = \dot{q}I_{y'} + rp(I_{x'} - I_{z'})$$

$$\Sigma N_{z'} = \dot{r}I_{z'} + pq(I_{y'} - I_{x'})$$

Because of the limited amount of data, it was assumed that the missile forces were independent of the angle of roll. Thus the missile normal force and side force lie in planes perpendicular and parallel to the xy reference plane, respectively, as shown in the sketch. This



assumption is partially substantiated by experimental data. Summing the applied forces in the x, y, z directions gives:

$$\Sigma F_x = T \cos \theta \cos \psi - W \sin \alpha - C_{N_m} q_m S_m \sin \theta \cos \psi - C_{Y_m} q_m S_m \sin \psi - C_{A_m} q_m S_m \cos \theta \cos \psi = \frac{W}{g} \ddot{x}$$

$$\Sigma F_y = C_{Y_m} q_m S_m \cos \psi + T \cos \theta \sin \psi - C_{N_m} q_m S_m \sin \theta \sin \psi - C_{A_m} q_m S_m \cos \theta \sin \psi = \frac{W}{g} \ddot{y}$$

$$\Sigma F_z = - C_{N_m} q_m S_m \cos \theta + W \cos \alpha - T \sin \theta + C_{A_m} q_m S_m \sin \theta = \frac{W}{g} \ddot{z}$$

and summing the applied moments about the x', y', z' axes gives:

$$\Sigma L_{x'} = C_{l_m} q_m S_m b_m = \dot{p} I_{x'}$$

$$\Sigma M_{y'} = C_{m_m} q_m S_m \bar{c}_m = \dot{q} I_{y'} + r p (I_{x'} - I_{z'})$$

$$\Sigma N_{z'} = C_{n_m} q_m S_m b_m = \dot{r} I_{z'} + p q (I_{y'} - I_{x'})$$

These equations for the translation and rotation of the missile comprise a system of nonlinear differential equations that are not solvable by ordinary methods. To effect a solution, the following assumptions are made:

1. The angular motions of the missile are small and the general rules for small disturbances apply. For the purpose of this analysis, this allows replacing cosines of angles by 1.0, sines by the angle, and

sines squared by zero. This disregards terms containing products of angular velocity components thereby neglecting motions due to inertia coupling. An estimate of angular velocities indicated inertia coupling may be of some significance in certain cases when the roll rate is large.

2. The missile thrust is large in comparison to other forces in the x direction.

3. Aerodynamic damping is small compared to the static forces and can be ignored.

4. The mass and distribution of mass of the missile remains fixed during the launch.

5. For a small finite interval, Δx , the attitude and coefficients of the missile can be averaged and are effectively constant.

When these assumptions are employed, the equations of motion become:

Translation

$$\frac{W}{g} \ddot{x} - T = 0$$

and for a finite interval, Δx

$$\frac{W}{g} \Delta \ddot{y} - C_{Y_m}' q_m S_m - T \psi' = 0$$

$$\frac{W}{g} \Delta \ddot{z} + C_{N_m}' q_m S_m + T \theta' = 0$$

Rotations

$$I_x \Delta \ddot{\phi} - C_{L_m}' q_m S_m b_m = 0$$

$$I_y \Delta \ddot{\theta} - C_{m_{\bar{m}}}' q_m S_m \bar{c}_m = 0$$

$$I_z \Delta \ddot{\psi} - C_{n_m}' q_m S_m b_m = 0$$

Substituting $q_m = \frac{1}{2} \rho (V + a_1 t + b_1)^2$ where a_1 is the missile acceleration and b_1 the initial velocity at the beginning of the interval relative to the airplane, the equations are easily solved by double quadrature after separating variables. The solutions are:

Translation in the x direction:

$$x = \frac{1}{2} a_1 t^2 + b_1 t + c_1$$

where

$$a_1 = \frac{T}{W} g$$

b_1 = initial velocity

c_1 = initial displacement

Translation in the y direction:

$$\Delta y = \frac{1}{12} a_2 \Delta t^4 + \frac{1}{6} b_2 \Delta t^3 + \frac{1}{2} c_2 \Delta t^2 + d_2 \Delta t$$

where

$$a_2 = \frac{C_{Y_m}' a_1^2}{2\bar{c}_m \mu} \quad \mu = \frac{W/g}{\rho S_m \bar{c}_m}$$

$$b_2 = \frac{C_{Y_m}' a_1 (V + b_1)}{\bar{c}_m \mu}$$

$$c_2 = \frac{C_{Y_m}' (V^2 + 2Vb_1 + b_1^2)}{2\bar{c}_m \mu} + a_1 \psi'$$

and d_2 is the initial velocity at the beginning of the interval

$$y = \Sigma \Delta y$$

Translation in the z direction:

$$\Delta z = \frac{1}{12} a_3 \Delta t^4 + \frac{1}{6} b_3 \Delta t^3 + \frac{1}{2} c_3 \Delta t^2 + d_3 \Delta t$$

where

$$a_3 = \frac{-C_{N_m}' a_1^2}{2\bar{c}_m \mu}$$

$$b_3 = \frac{-C_{N_m}' a_1 (V + b_1)}{\bar{c}_m \mu}$$

$$c_3 = \frac{-C_{N_m}' (V^2 + 2Vb_1 + b_1^2)}{2\bar{c}_m \mu} + g \cos \alpha - a_1 \theta'$$

and d_3 is the initial velocity at the beginning of the interval

$$z = \Sigma \Delta z$$

Rotation of the x' axis:

$$\Delta\phi = \frac{1}{12} a_4 \Delta t^4 + \frac{1}{6} b_4 \Delta t^3 + \frac{1}{2} c_4 \Delta t^2 + d_4 \Delta t$$

where

$$a_4 = \frac{C_{l_m}' b_m a_1^2}{2 \bar{c}_m K_{x'}^2 \mu} \quad K_{x'}^2 = \frac{g}{W} I_{x'}$$

$$b_4 = \frac{C_{l_m}' b_m a_1 (V + b_1)}{\bar{c}_m K_{x'}^2 \mu}$$

$$c_4 = \frac{C_{l_m}' b_m (V^2 + 2Vb_1 + b_1^2)}{2 \bar{c}_m K_{x'}^2 \mu}$$

and d_4 is the initial velocity at the beginning of the interval

$$\phi = \Sigma \Delta\phi$$

Rotation of the y' axis:

$$\Delta\theta = \frac{1}{12} a_5 \Delta t^4 + \frac{1}{6} b_5 \Delta t^3 + \frac{1}{2} c_5 \Delta t^2 + d_5 \Delta t$$

where

$$a_5 = \frac{C_{m_m}' a_1^2}{2 K_{y'}^2 \mu} \quad K_{y'}^2 = \frac{g}{W} I_{y'}$$

$$b_5 = \frac{C_{m_m}' a_1 (V + b_1)}{K_{y'}^2 \mu}$$

$$c_5 = \frac{C_{m_m}' (V^2 + 2Vb_1 + b_1^2)}{2 K_{y'}^2 \mu}$$

and d_5 is the initial velocity at the beginning of the interval

$$\theta = \Sigma \Delta\theta$$

Rotation of the z' axis:

$$\Delta\psi = \frac{1}{12} a_6 \Delta t^4 + \frac{1}{6} b_6 \Delta t^3 + \frac{1}{2} c_6 \Delta t^2 + d_6 \Delta t$$

where

$$a_e = \frac{C_{n_m} b_m a_1^2}{2 \bar{c}_m K_Z \mu} \quad K_Z^2 = \frac{g}{W} I_Z$$

$$b_e = \frac{C_{n_m} b_m a_1 (V + b_1)}{\bar{c}_m K_Z \mu}$$

$$c_e = \frac{C_{n_m} b_m (V^2 + 2Vb_1 + b_1^2)}{2 \bar{c}_m K_Z \mu}$$

and d_e is the initial velocity at the beginning of the interval

$$\psi = \Sigma \Delta \psi$$

REFERENCES

1. Alford, William J., Jr., and King, Thomas J., Jr.: Experimental Static Aerodynamic Forces and Moments at High Subsonic Speeds on a Missile Model During Simulated Launching From the Mid-Semispan Location of a 45° Sweptback Wing-Fuselage-Pylon Combination. NACA RM L56J05, 1957.
2. Froning, H. D., Munter, P. L., and Pedraglia, R. M.: A Study of the Aerodynamic Phenomena Arising From the External Carriage of Air-To-Air Missiles. Rep. No. SM-27101, Douglas Aircraft Co., Inc., Aug. 17, 1956.
3. Livezey, W. F., and Mixon, M. S.: Stability and Control Data from Subsonic, Transonic, and Supersonic Wind Tunnel Tests on an 11-Percent-Scale Model of the Sparrow II Missile. Rep. No. SM-19468, Douglas Aircraft Co., Inc., Dec. 20, 1955.
4. Perkins, Courtland D., and Hage, Robert E.: Airplane Performance Stability and Control. John Wiley and Sons, N. Y., 1949.

TABLE I.- GEOMETRIC PROPERTIES OF THE AIRPLANE MODEL

| | |
|--------------------------------------|----------------------|
| Wing | |
| Airfoil sections | |
| Root | NACA 0005 modified |
| Tip | NACA 0003.2 modified |
| Area, sq ft | 2.729 |
| Span, ft | 2.34 |
| Root chord, ft | 1.756 |
| Tip chord, ft | 0.583 |
| Mean aerodynamic chord, ft | 1.278 |
| Aspect ratio | 2.02 |
| Taper ratio | 0.332 |
| Sweepback 0.25c, deg | 46.5 |
| Dihedral, deg | 0 |
| Incidence, deg | 0 |
| Geometric twist, deg | 0 |
| Vertical tail | |
| Airfoil sections | |
| Root (rudder base). | NACA 0005.1 modified |
| Tip | NACA 0003.2 modified |
| Area, sq ft | 0.342 |
| Span, ft | 0.662 |
| Mean aerodynamic chord, ft | 0.549 |
| Sweepback 0.25c, deg | 48.2 |
| Aspect ratio | 1.28 |
| Taper ratio | 0.455 |
| Fuselage | |
| Length, ft | 3.278 |
| Maximum depth, ft | 0.332 |
| Maximum width, ft | 0.332 |
| Fineness ratio | 9.86 |

TABLE II.- GEOMETRIC PROPERTIES OF THE MISSILE MODEL

| | |
|---|--------------|
| Wing | |
| Airfoil sections, double wedge | t/c = 0.0415 |
| Area, exposed two panels, sq ft | 0.01235 |
| Span, ft | 0.2341 |
| Root chord, exposed, ft | 0.1132 |
| Tip chord, ft | 0.0194 |
| Mean aerodynamic chord, exposed, ft | 0.0772 |
| Aspect ratio, based on total area and span | 3.0 |
| Taper ratio, ratio of tip chord to root chord at plane of symmetry | 0.142 |
| Sweepback, deg | 45 |
| Incidence, deg | 0 |
| Tail | |
| Airfoil sections, double wedge | t/c = 0.0290 |
| Area, exposed two panels, sq ft | 0.01007 |
| Span, ft | 0.2332 |
| Root chord, exposed, ft | 0.1079 |
| Tip chord | 0 |
| Mean aerodynamic chord, exposed, ft | 0.0720 |
| Aspect ratio | 3.46 |
| Taper ratio | 0 |
| Sweepback, leading edge, deg | 57 |
| Incidence, deg | 0 |
| Fuselage | |
| Length, ft | 0.866 |
| Maximum diameter, ft | 0.0467 |
| Fineness ratio | 18.8 |

TABLE III.- INERTIA PROPERTIES OF THE MISSILE

| | |
|---|-------|
| Missile weight, lb | 381 |
| Pitching and yawing moment of inertia, slug-ft ² | 109.5 |
| Rolling moment of inertia, slug-ft ² | 1.325 |

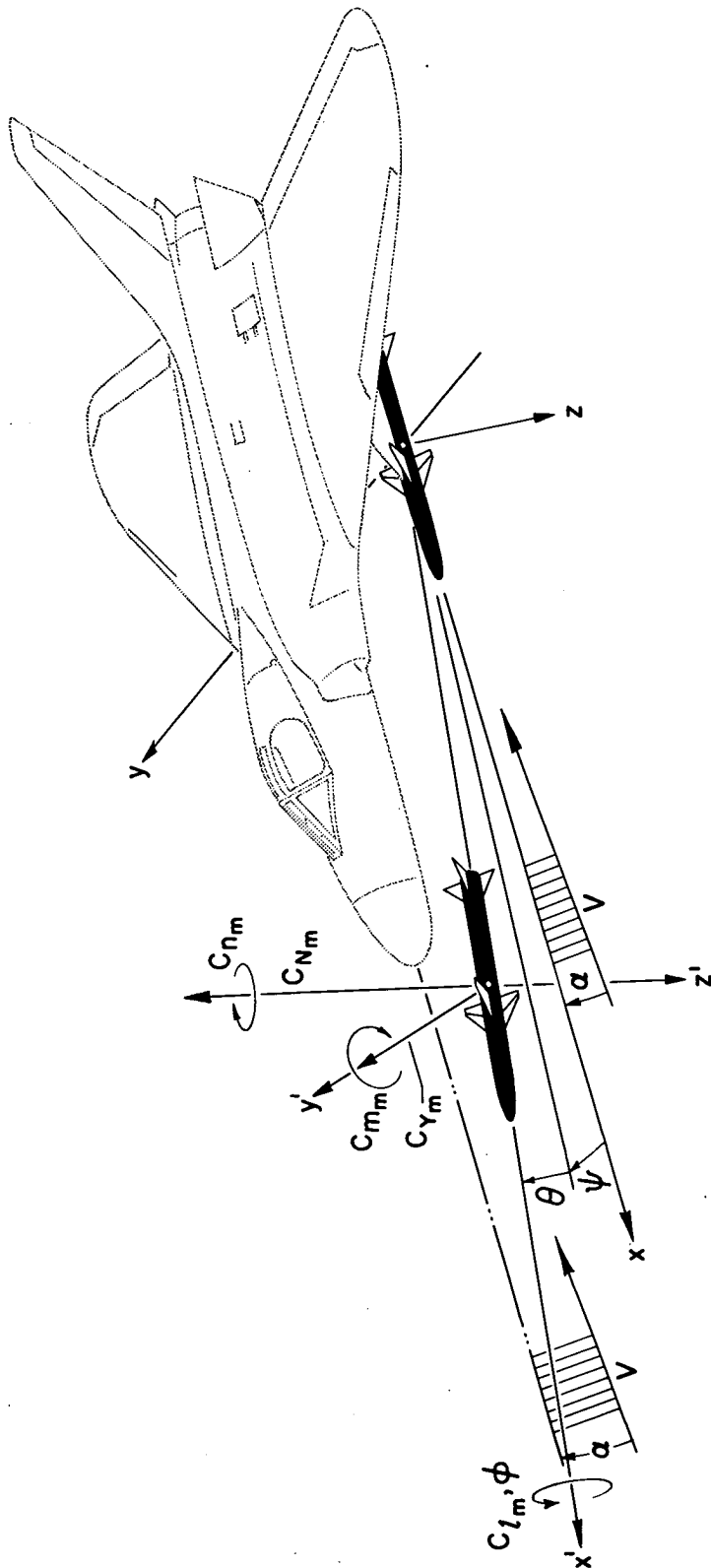


Figure 1.- Systems of axes showing positive forces and displacements of the missile.

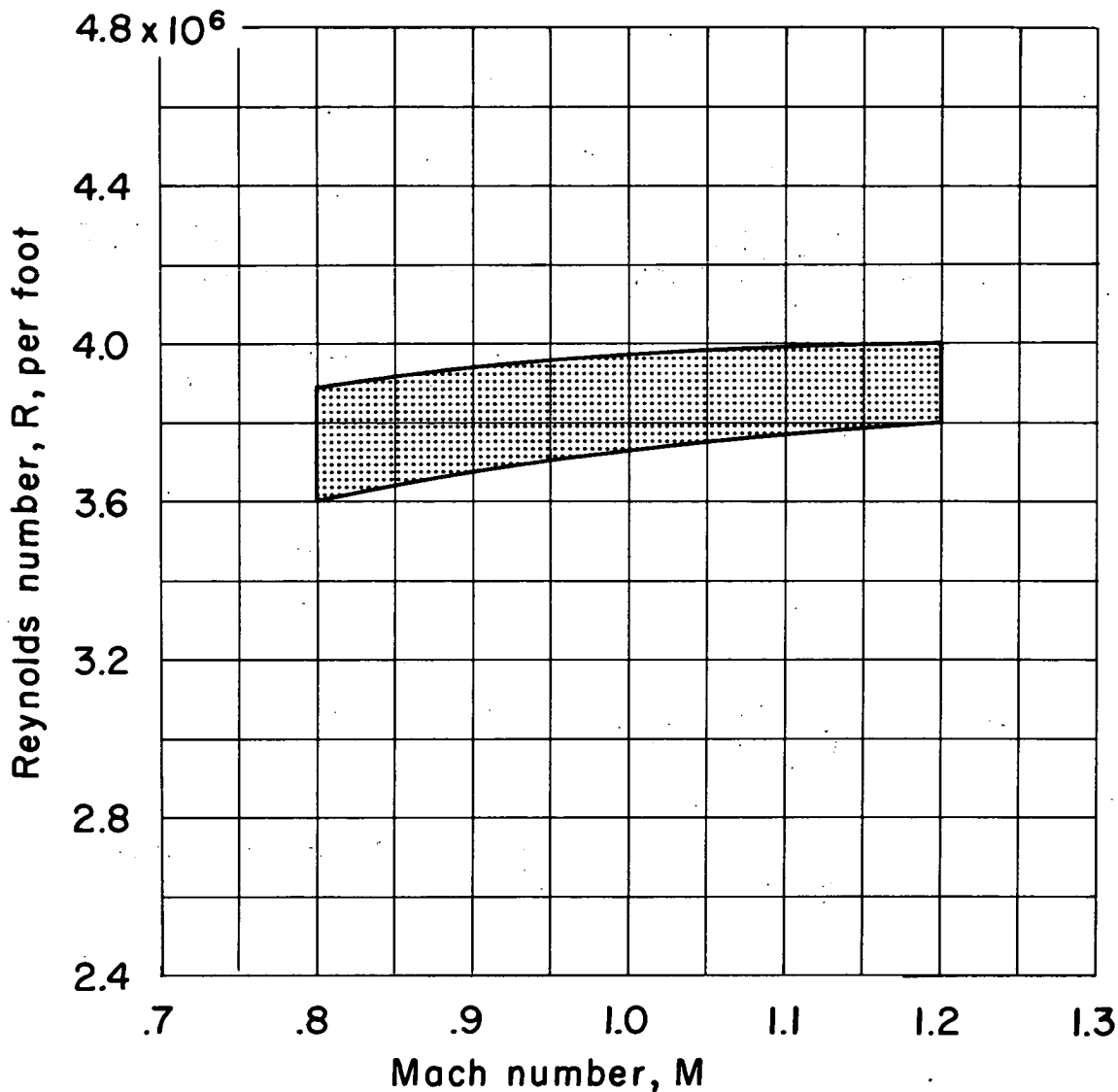


Figure 3.- Variation of Reynolds number with Mach number.

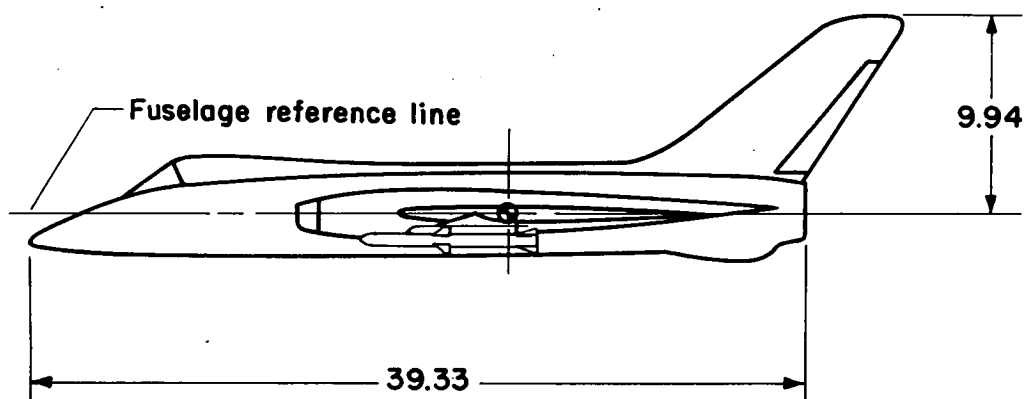
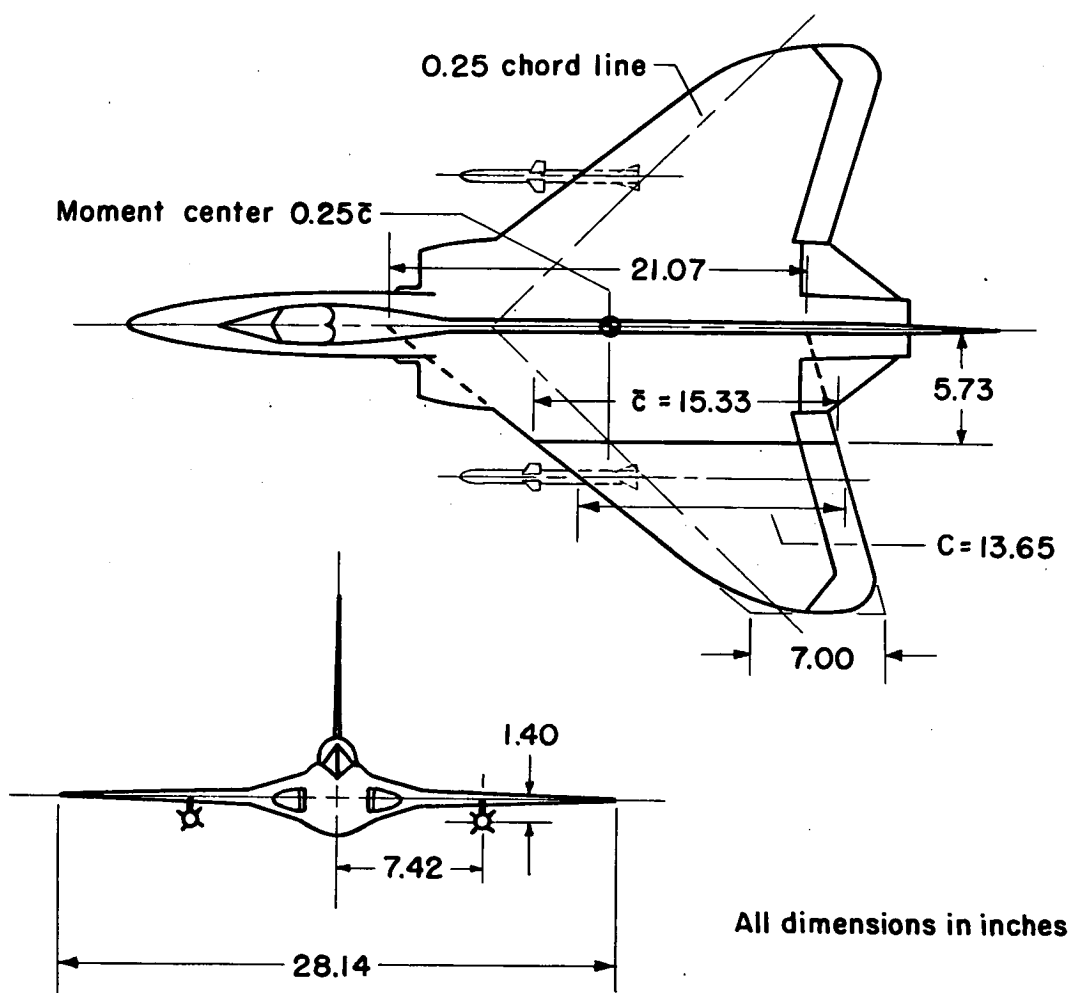
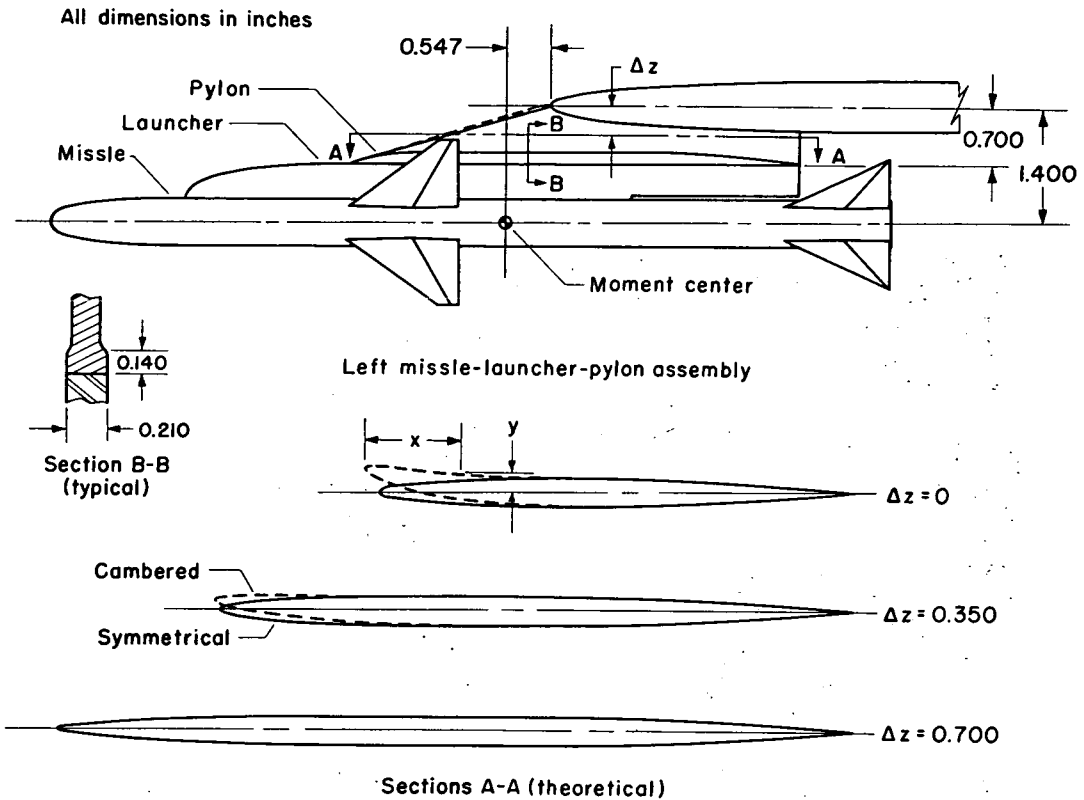


Figure 4.- The 0.07-scale model of the airplane.



| Section A-A basic pylon | | | | Section A-A cambered pylon | | | | |
|-------------------------|-------|------------|-------|----------------------------|--------------------|--------------------|------------|-------|
| Δz = 0 | | Δz = 0.700 | | Δz = 0 | | | Δz = 0.700 | |
| x | y | x | y | x | y _{lower} | y _{upper} | x | y |
| 0 | 0 | 0 | 0 | 0 | 0.160 | 0.160 | 0 | 0 |
| 0.038 | 0.028 | 0.069 | 0.028 | 0.020 | .137 | .167 | 0.069 | 0.028 |
| .075 | .038 | .138 | .038 | .038 | .123 | .170 | .138 | .038 |
| .150 | .052 | .275 | .052 | .073 | .101 | .171 | .275 | .052 |
| .225 | .061 | .412 | .061 | .125 | .075 | .167 | .412 | .061 |
| .300 | .068 | .550 | .068 | .195 | .048 | .158 | .550 | .068 |
| .450 | .079 | .826 | .079 | .300 | .013 | .145 | .826 | .079 |
| .600 | .084 | 1.100 | .084 | .405 | -.017 | .131 | 1.100 | .084 |
| .750 | .087 | 1.376 | .087 | .510 | -.039 | .119 | 1.376 | .087 |
| .900 | .088 | 1.650 | .088 | .615 | -.057 | .109 | 1.650 | .088 |
| 1.091 | .088 | 3.400 | .088 | .720 | -.071 | .101 | 3.400 | .088 |
| 1.091 | .088 | 3.591 | .088 | .825 | -.081 | .094 | 3.591 | .088 |
| 1.419 | .085 | 3.919 | .085 | .914 | -.086 | .090 | 3.919 | .085 |
| 1.729 | .078 | 4.229 | .078 | 1.033 | -.088 | .088 | 4.229 | .078 |
| 2.047 | .065 | 4.547 | .065 | 1.103 | -.088 | .088 | 4.547 | .065 |
| 2.362 | .048 | 4.862 | .048 | 1.294 | -.088 | .088 | 4.862 | .048 |
| 2.685 | .027 | 5.185 | .027 | 1.622 | -.085 | .085 | 5.185 | .027 |
| 2.841 | .015 | 5.341 | .015 | 1.932 | -.078 | .078 | 5.341 | .015 |
| 3.000 | .002 | 5.500 | .002 | 2.250 | -.065 | .065 | 5.500 | .002 |
| | | | | 2.565 | -.048 | .048 | | |
| | | | | 2.888 | -.027 | .027 | | |
| | | | | 3.044 | -.015 | .015 | | |
| | | | | 3.203 | .002 | .002 | | |

Figure 5.- Details of the symmetrical and the cambered pylons.



(a) Missiles pylon mounted.

A-21349

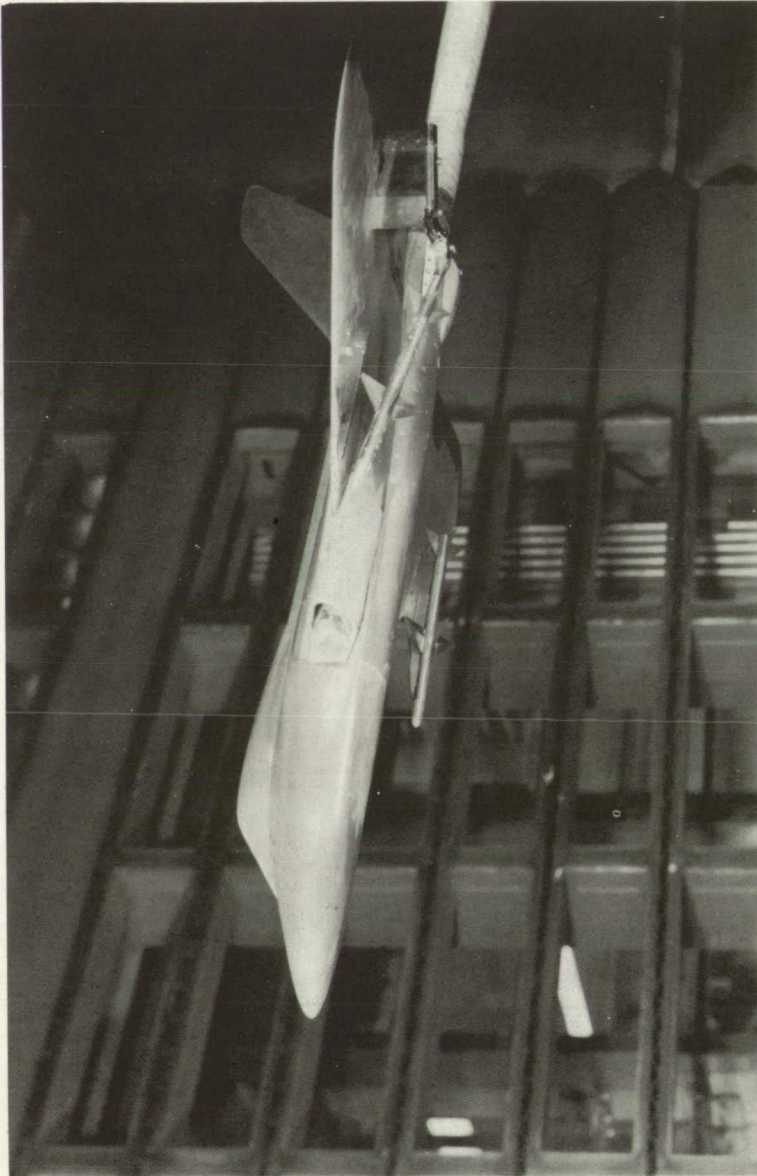
Figure 6.- The airplane model equipped with missiles and installed in the test section.



A-21308

(b) Left missile sting mounted at $x/c = 0.369$.

Figure 6.- Continued.



A-21387

(c) Left missile sting mounted at $z/c = 0.0923$.

Figure 6.- Concluded.

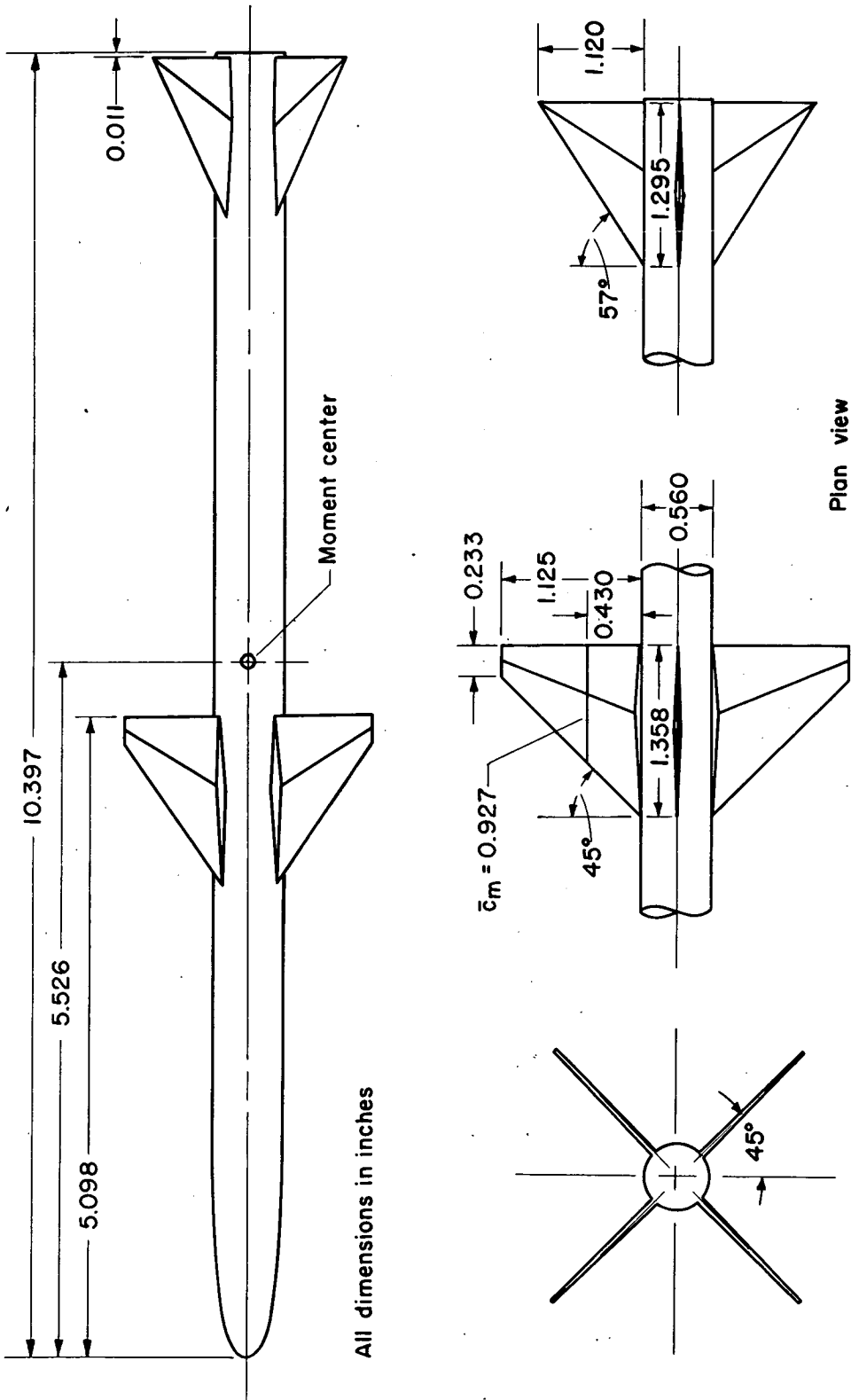
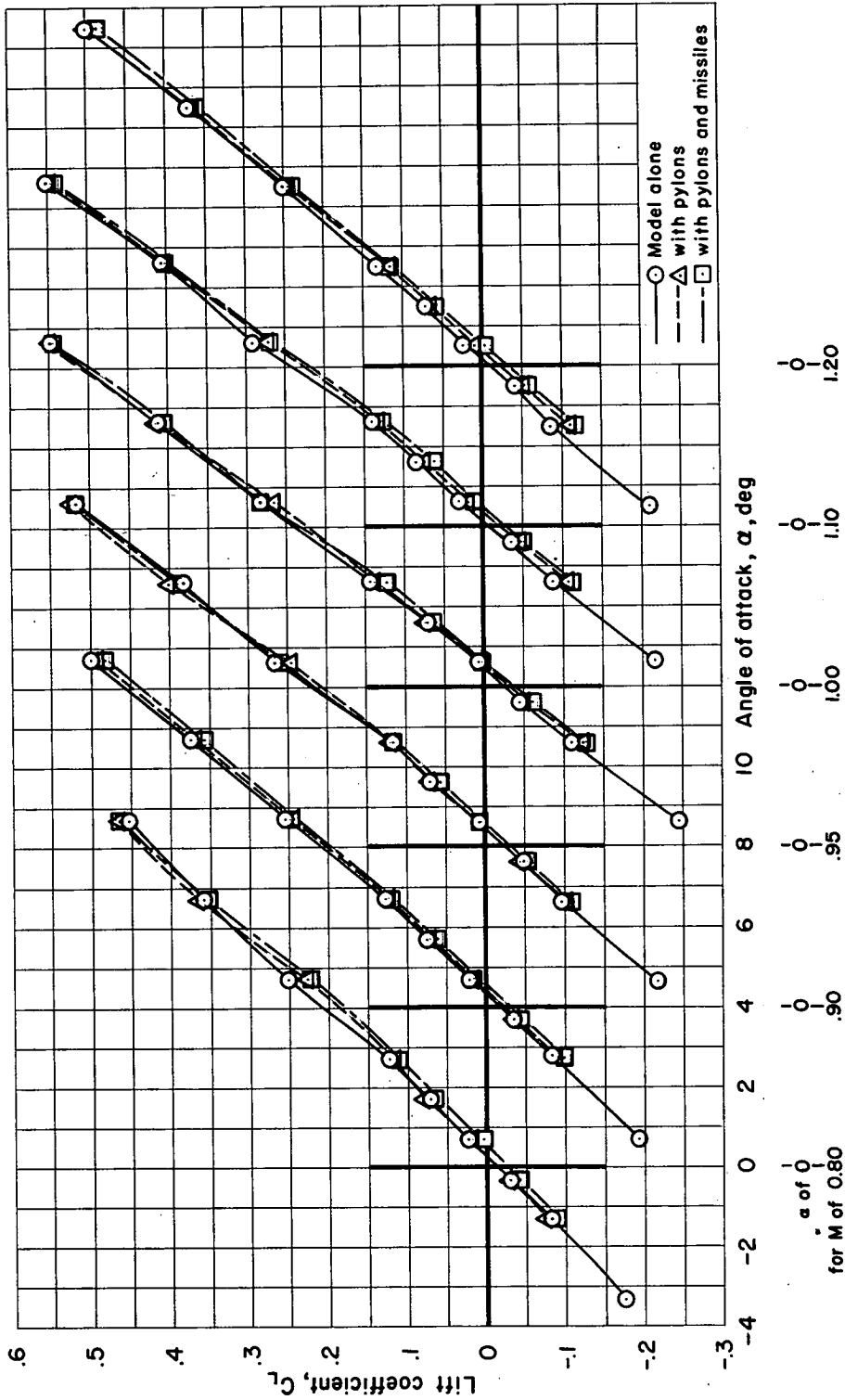
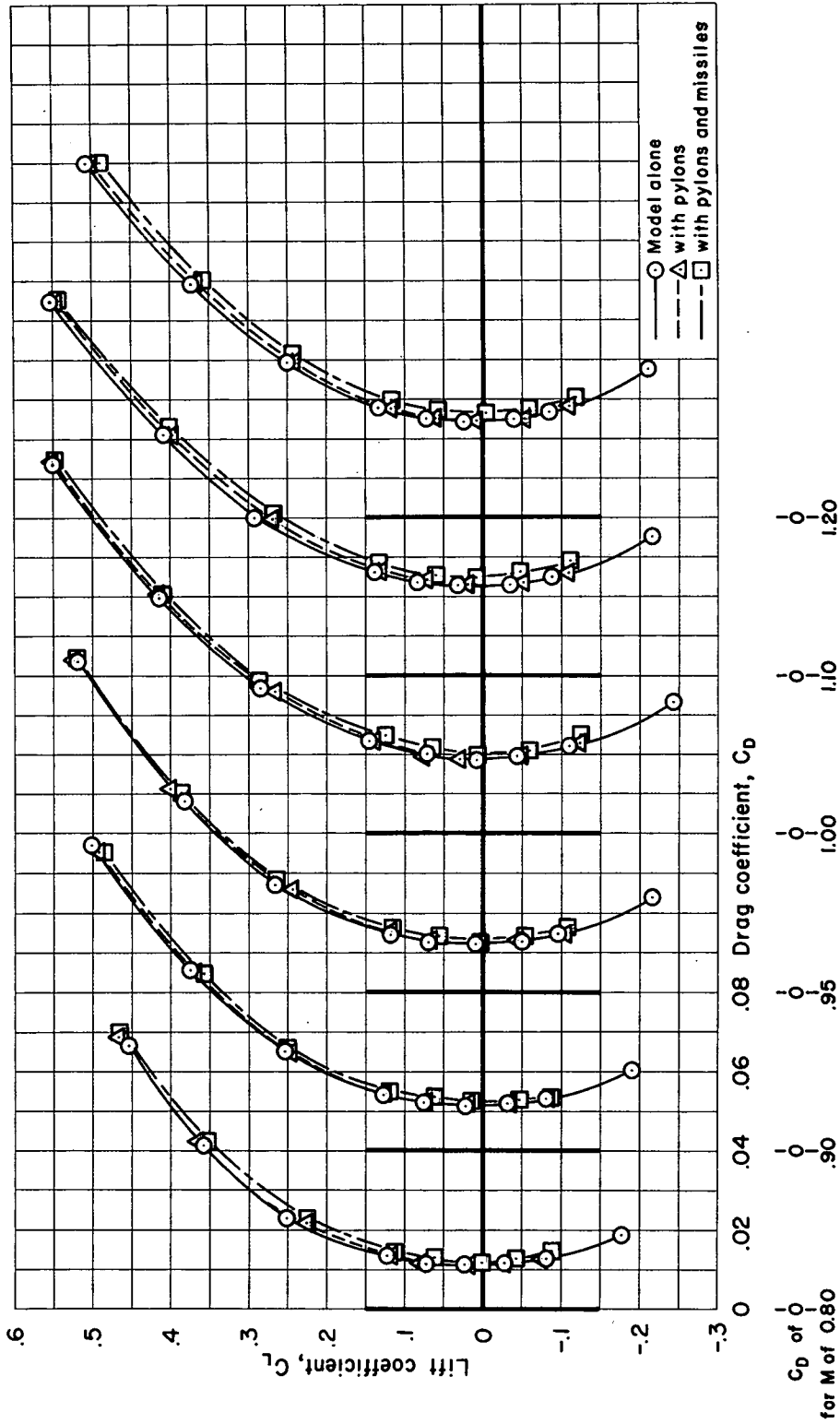


Figure 7.- The 0.07-scale model of the missile.

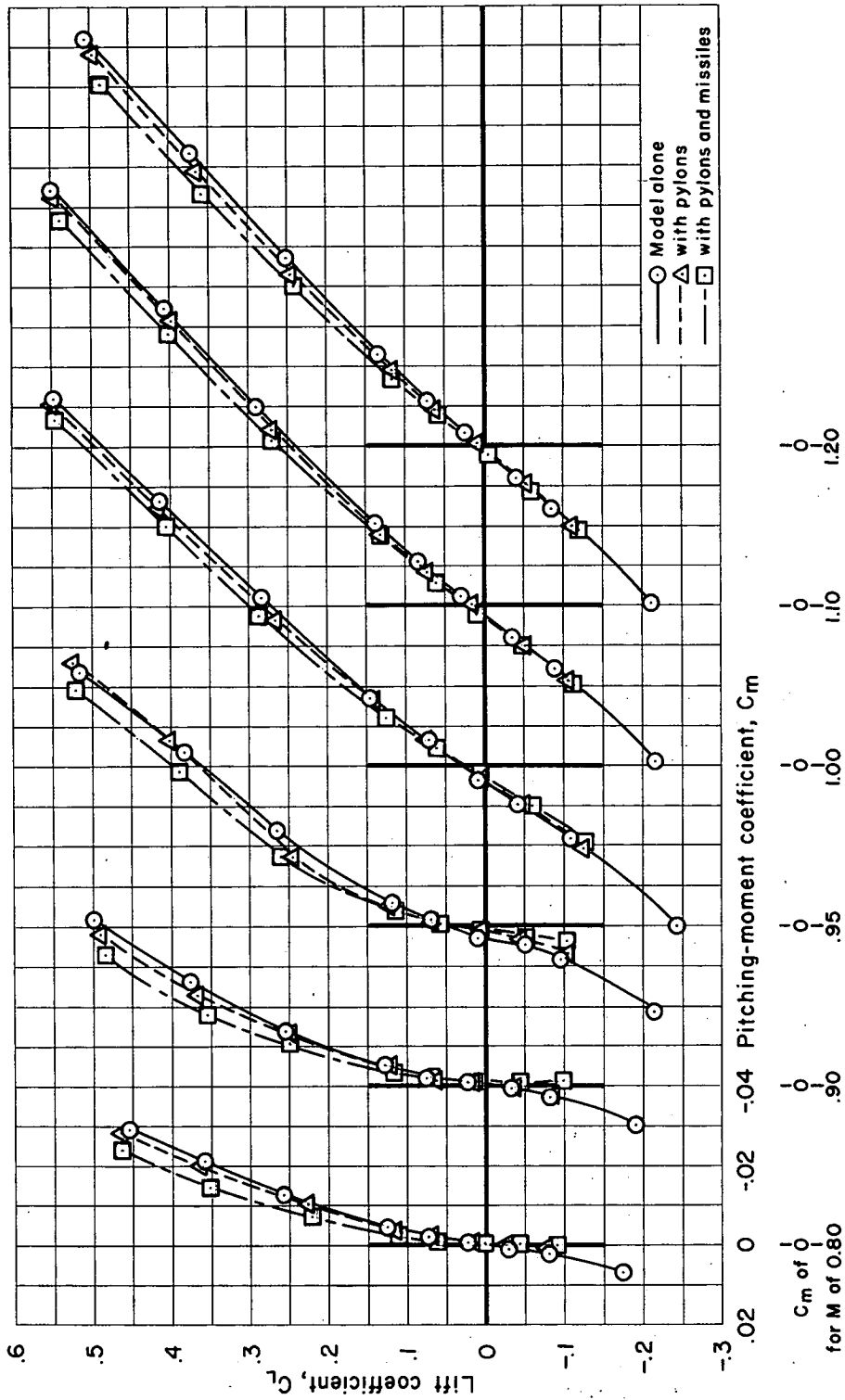


(a) Lift characteristics.

Figure 8.- The effect of the symmetrical pylons and missiles on the aerodynamic characteristics of the airplane model.

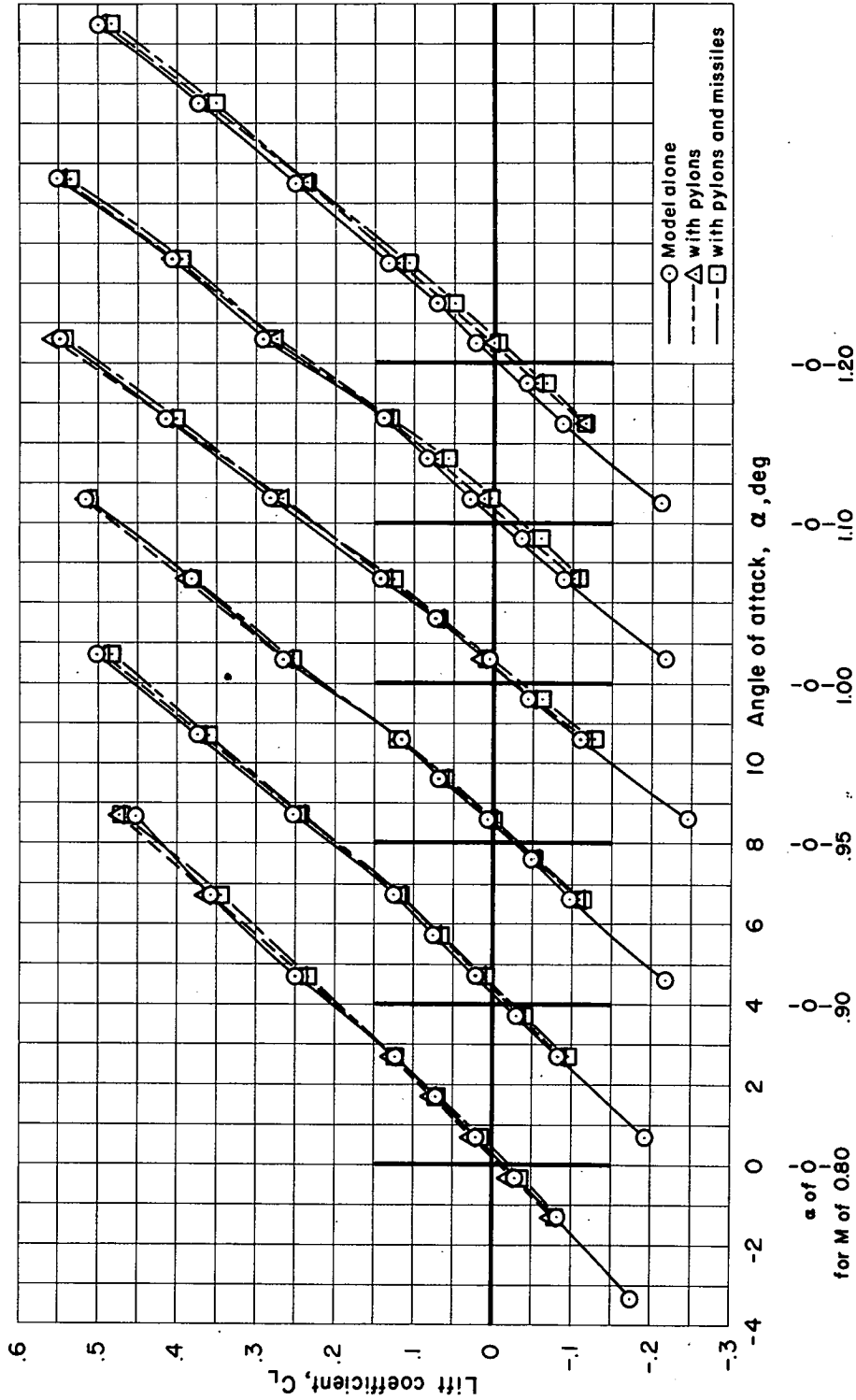


(b) Drag characteristics.
Figure 8.- Continued.

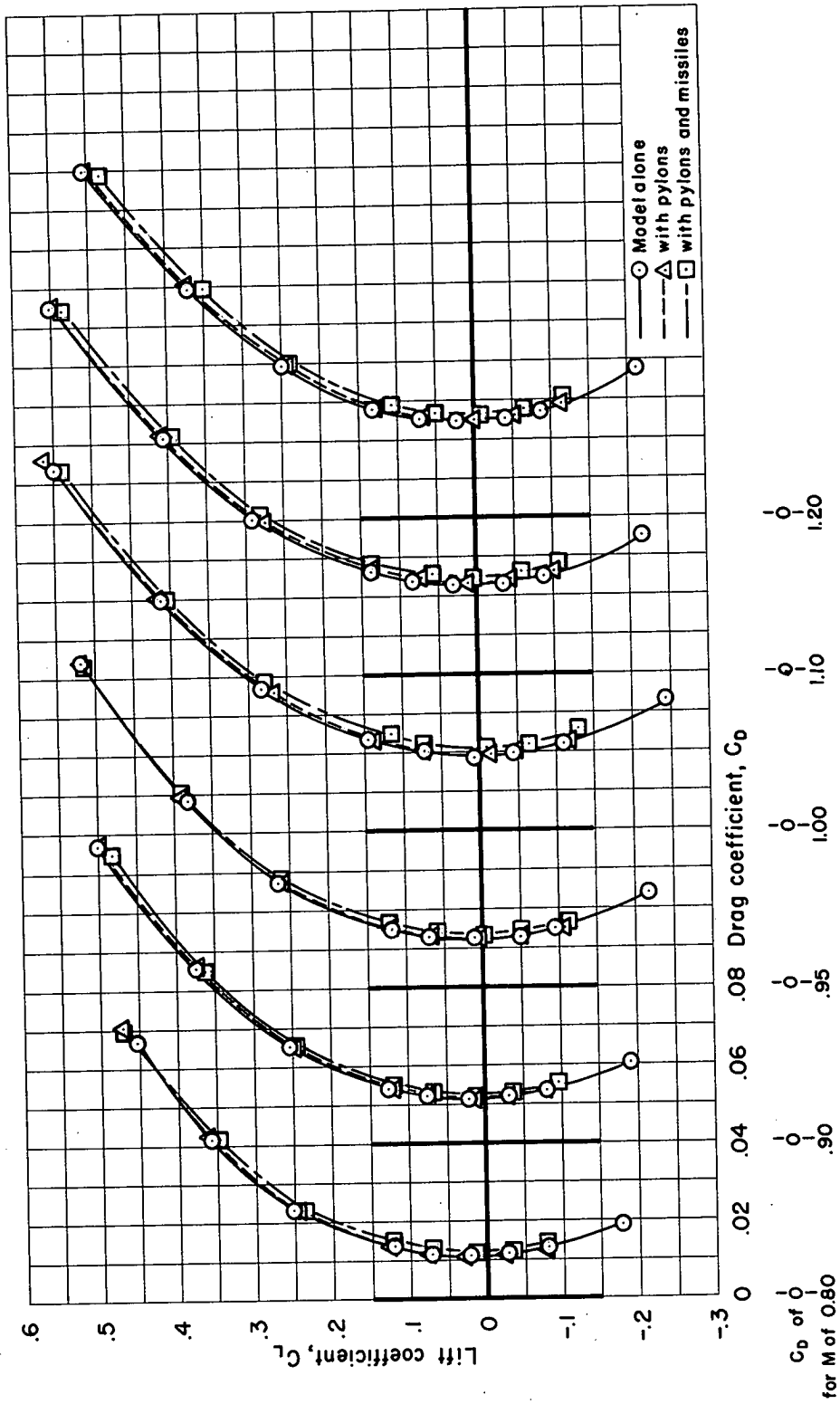


(c) Pitching-moment characteristics.

Figure 8.- Concluded.

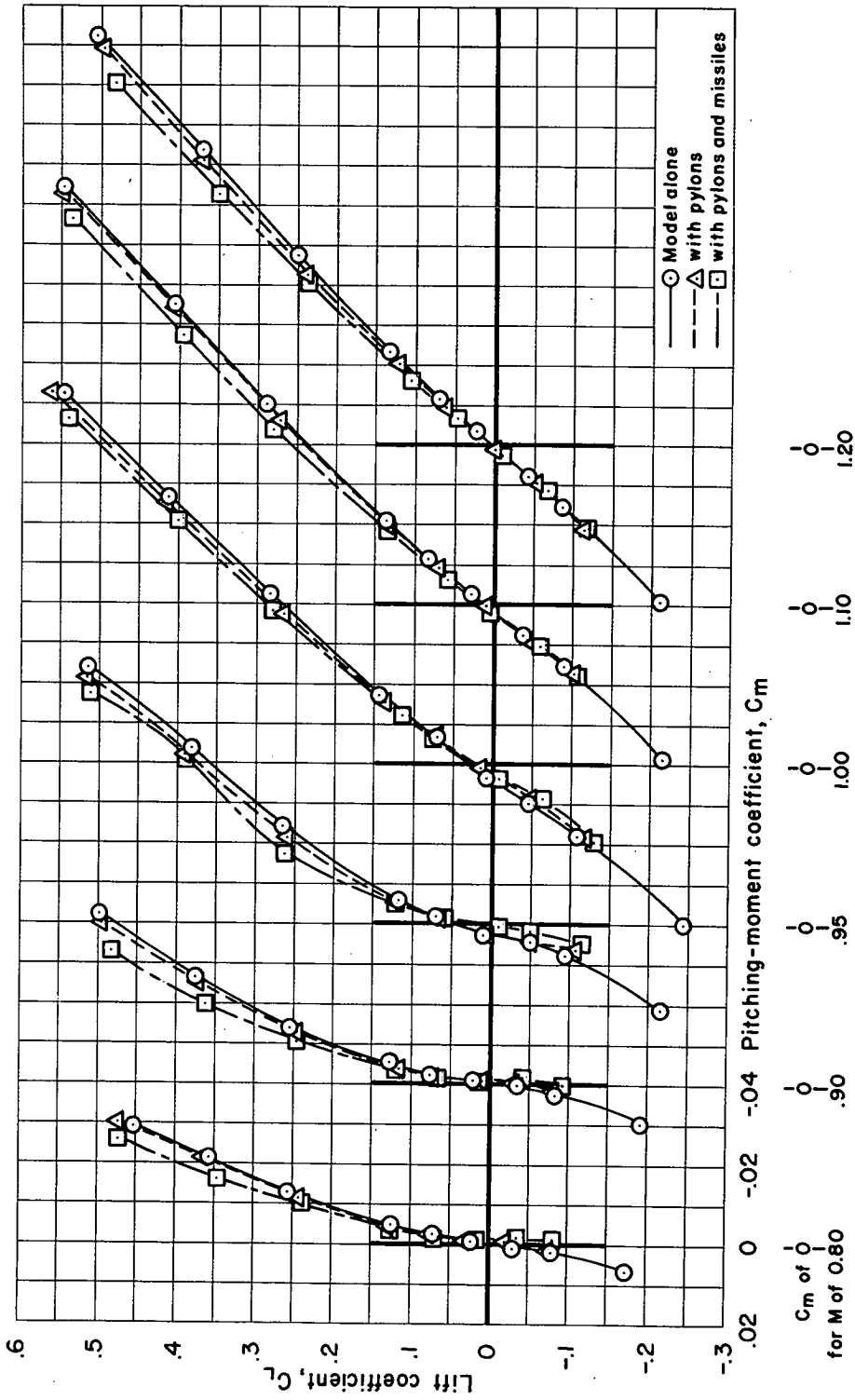


(a) Lift characteristics.
 Figure 9.- The effect of the canted symmetrical pylons and missiles on the aerodynamic characteristics of the airplane model.



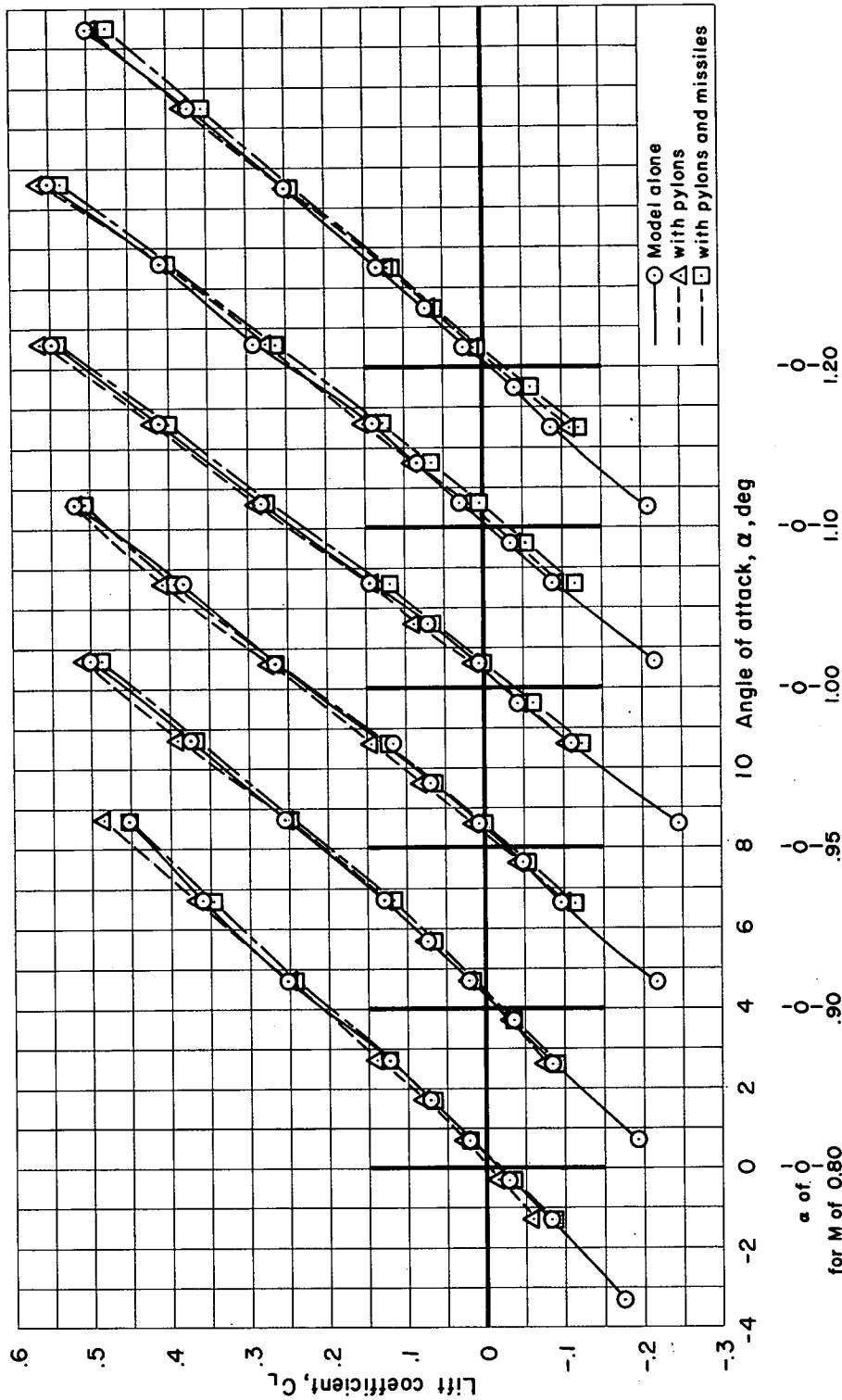
(b) Drag characteristics.

Figure 9.- Continued.



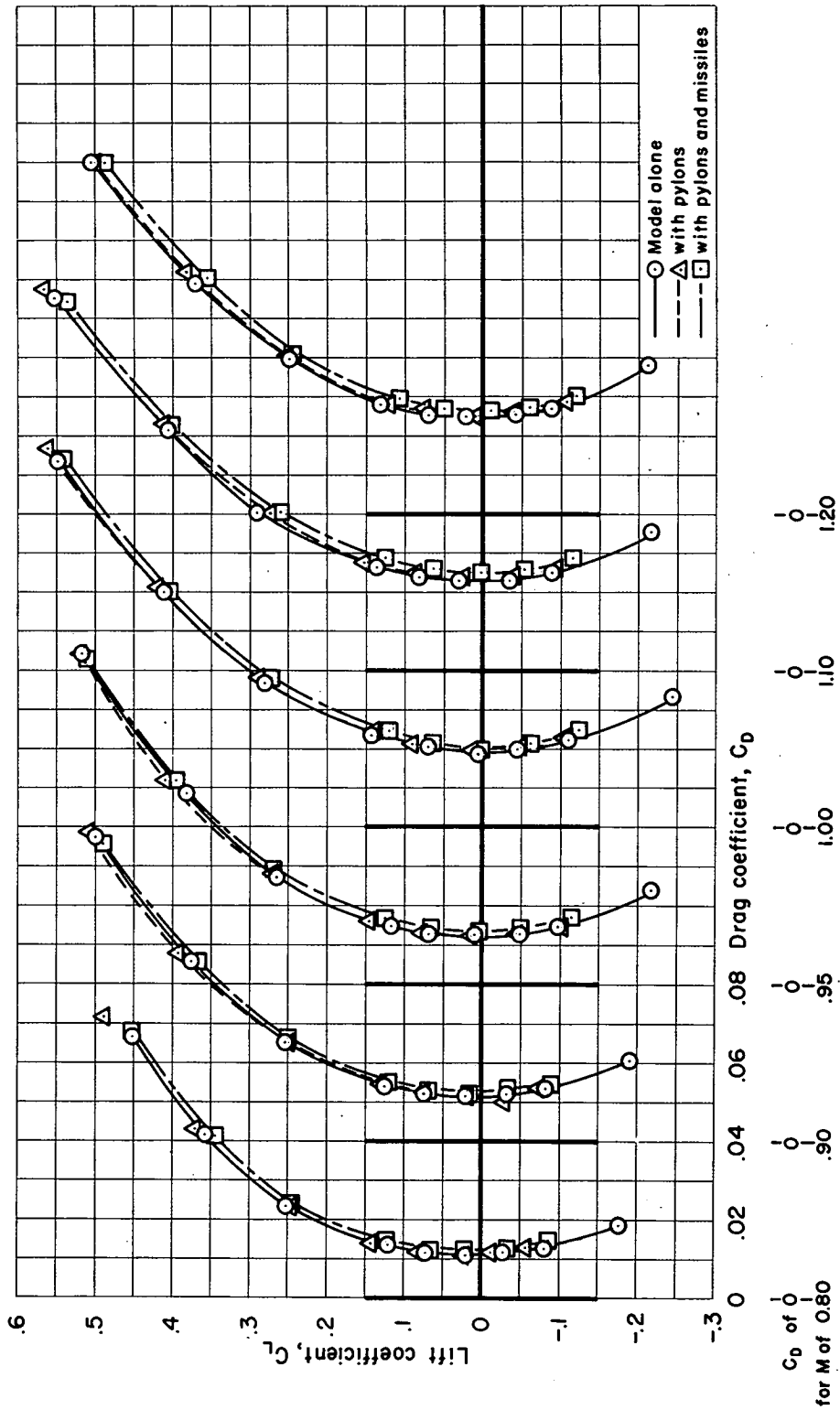
(c) Pitching-moment characteristics.

Figure 9.- Concluded.



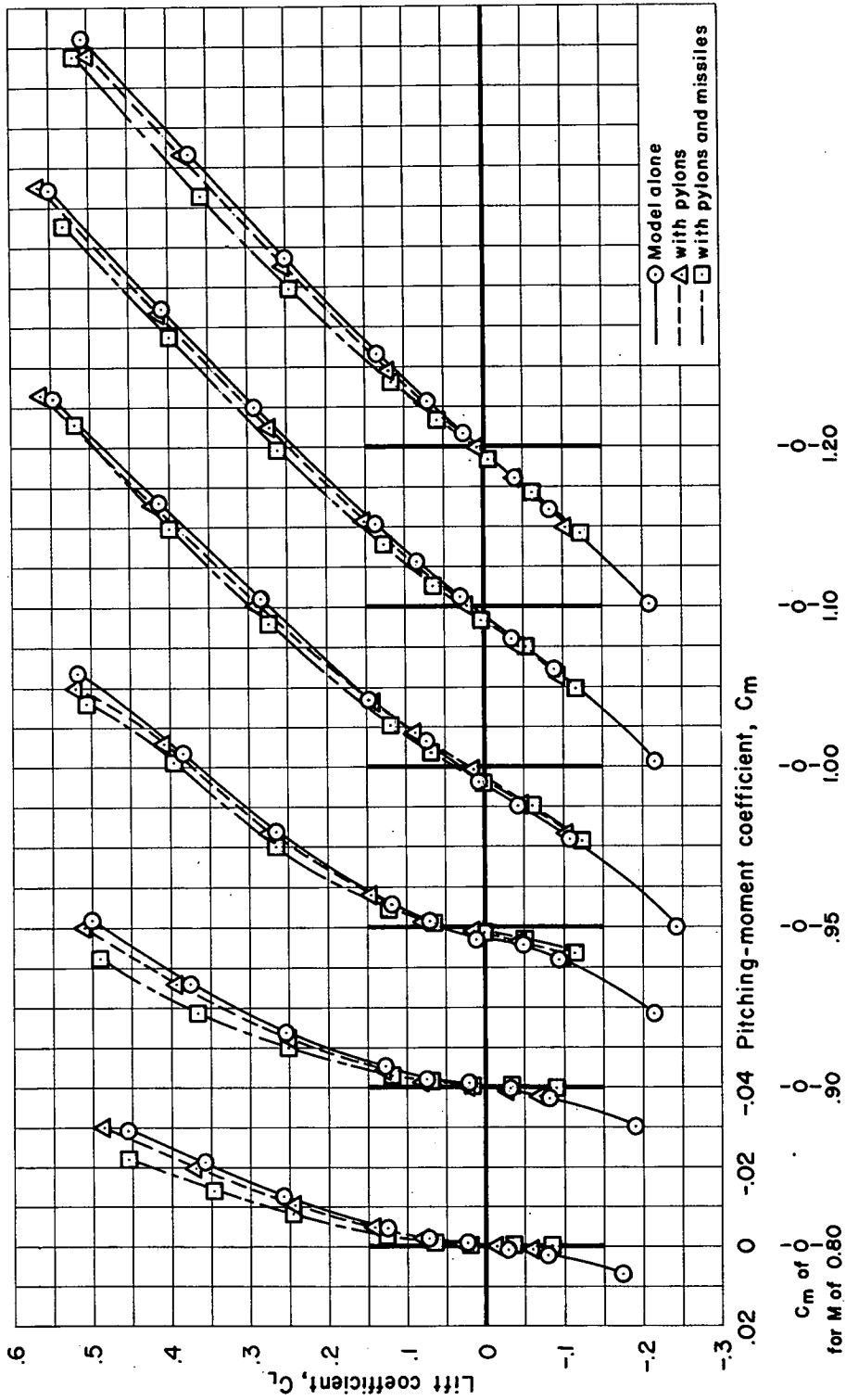
(a) Lift characteristics.

Figure 10.- The effect of the cambered pylons and missiles on the aerodynamic characteristics of the airplane model.



(b) Drag characteristics.

Figure 10.- Continued.



(c) Pitching-moment characteristics.

Figure 10.- Concluded.

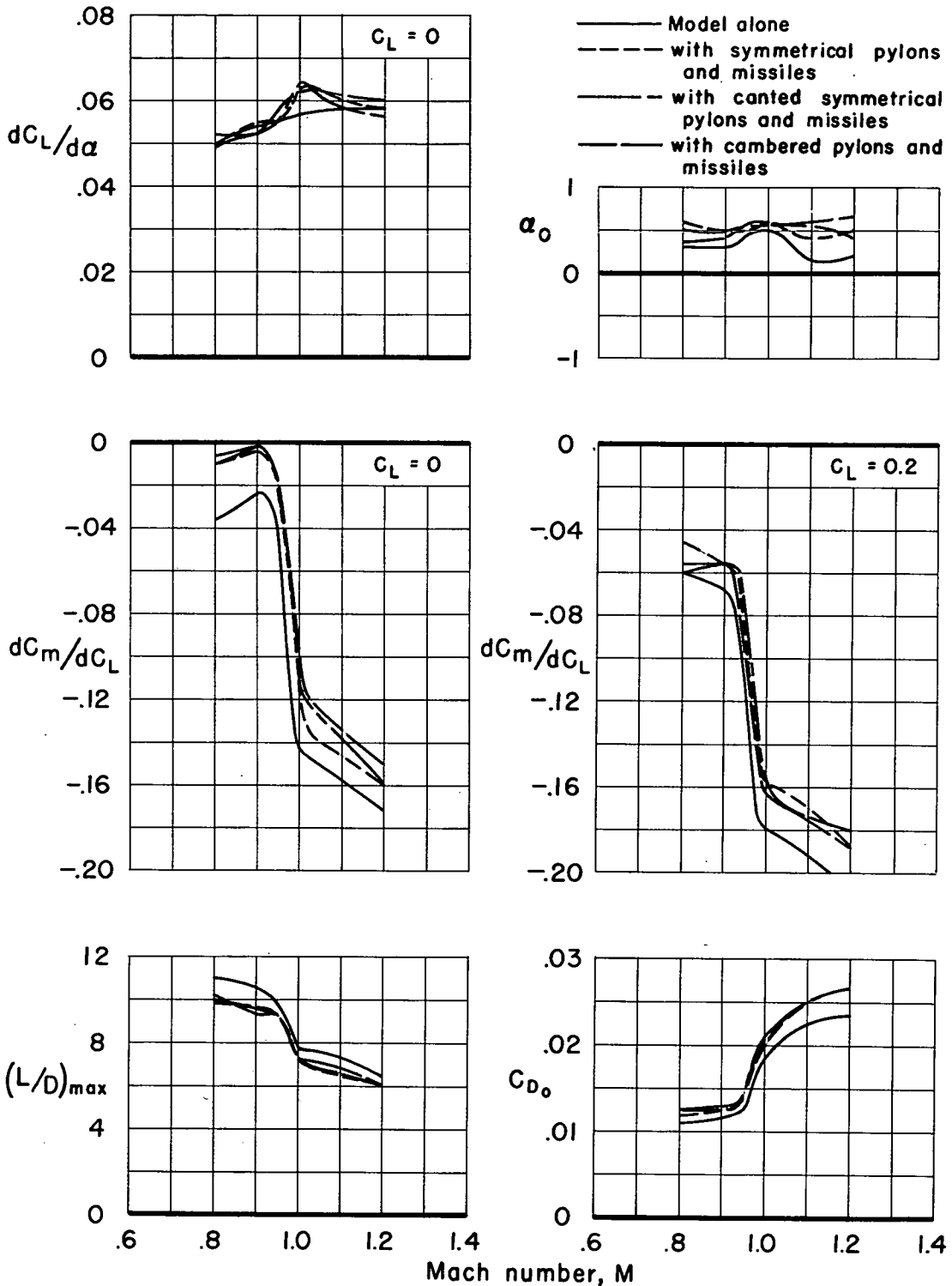
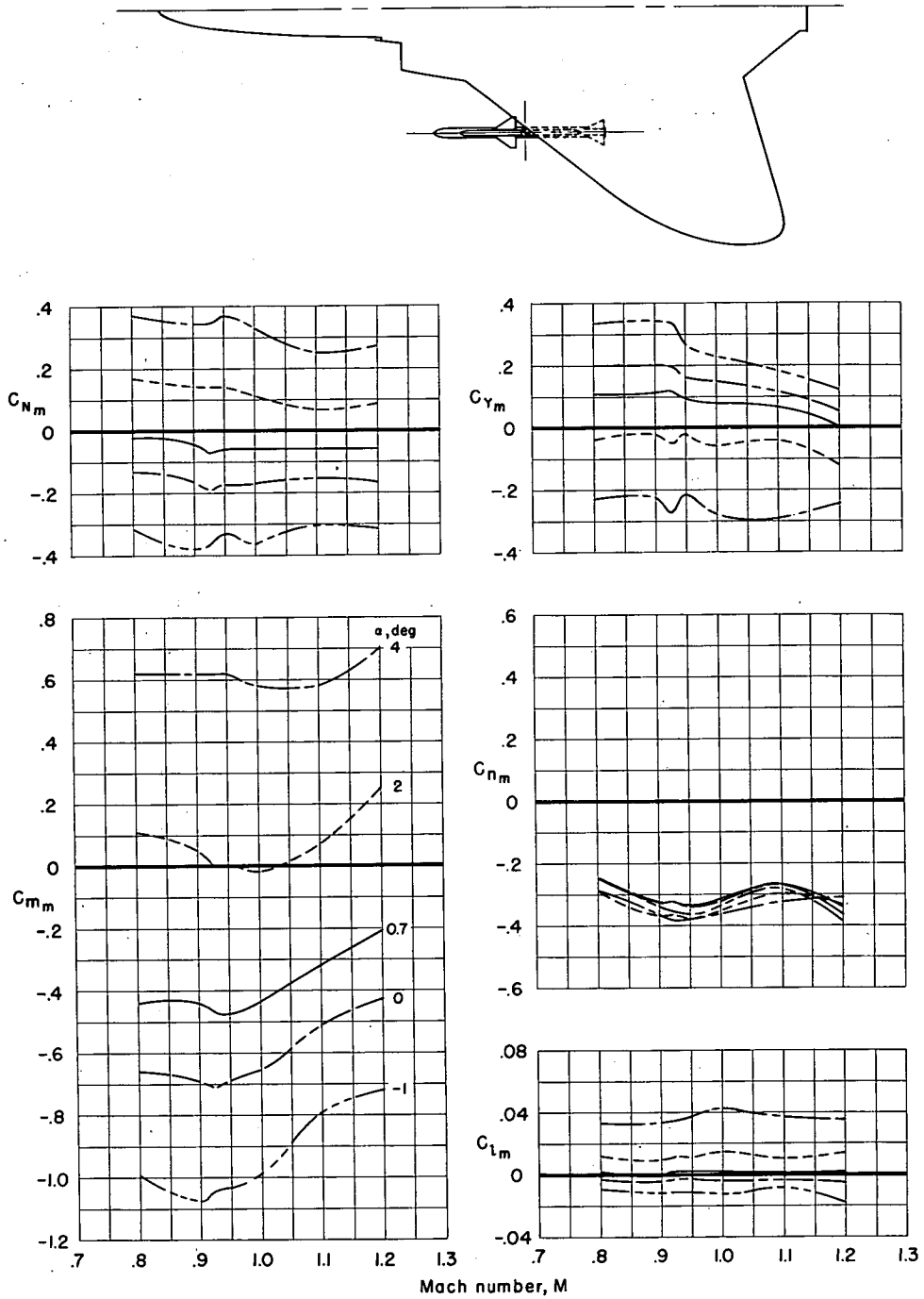
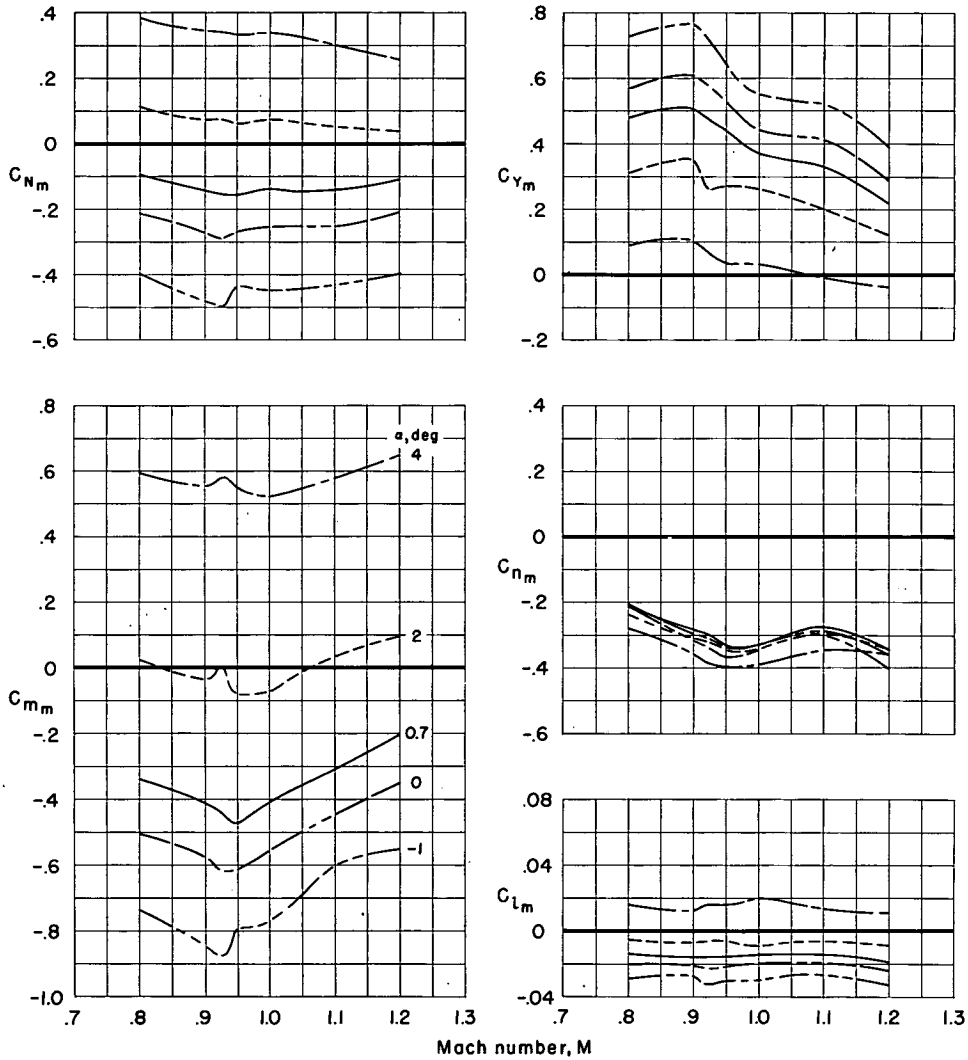
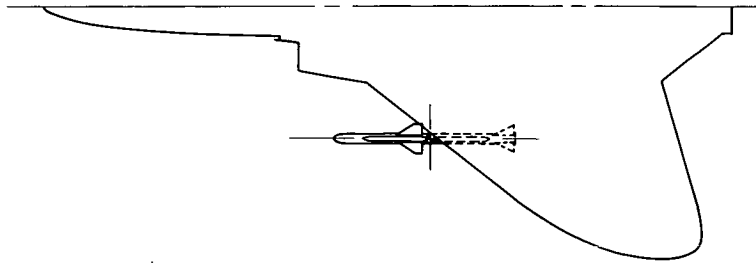


Figure 11.- Longitudinal aerodynamic parameters of the airplane model.



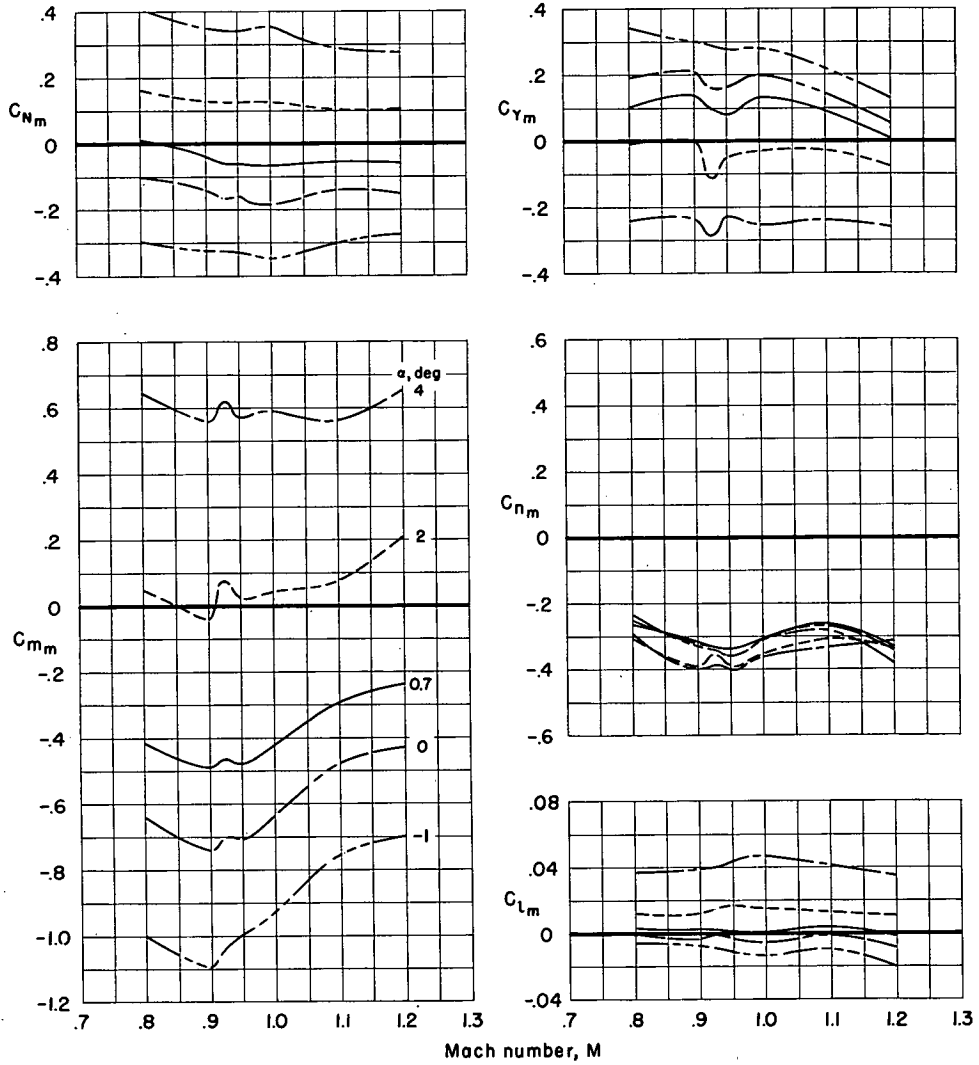
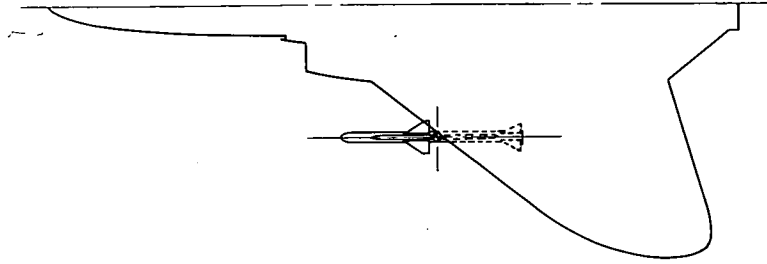
(a) Symmetrical pylons.

Figure 12.- Force and moment characteristics of the missile mounted on pylons; $x/c = 0$.



(b) Canted symmetrical pylons.

Figure 12.- Continued.



(c) Cambered pylons.

Figure 12.- Concluded.

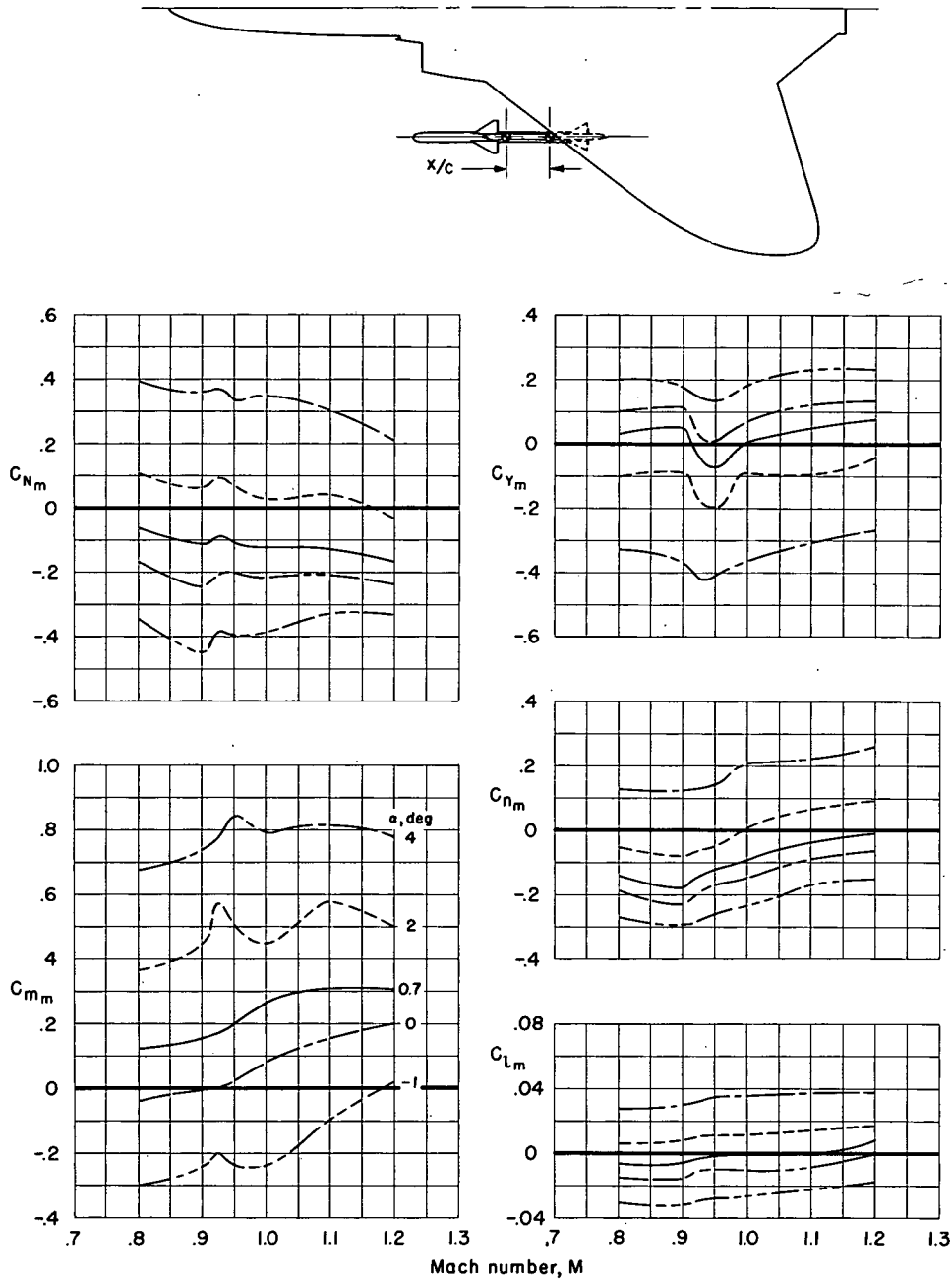
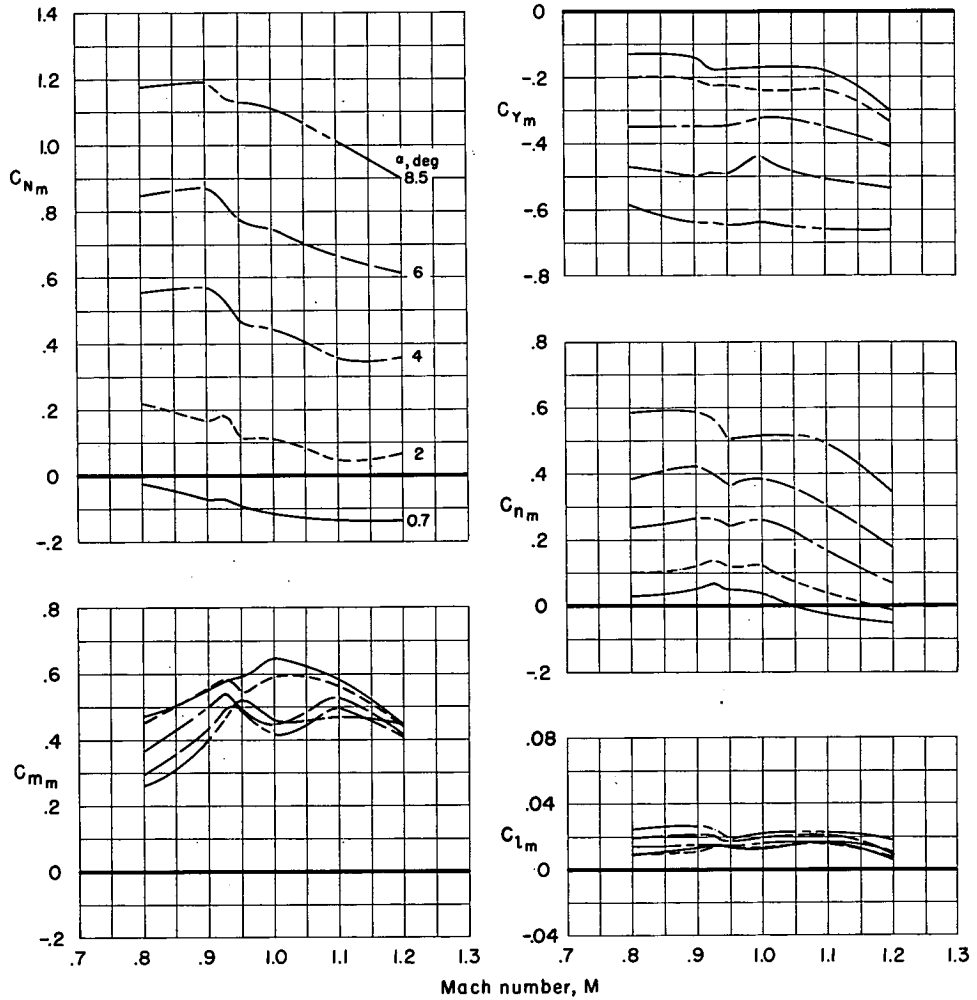
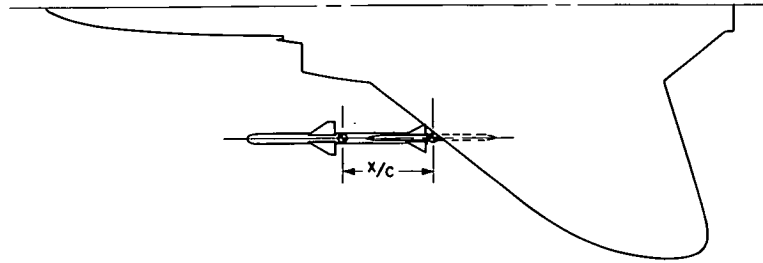
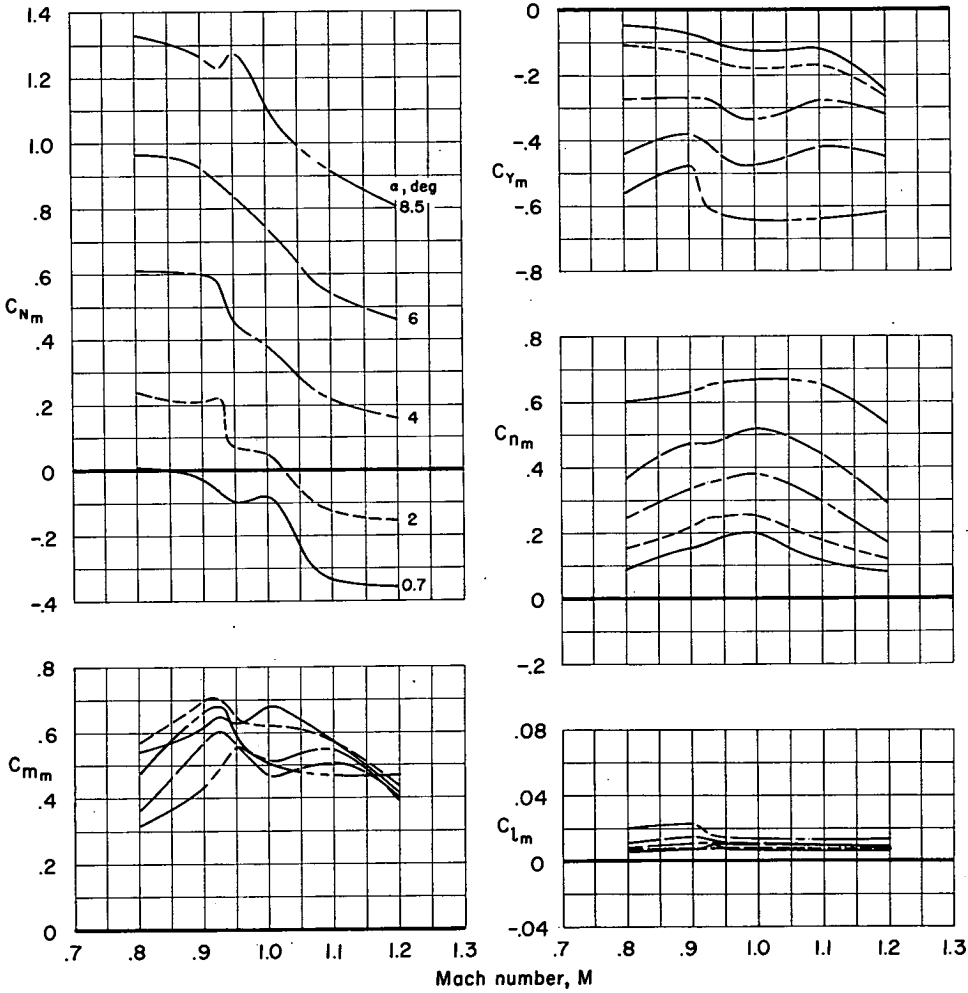
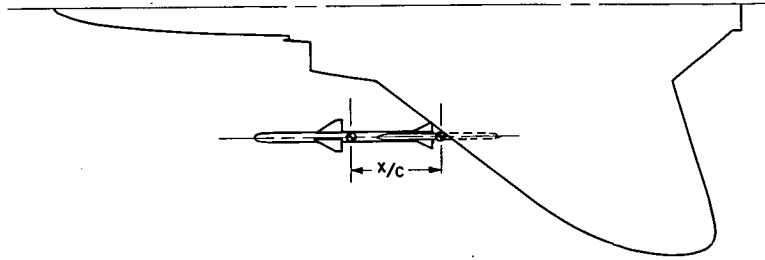


Figure 13.- Force and moment characteristics of the missile in launch position $x/c = 0.185$; $\theta = \psi = \phi = 0^\circ$.



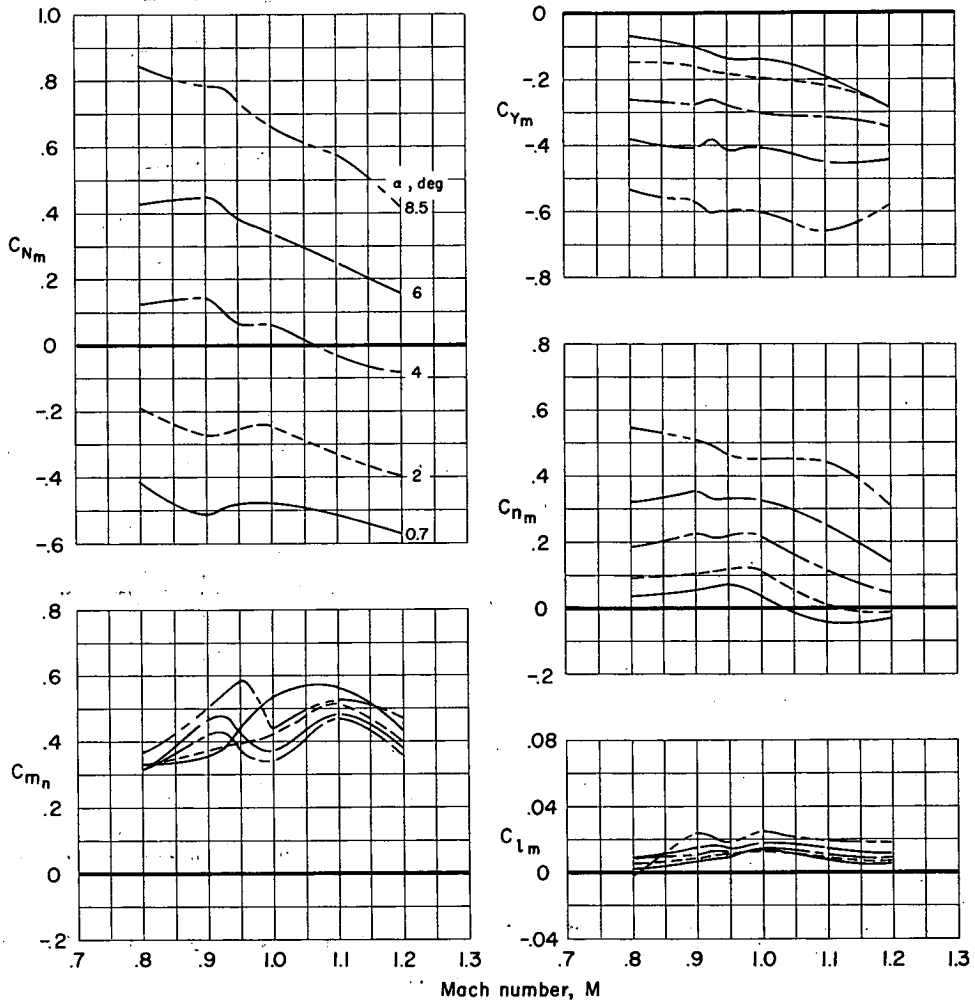
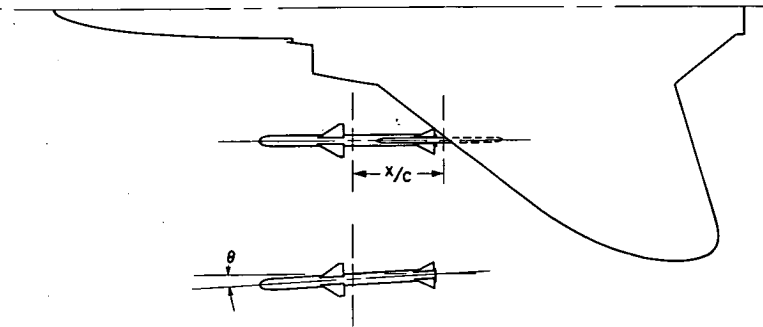
(a) $\theta = \psi = \phi = 0^\circ$.

Figure 14.- Force and moment characteristics of the missile in launch position $x/c = 0.369$.



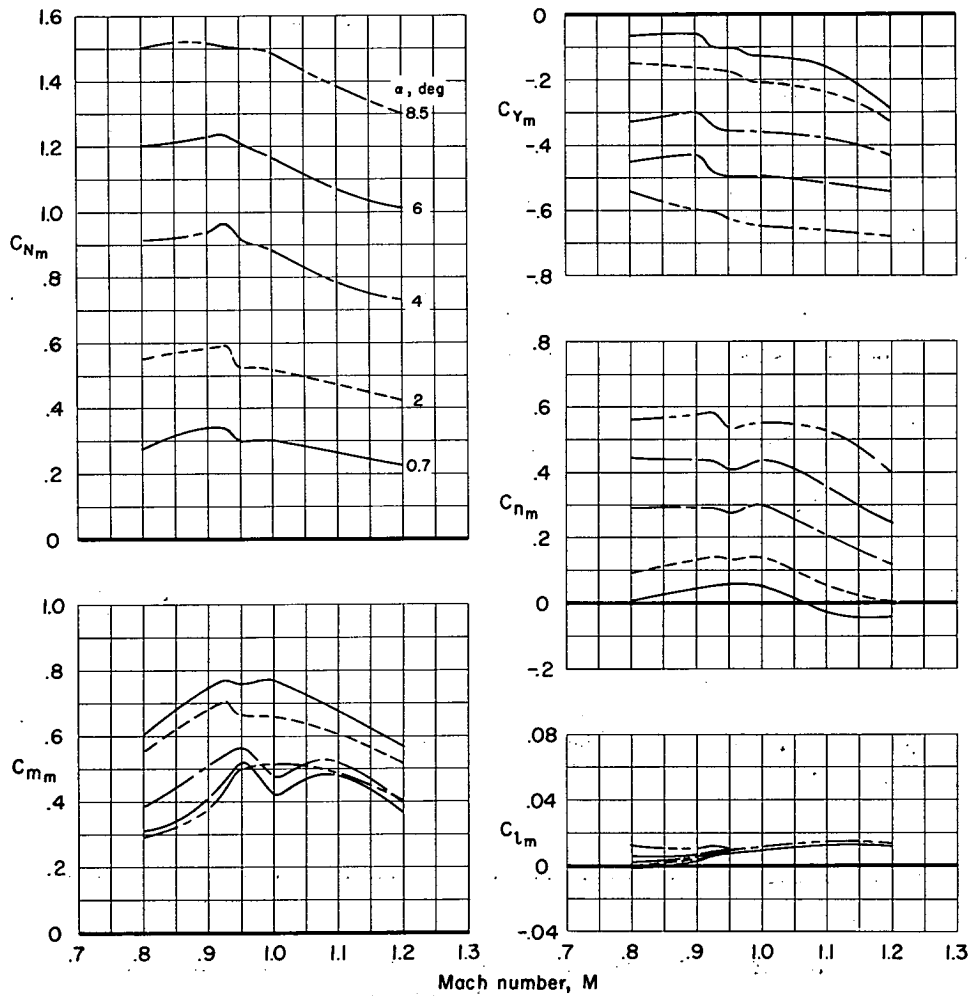
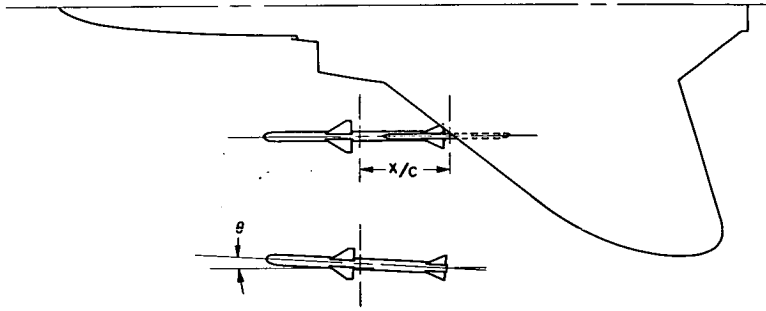
(b) $\phi = 15^\circ$; $\theta = \psi = 0^\circ$.

Figure 14.- Continued.



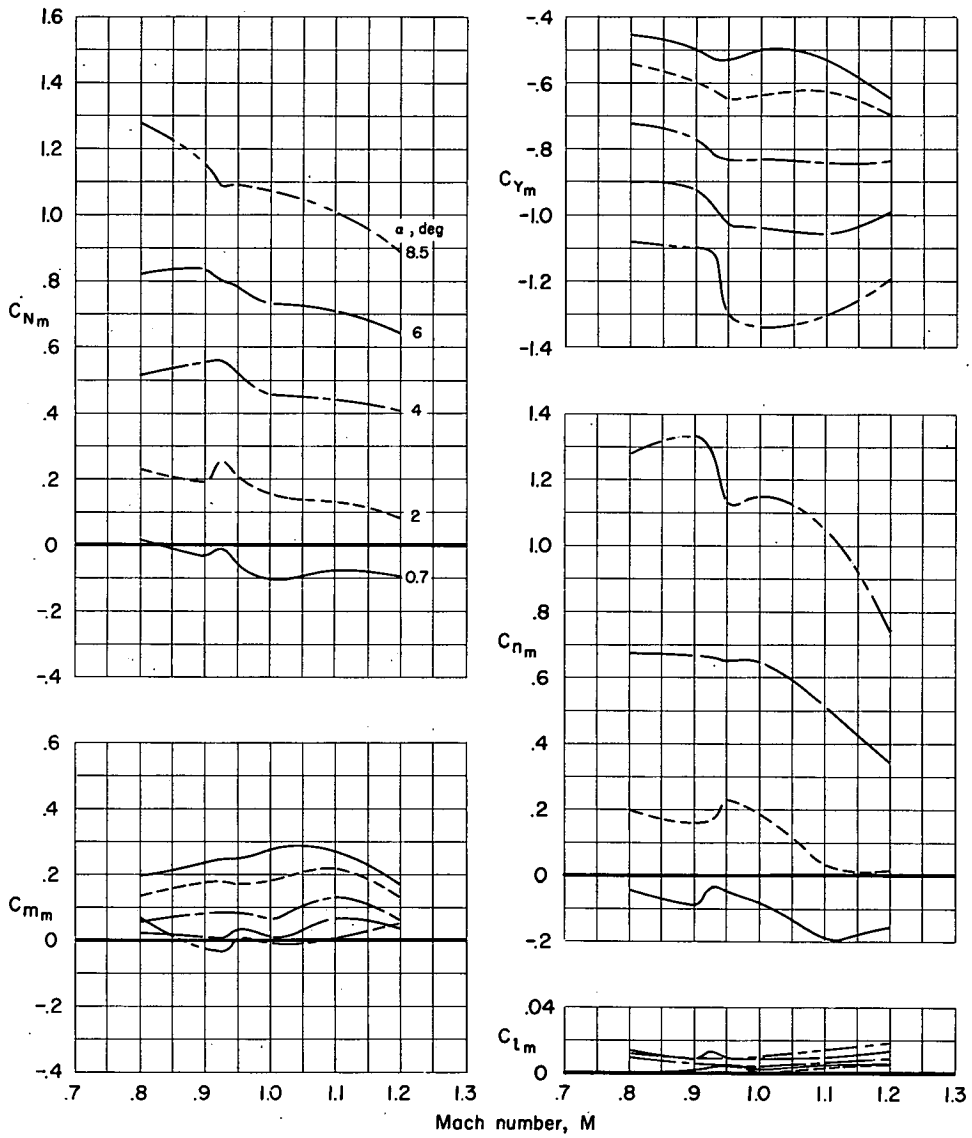
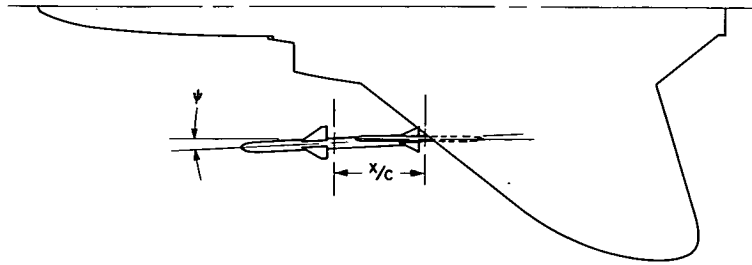
(c) $\theta = 3^\circ$; $\psi = \phi = 0^\circ$.

Figure 14.- Continued.



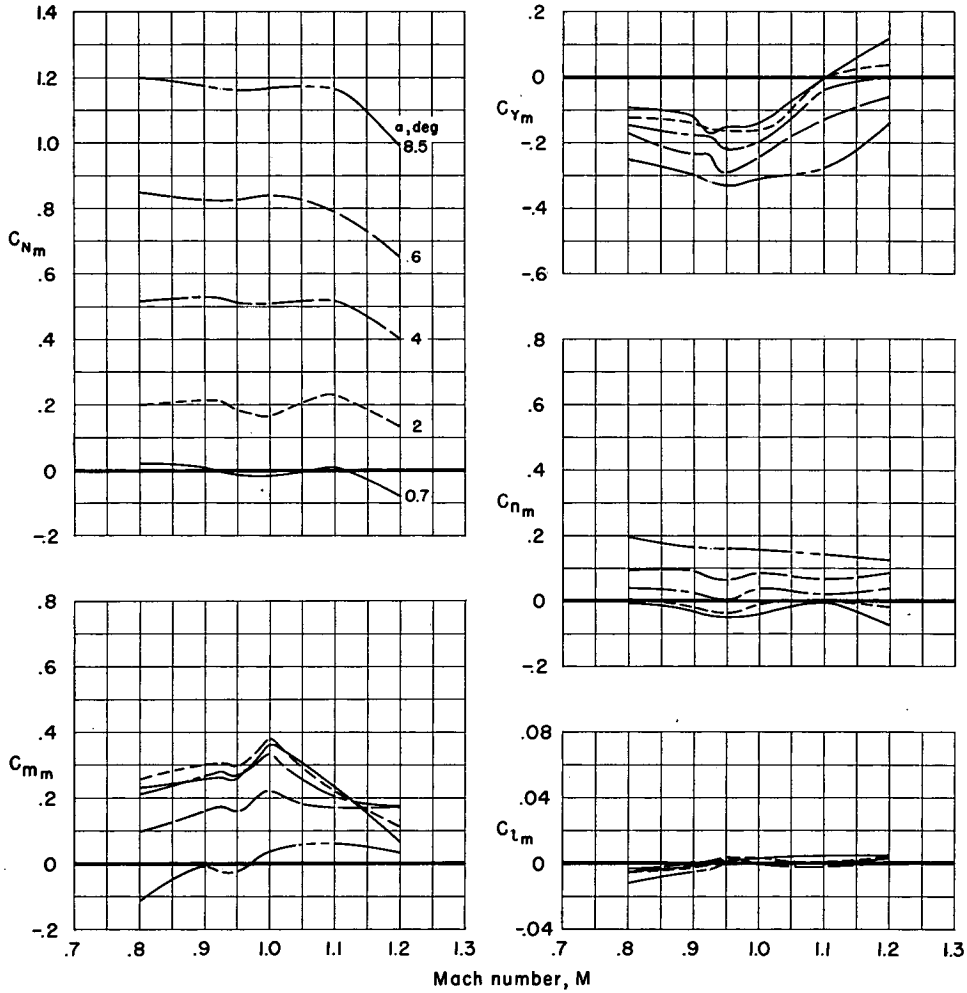
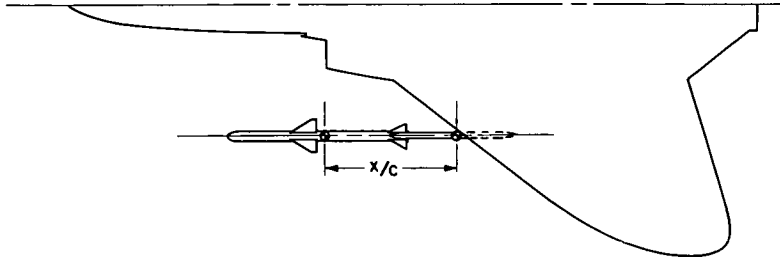
(d) $\theta = -3^\circ$; $\psi = \phi = 0^\circ$.

Figure 14.- Continued.



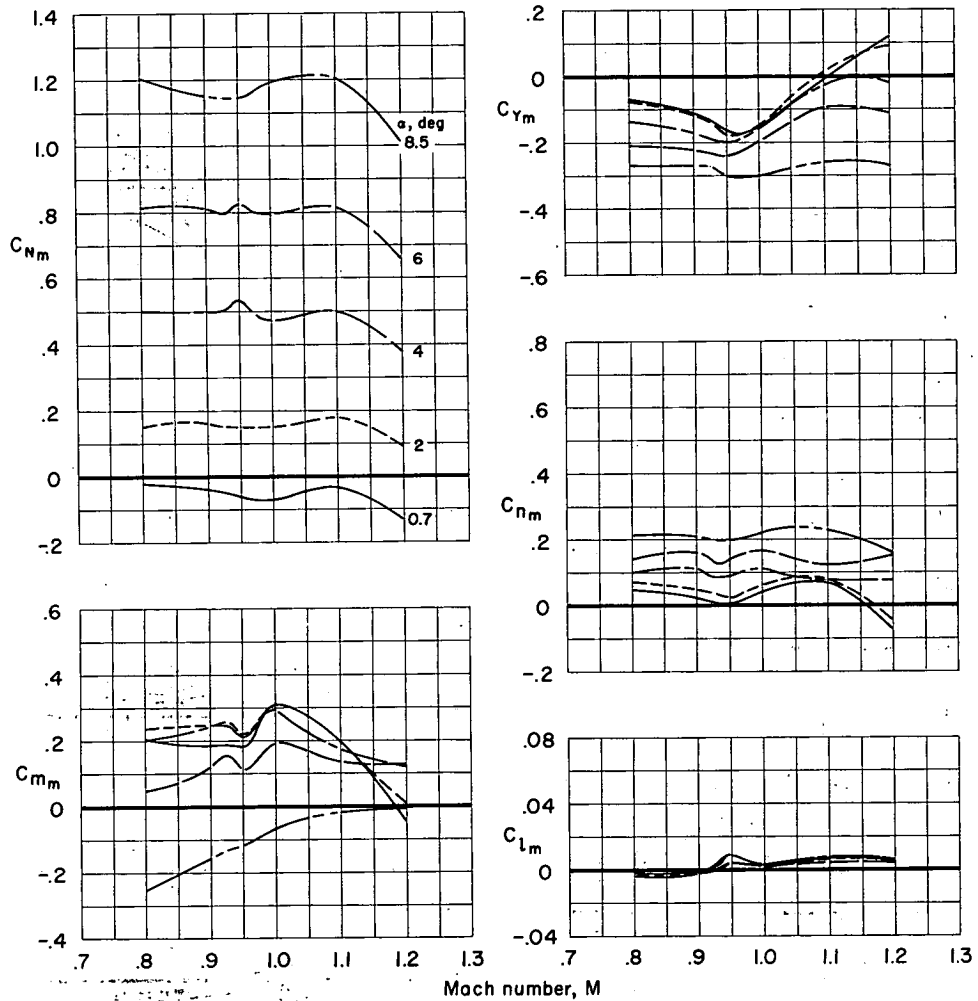
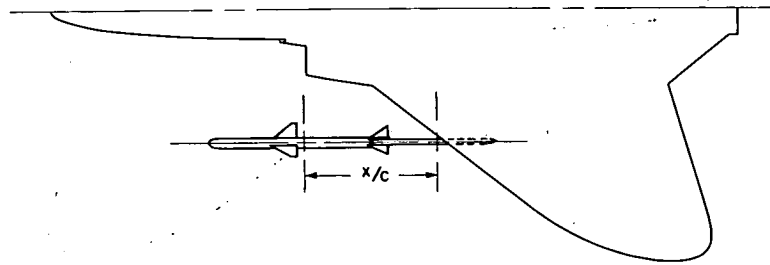
(e) $\psi = -3^\circ$; $\theta = \phi = 0^\circ$.

Figure 14.- Concluded.



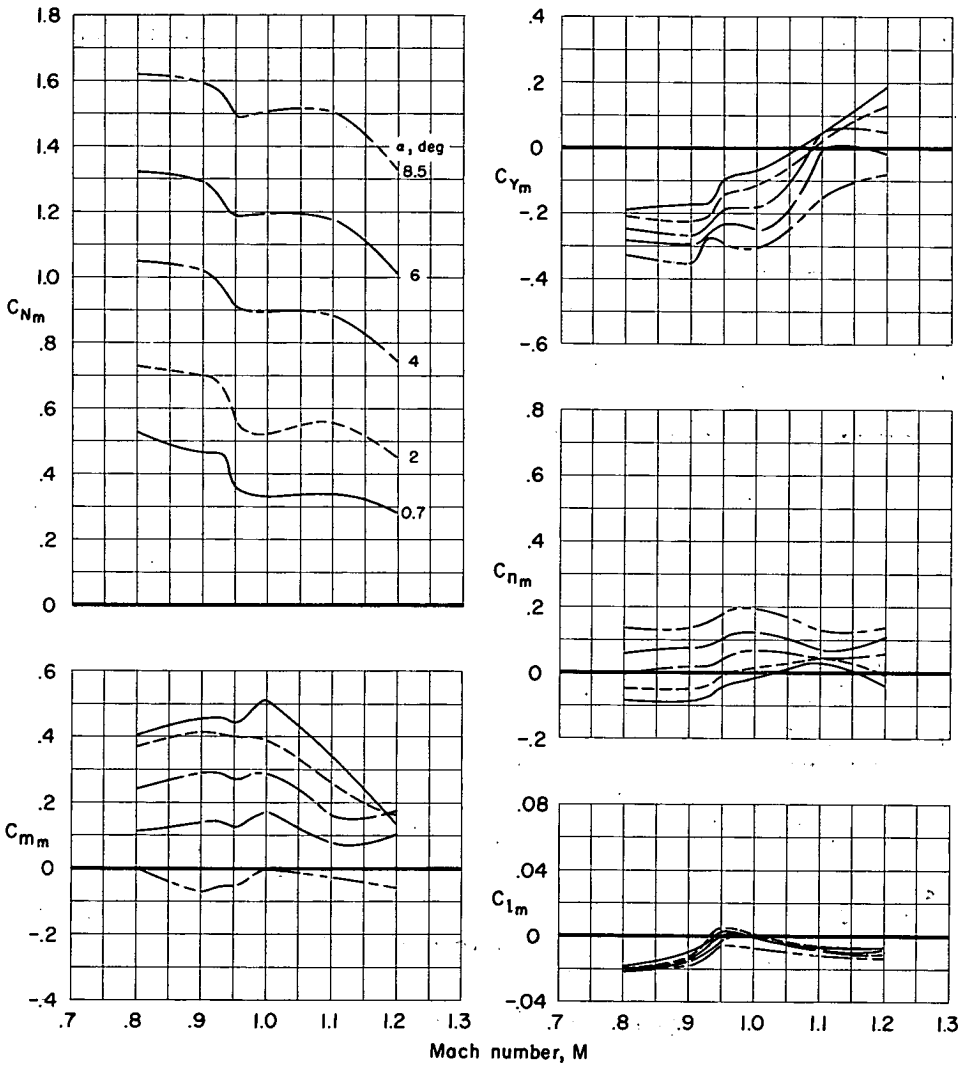
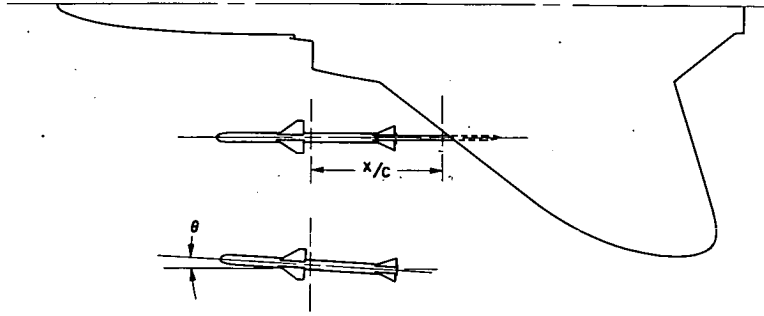
(a) $\theta = \psi = \phi = 0^\circ$.

Figure 15.- Force and moment characteristics of the missile in launch position $x/c = 0.554$.



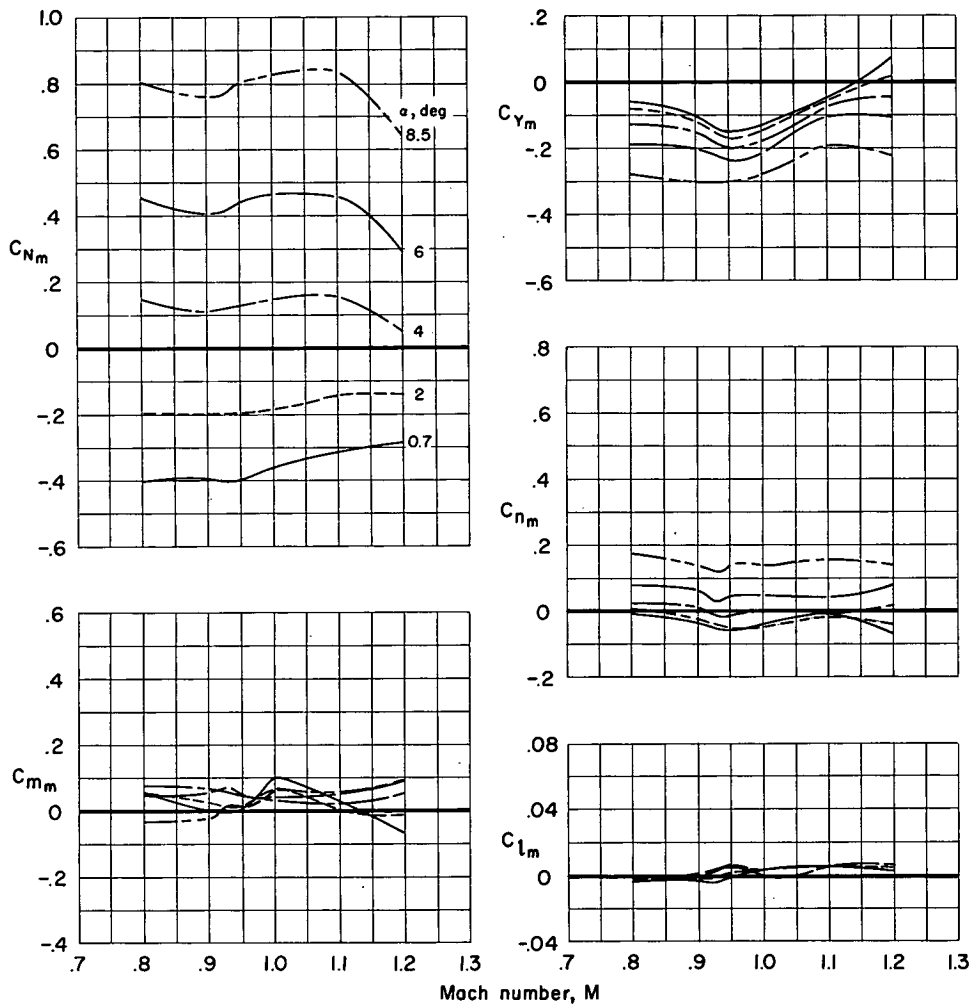
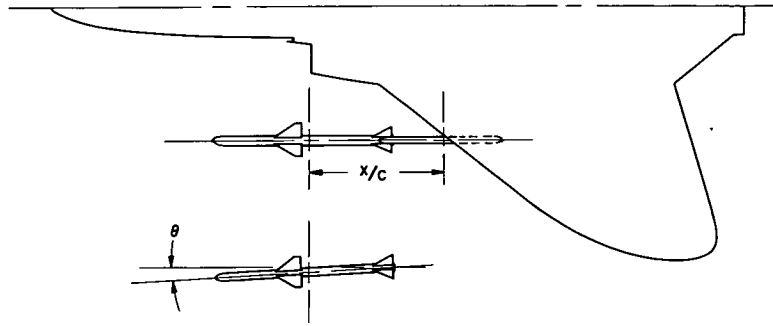
(b) $\phi = 15^\circ$; $\theta = \psi = 0^\circ$.

Figure 15.- Continued.



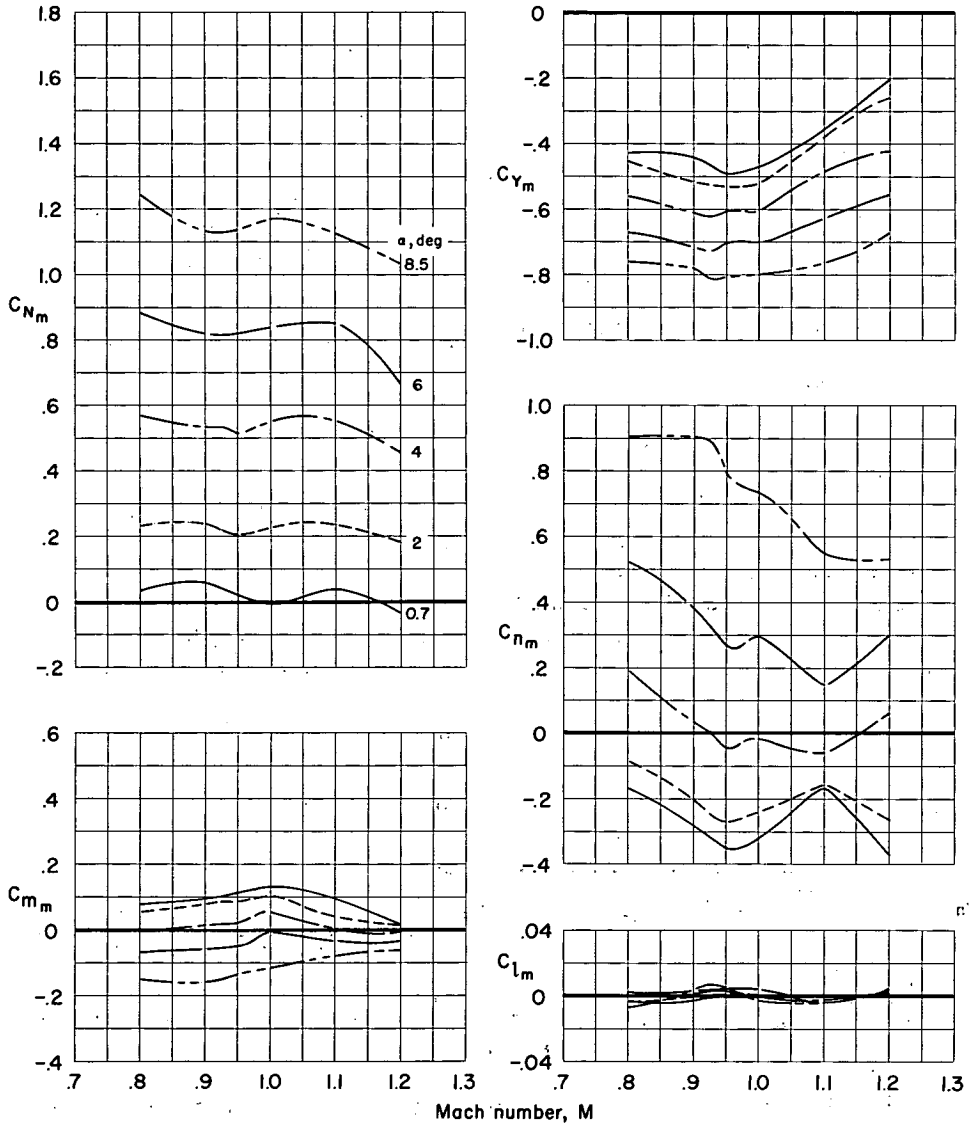
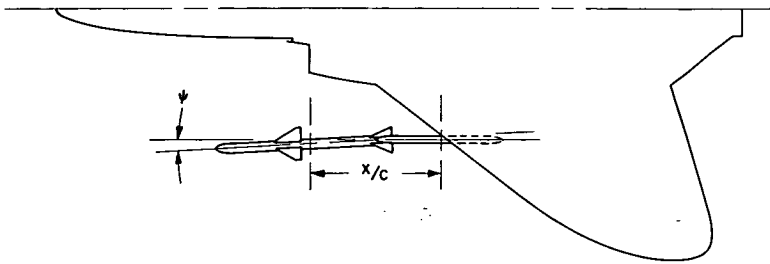
(c) $\theta = 3^\circ$; $\psi = \phi = 0^\circ$.

Figure 15.- Continued.



(d) $\theta = -3^\circ$; $\psi = \phi = 0^\circ$.

Figure 15.- Continued.



(e) $\psi = -3^\circ$; $\theta = \phi = 0^\circ$.

Figure 15.- Concluded.

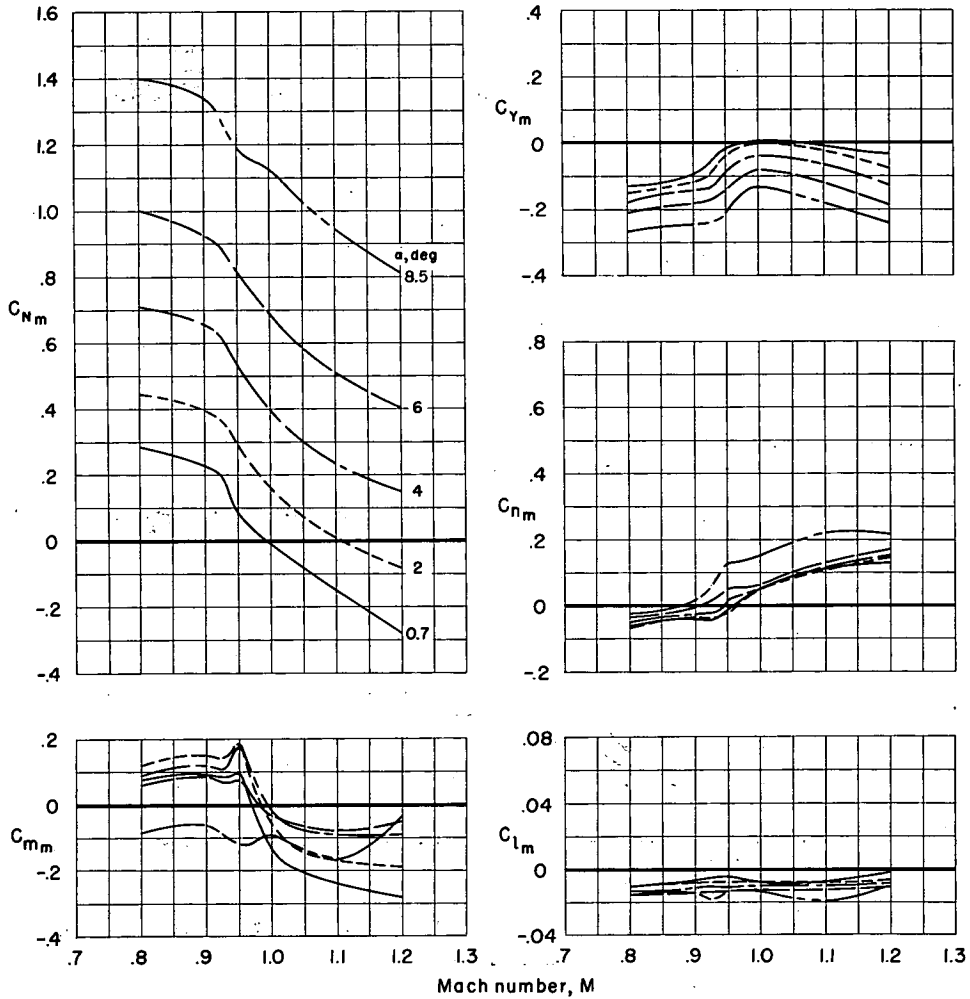
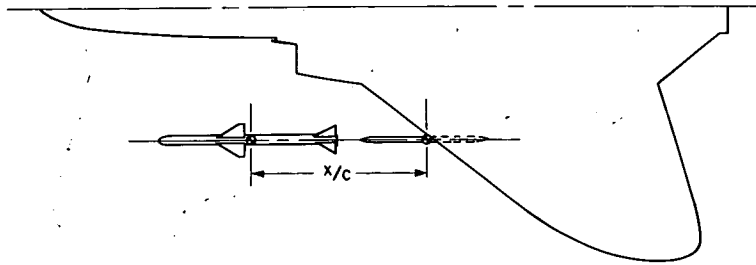
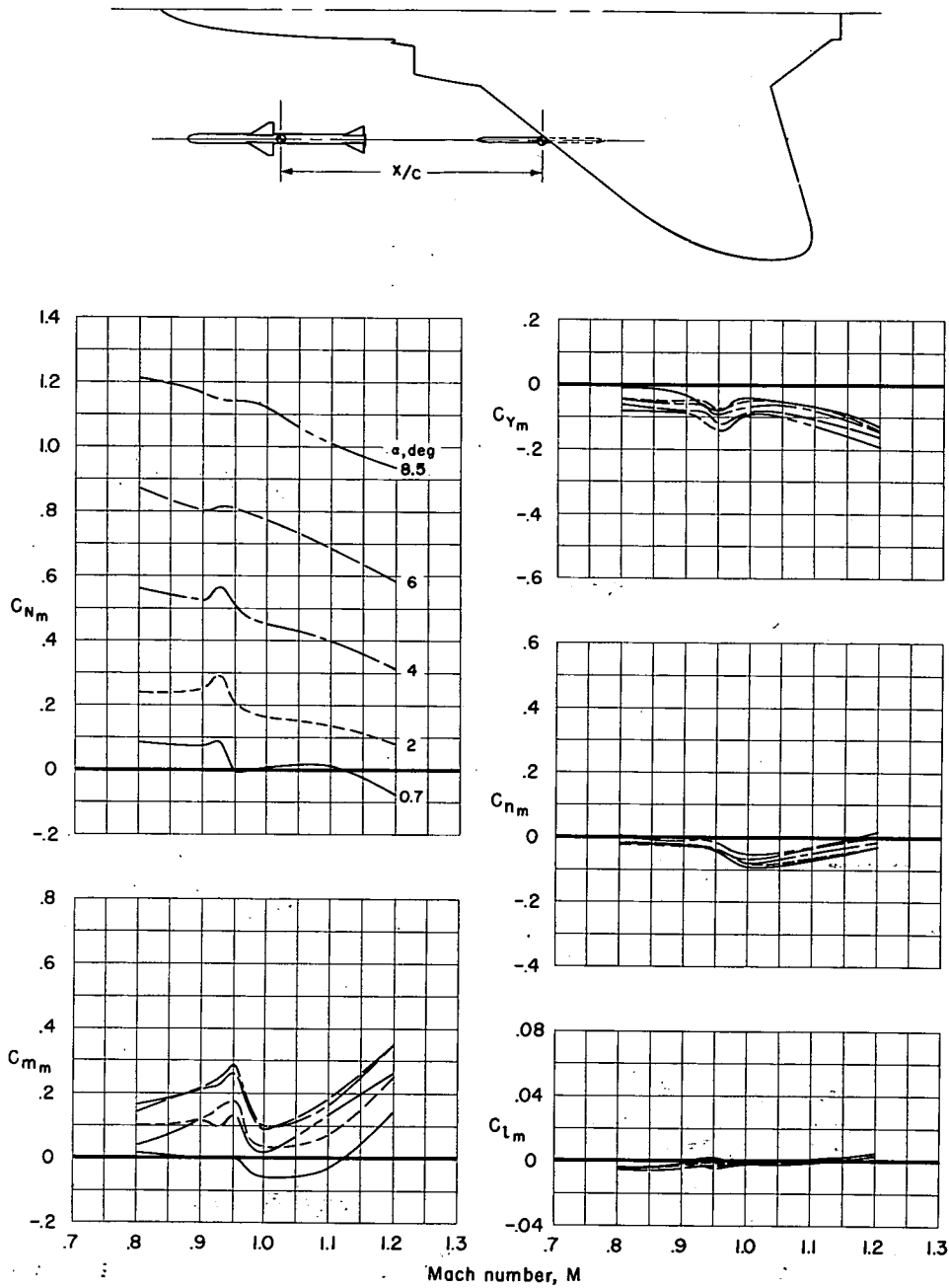
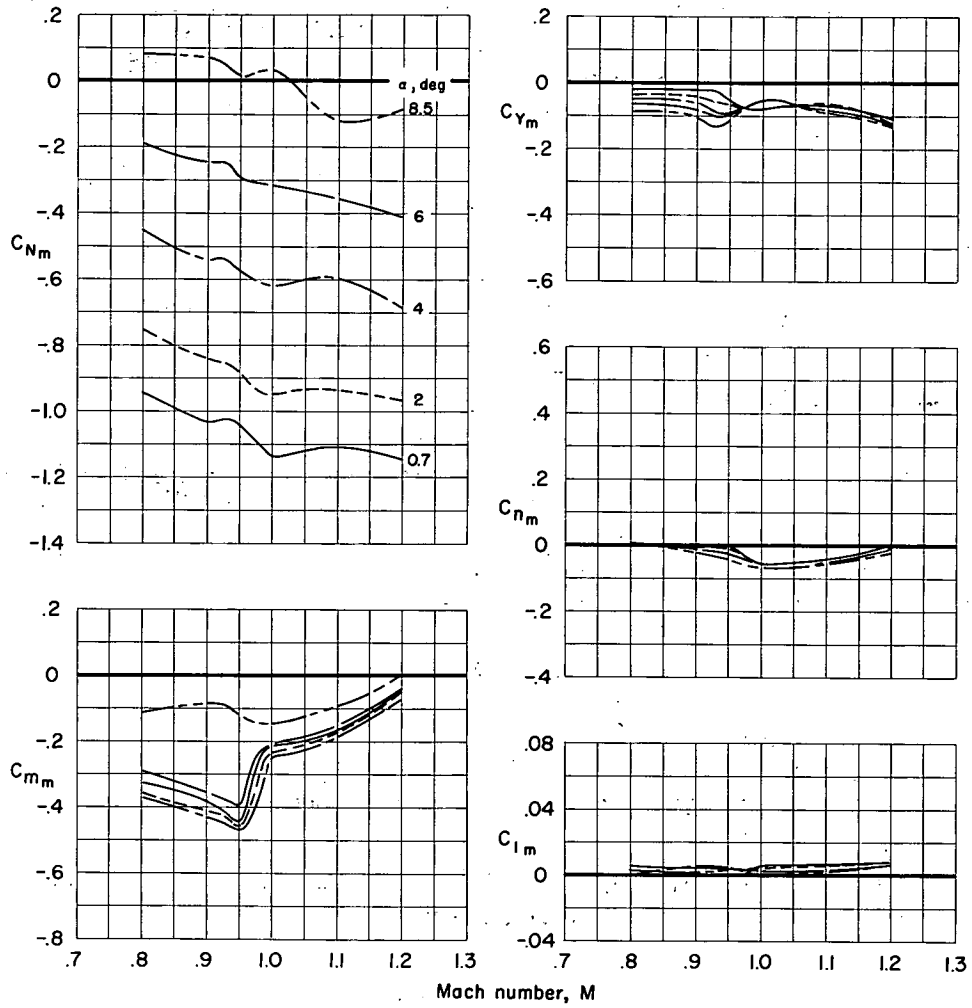
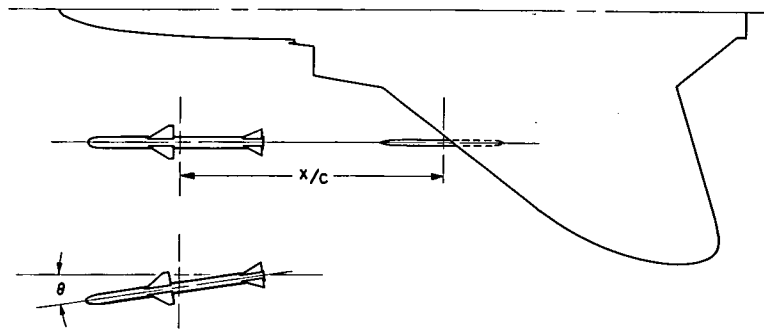


Figure 16.- Force and moment characteristics of the missile in launch position $x/c = 0.738$; $\theta = \psi = \phi = 0^\circ$.



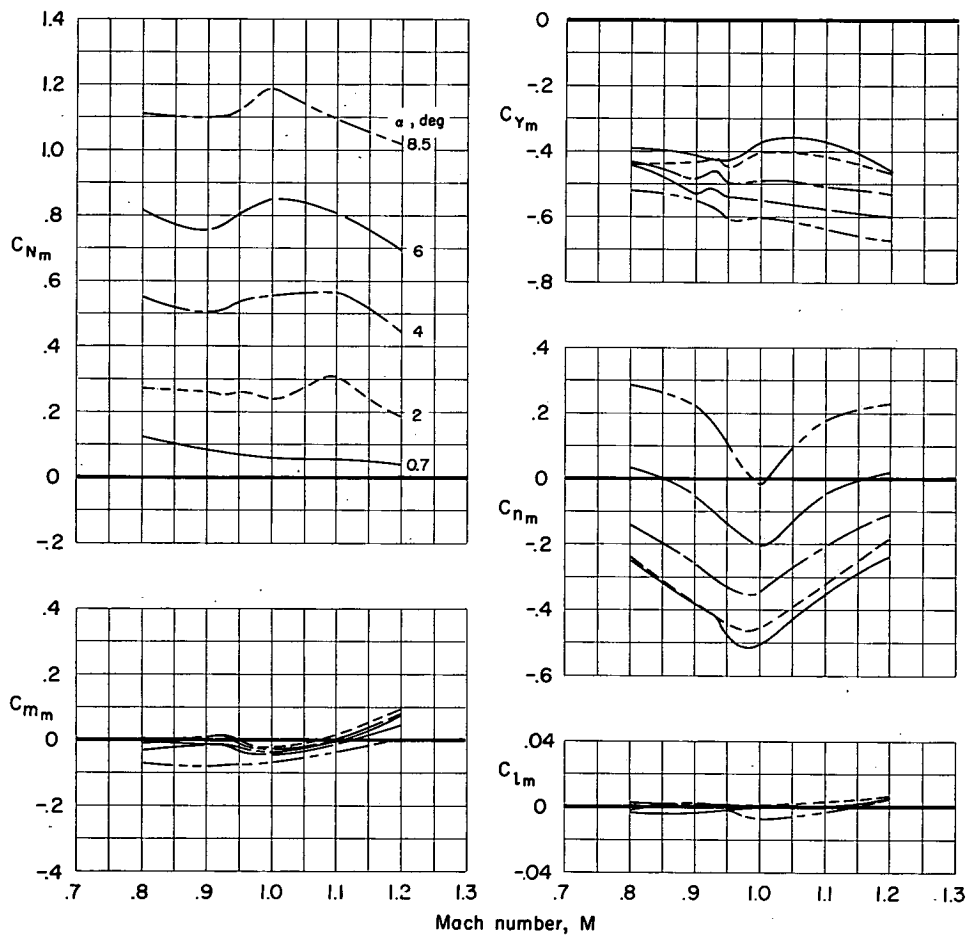
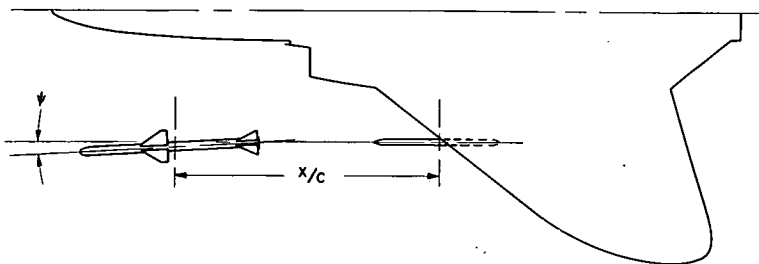
(a) $\theta = \psi = \phi = 0^\circ$.

Figure 17.- Force and moment characteristics of the missile in launch position $x/c = 1.108$.



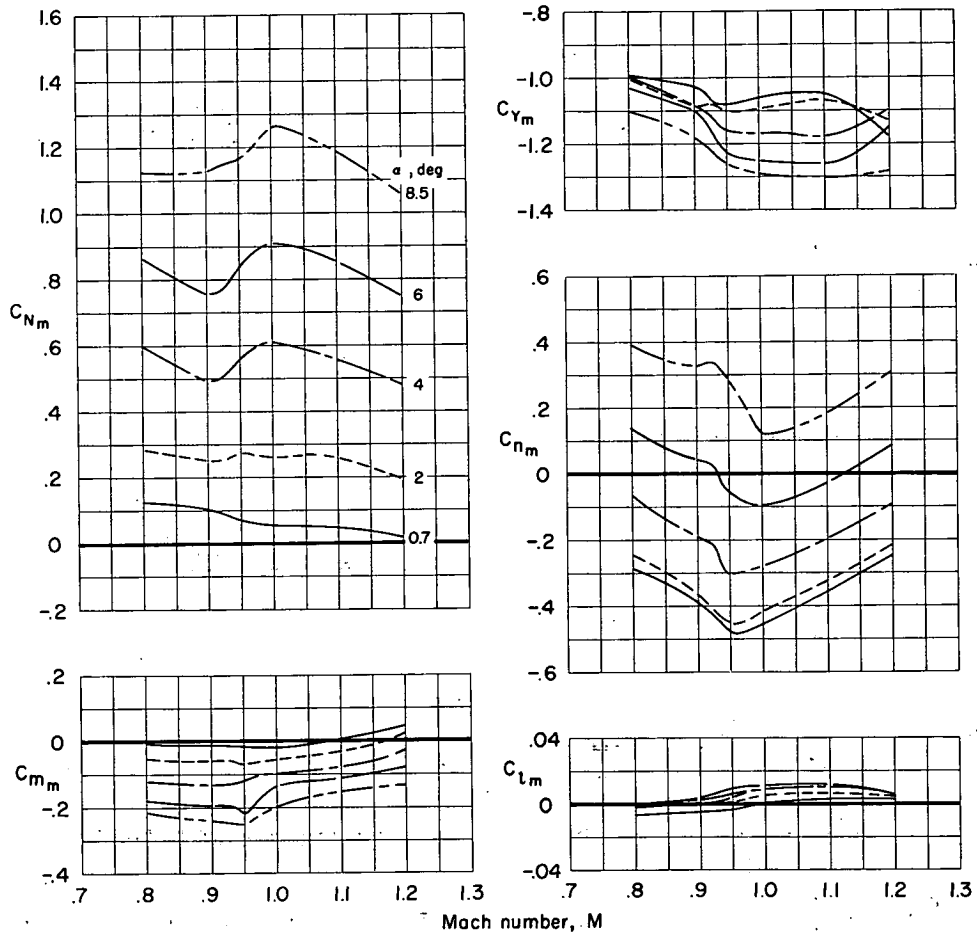
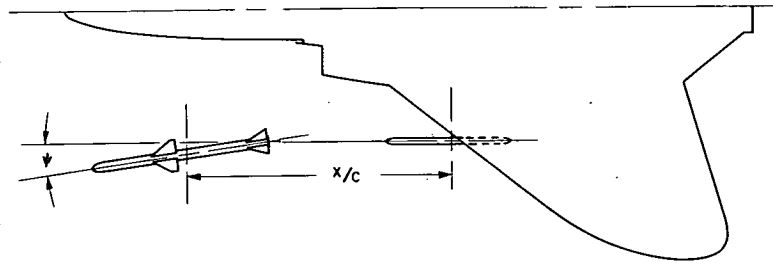
(b) $\theta = 8^\circ$; $\psi = \phi = 0^\circ$.

Figure 17.- Continued.



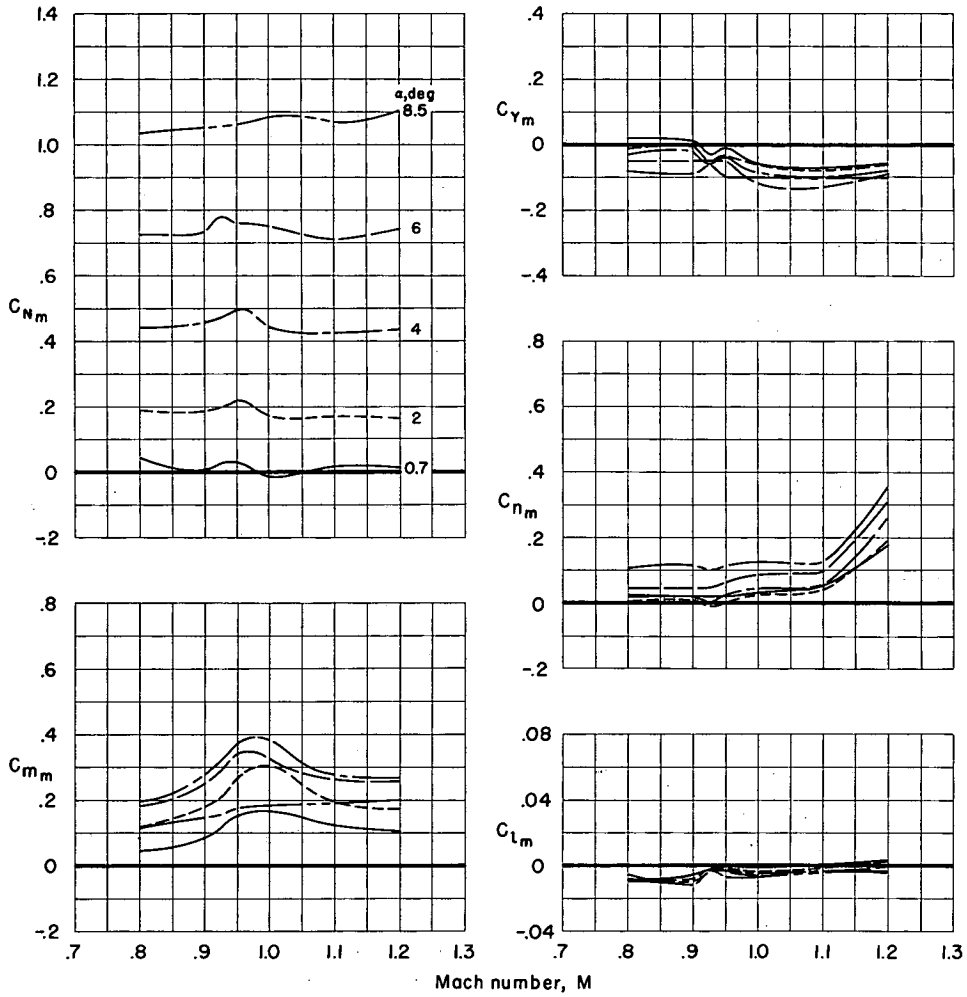
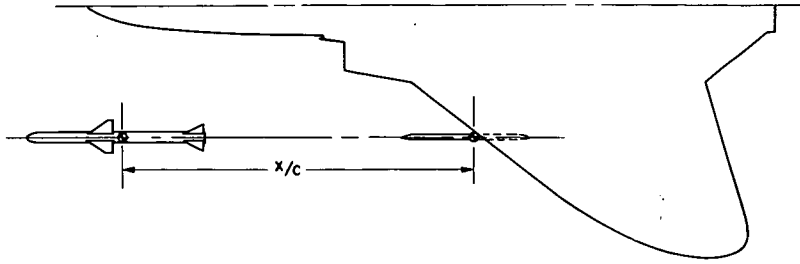
(c) $\psi = -3$; $\theta = \phi = 0^\circ$.

Figure 17.- Continued.



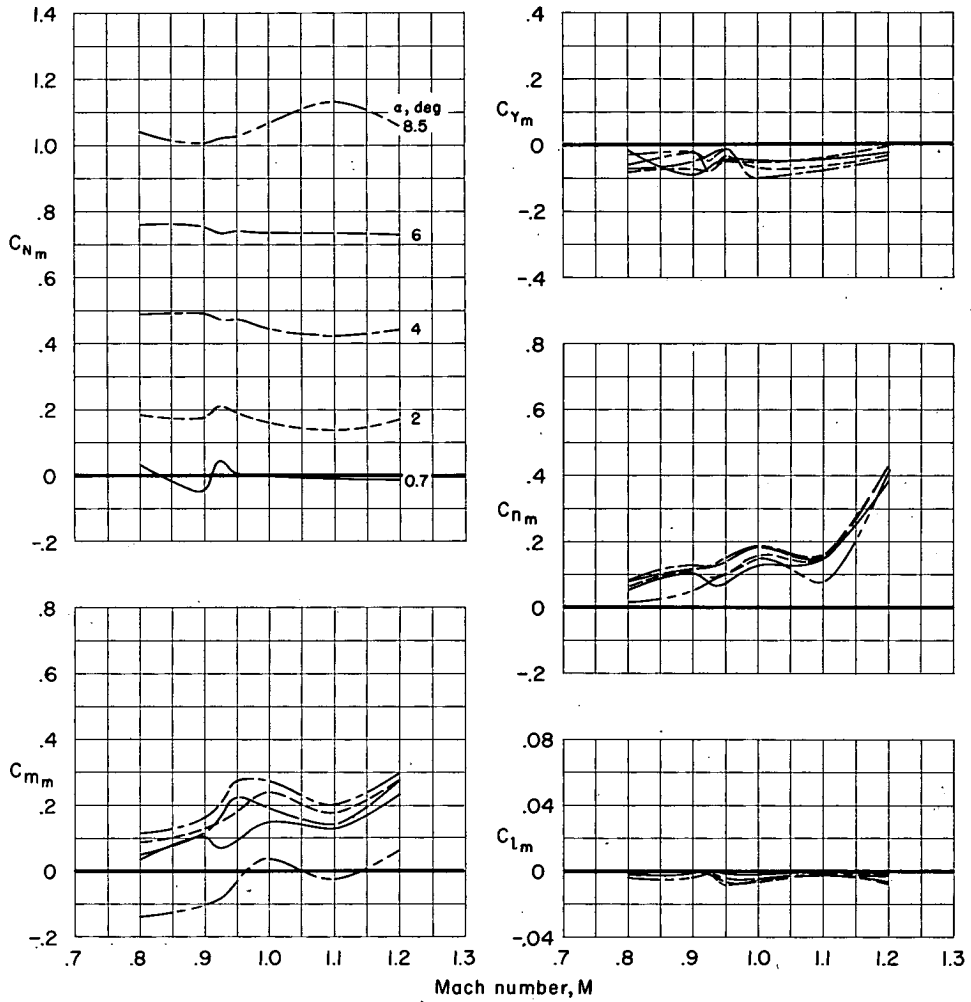
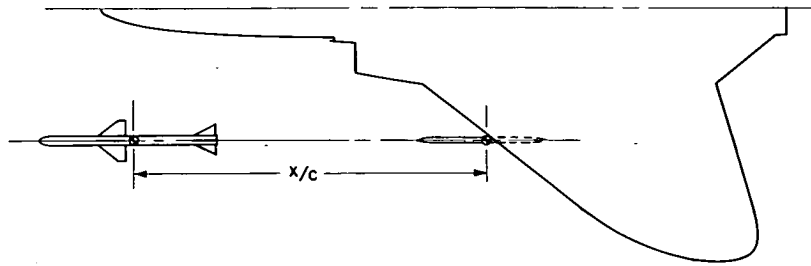
(d) $\psi = -8$; $\theta = \phi = 0^\circ$.

Figure 17.- Concluded.



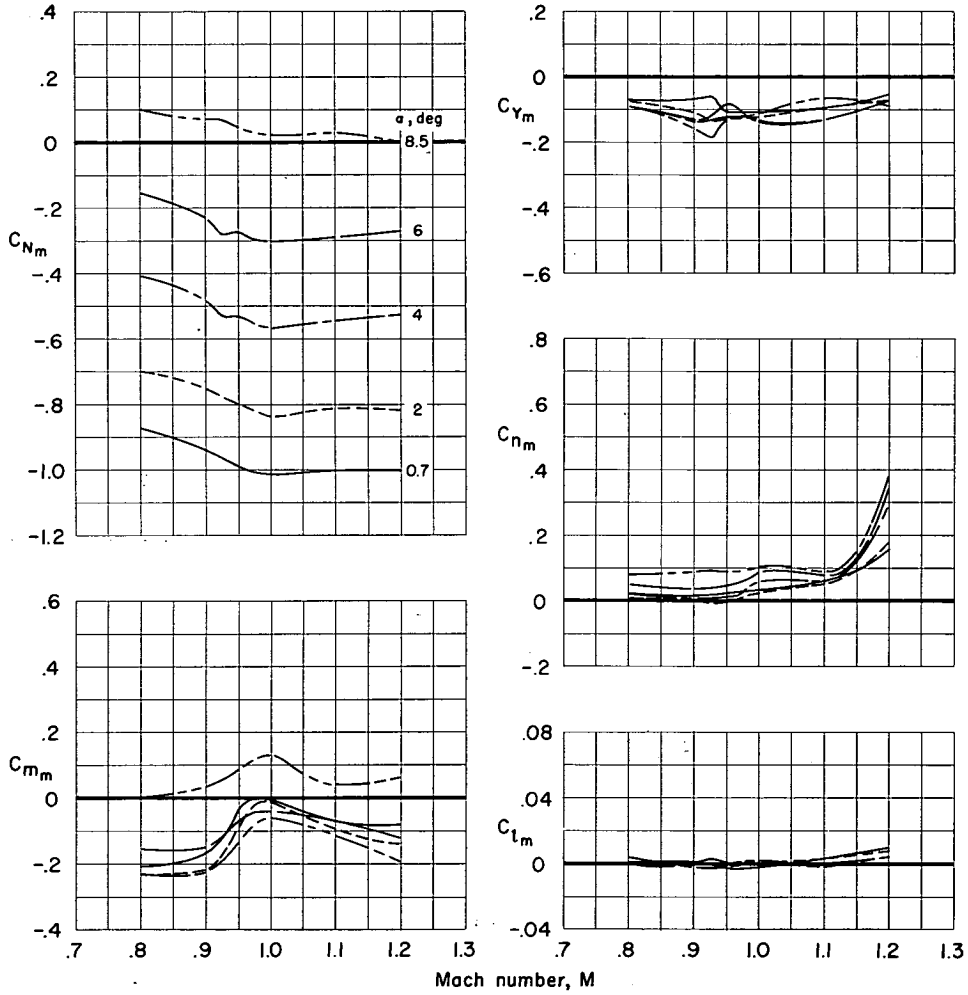
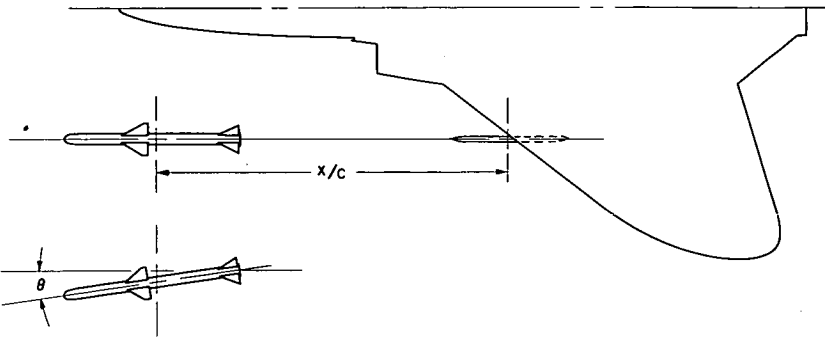
(a) $\theta = \psi = \phi = 0^\circ$.

Figure 18.- Force and moment characteristics of the missile in launch position $x/c = 1.477$.



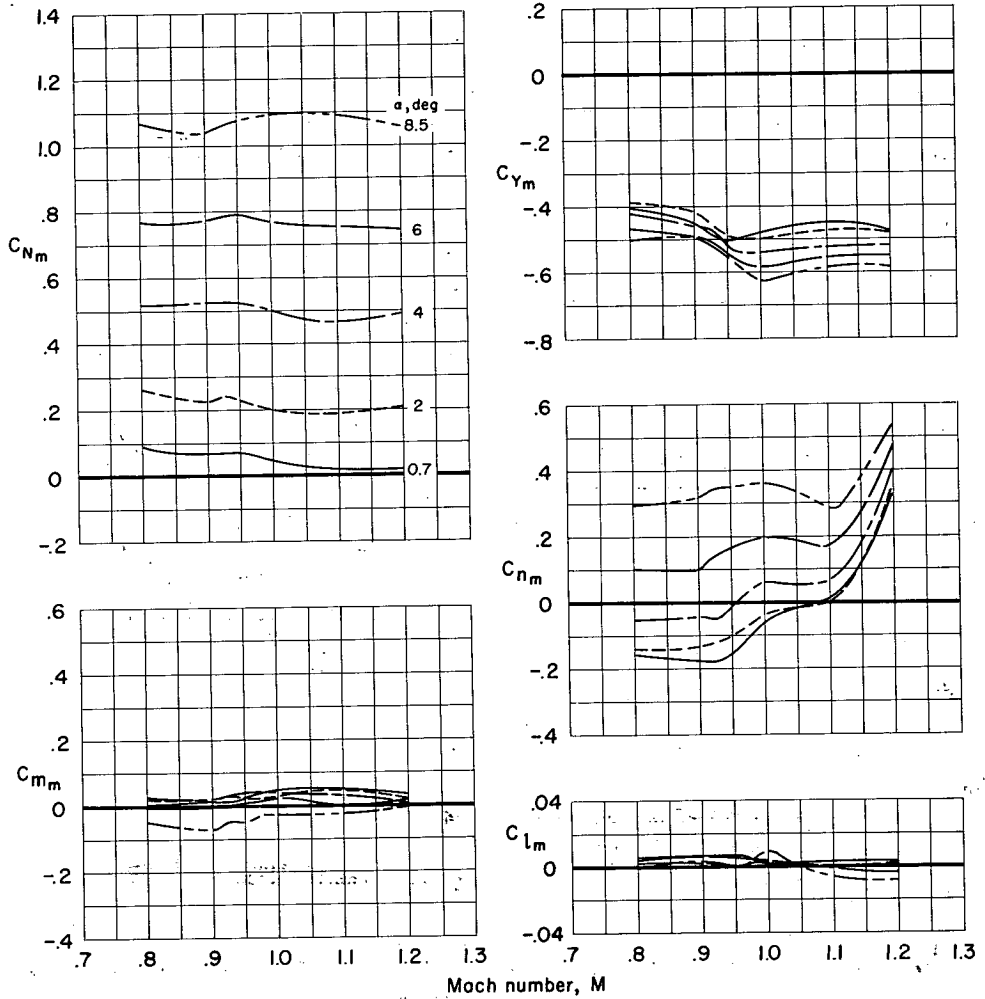
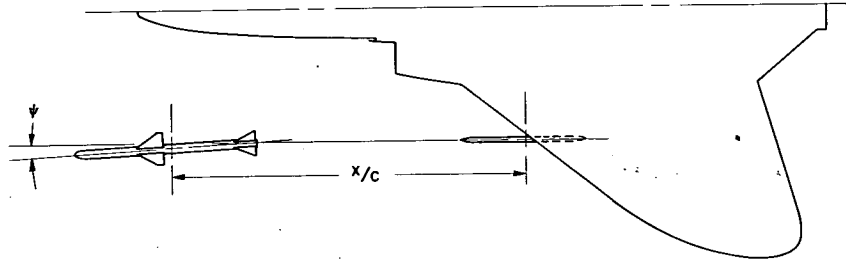
(b) $\varphi = 45^\circ$; $\theta = \psi = 0^\circ$.

Figure 18.- Continued.



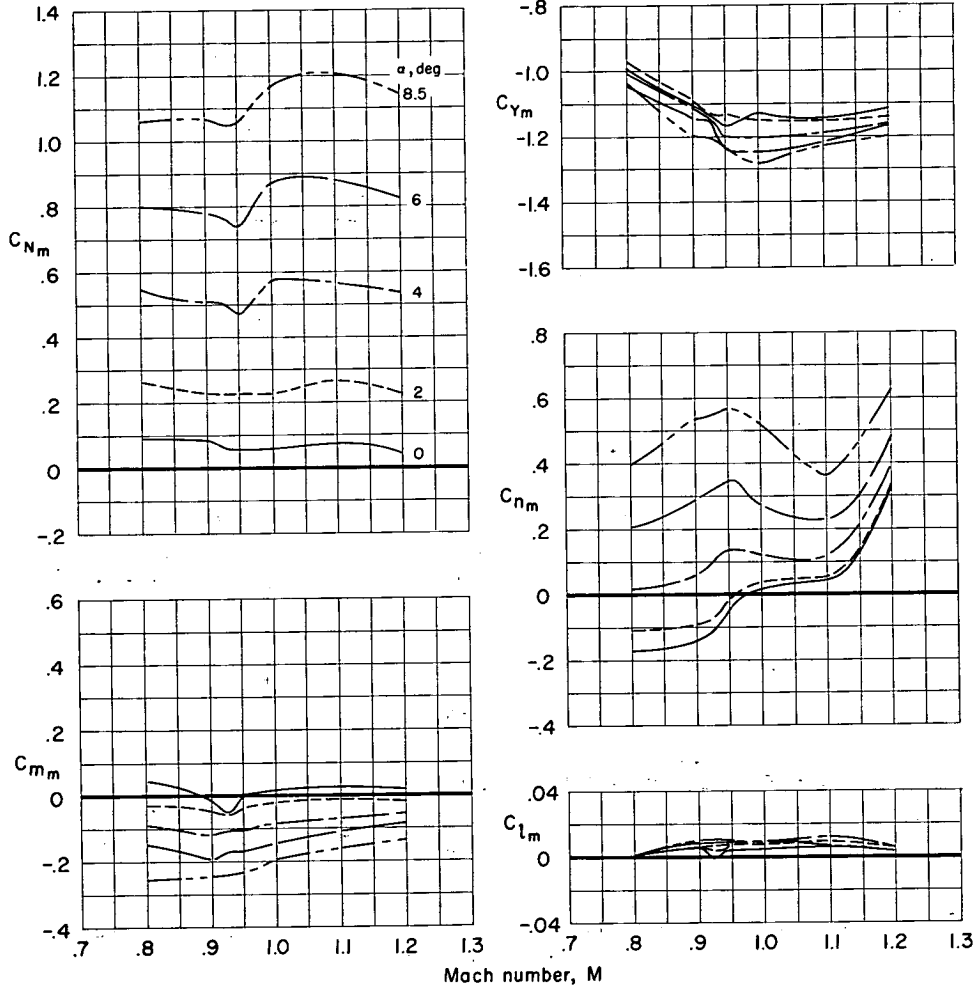
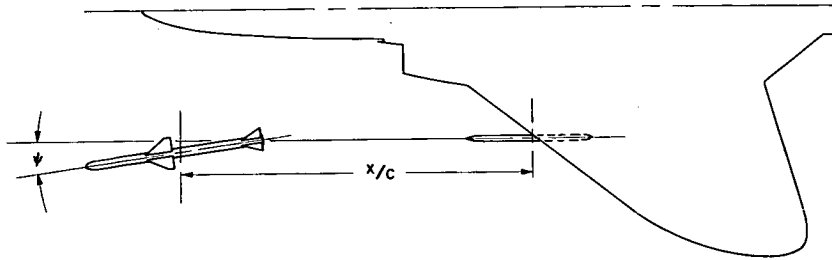
(c) $\theta = -8^\circ$; $\phi = \psi = 0^\circ$.

Figure 18.- Continued.



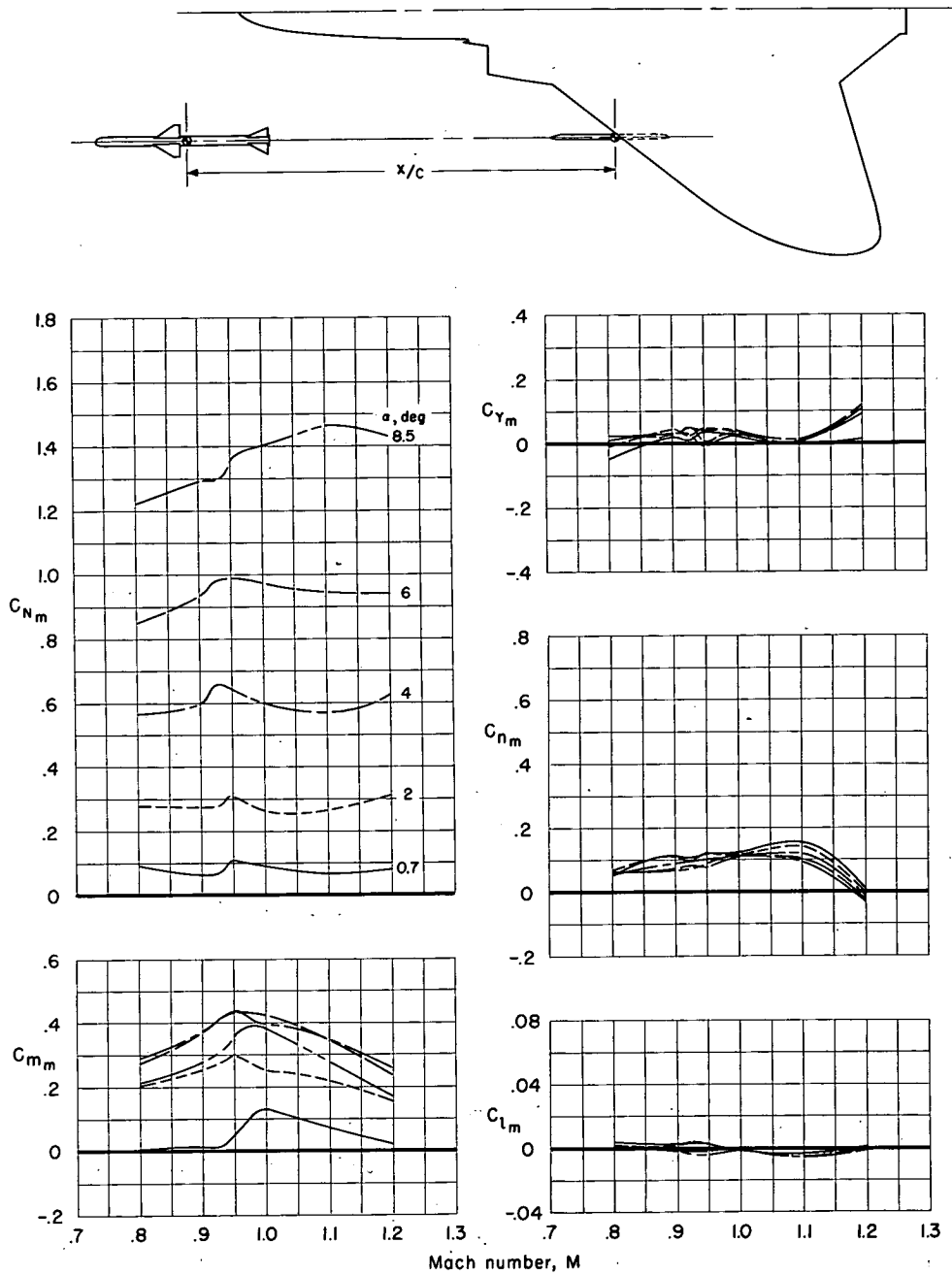
(d) $\psi = -3^\circ$; $\theta = \phi = 0^\circ$.

Figure 18.- Continued.



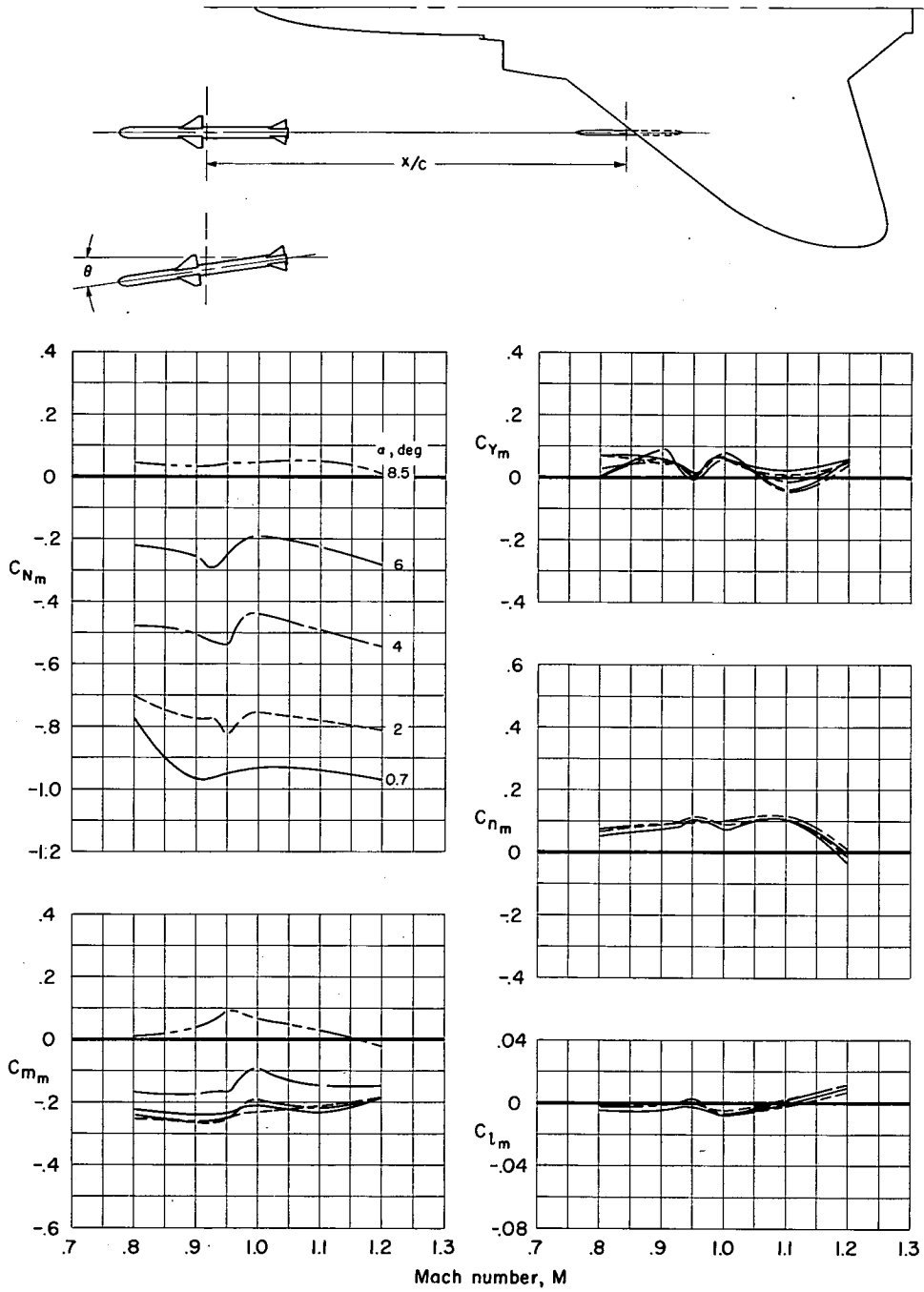
(e) $\psi = -8^\circ$; $\theta = \phi = 0^\circ$.

Figure 18.- Concluded.



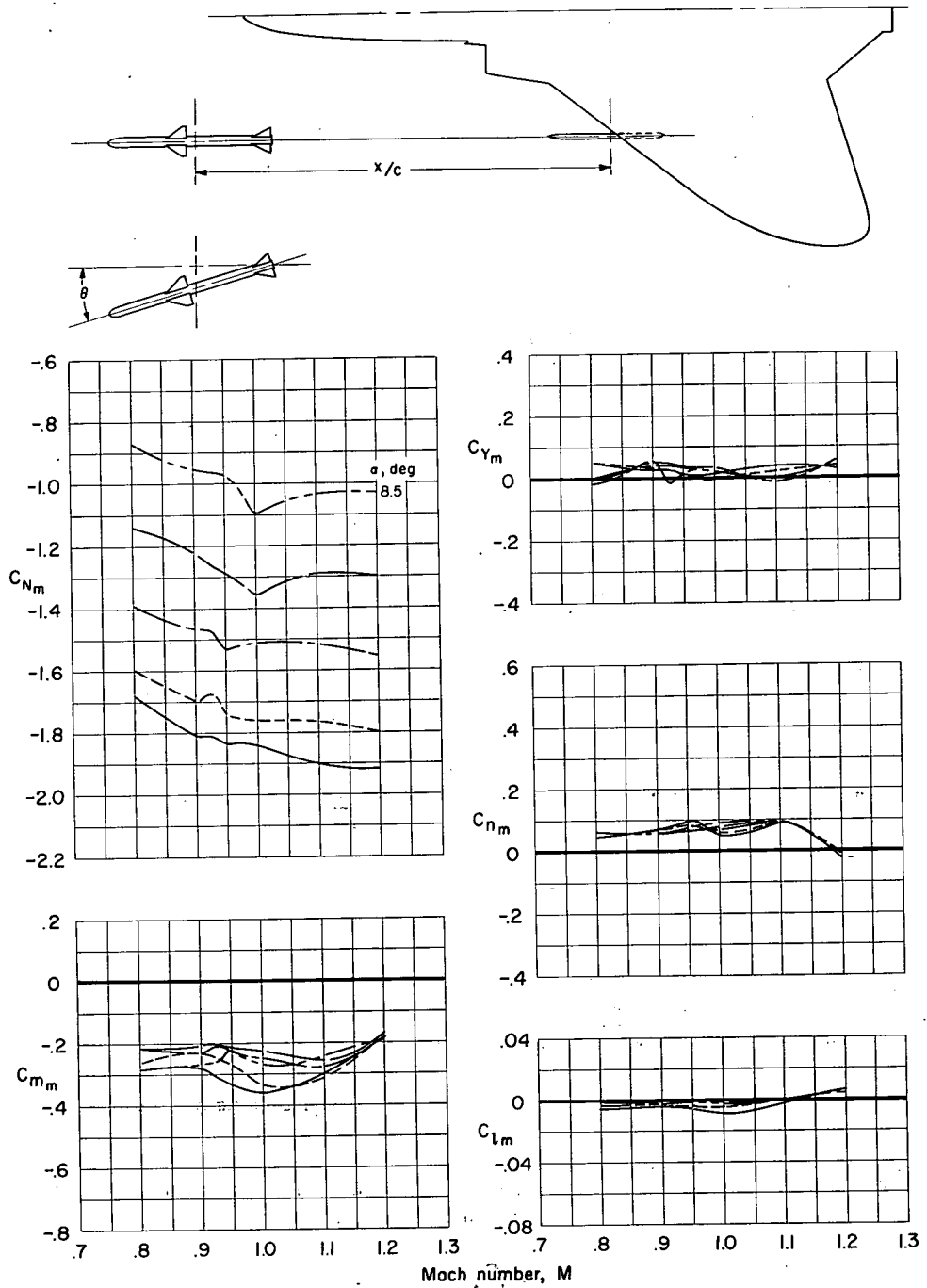
(a) $\theta = \psi = \phi = 0^\circ$.

Figure 19.- Force and moment characteristics of the missile in launch position $x/c = 1.846$.



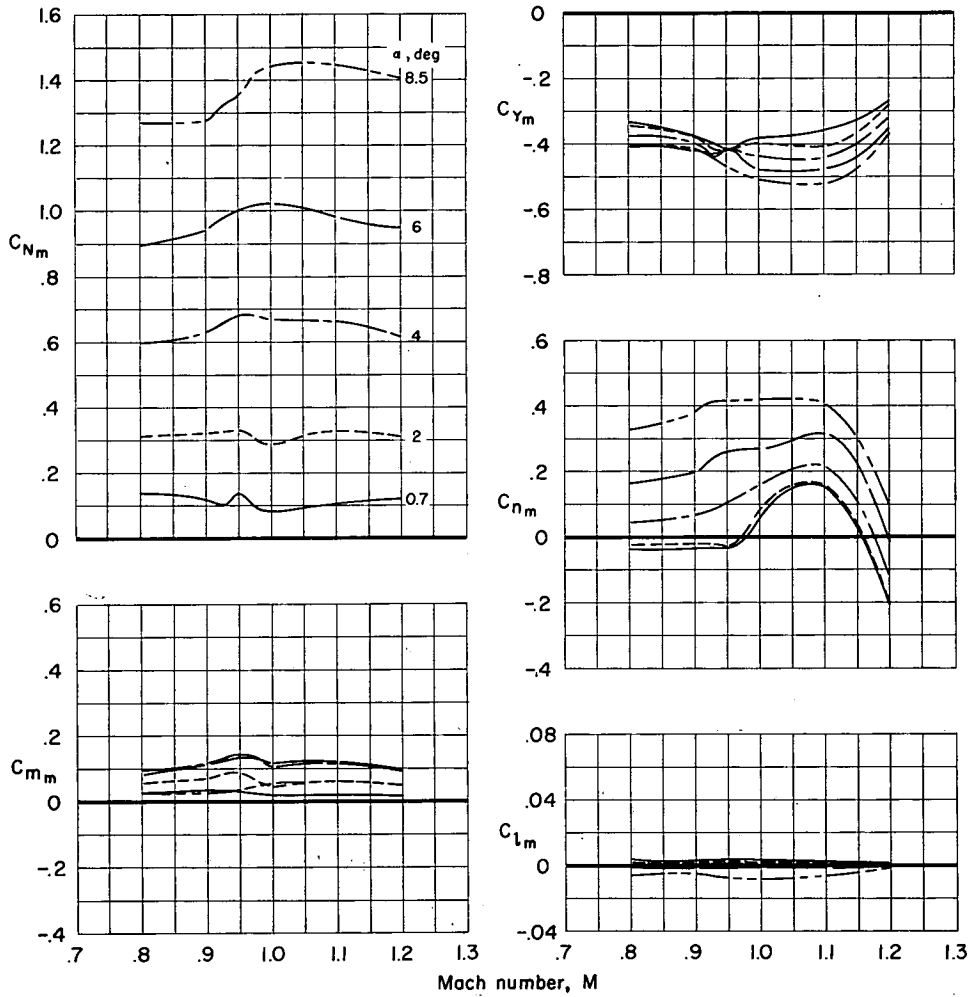
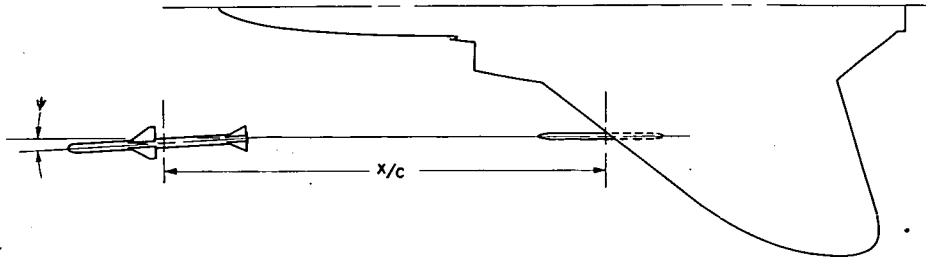
(b) $\theta = -3^\circ$; $\psi = \phi = 0^\circ$.

Figure 19.- Continued.



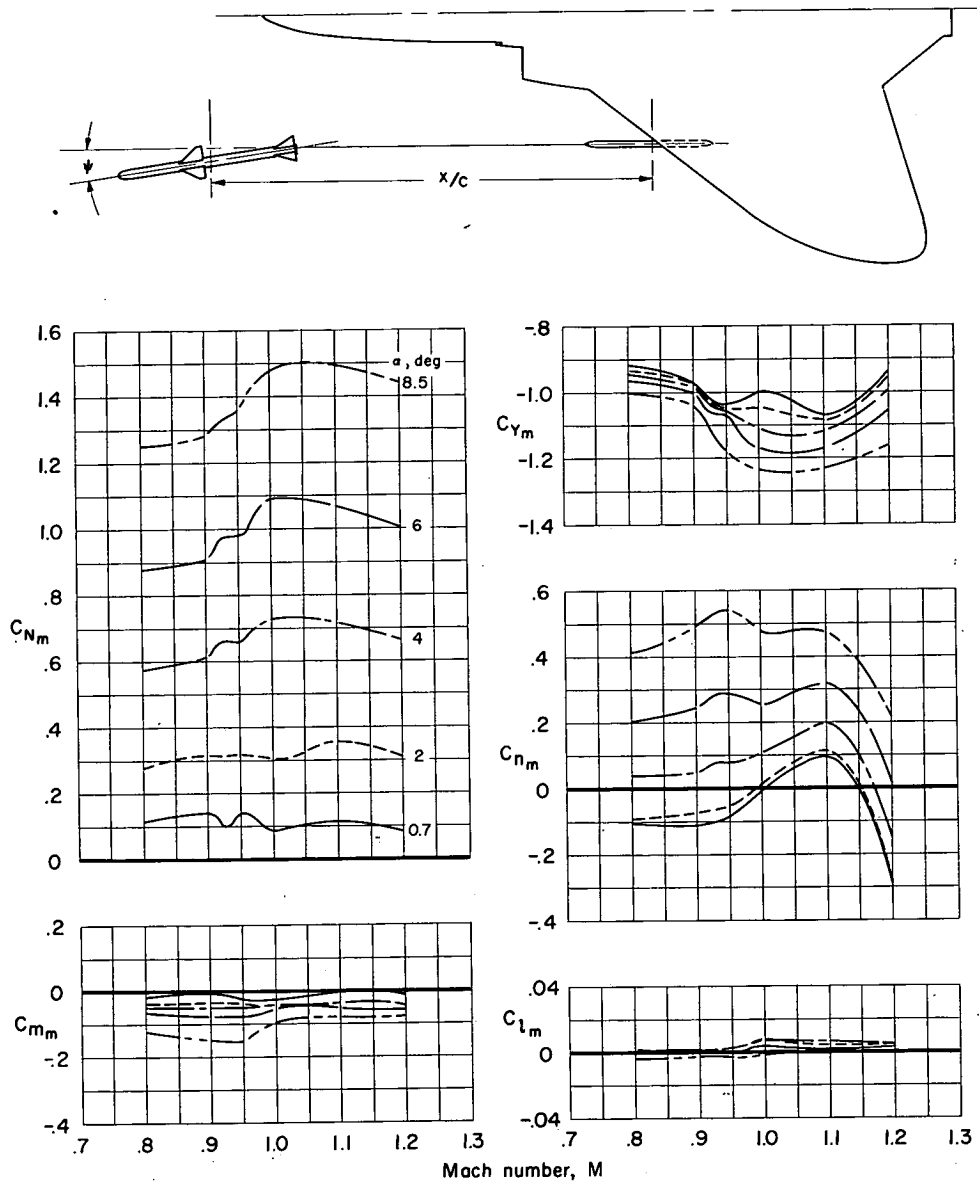
(c) $\theta = -16^\circ$; $\psi_i = \varphi = 0^\circ$.

Figure 19.- Continued.



(d) $\psi = -3^\circ$; $\theta = \phi = 0^\circ$.

Figure 19.- Continued.



(e). $\psi = -8^\circ$; $\theta = \phi = 0^\circ$.

Figure 19.- Concluded.

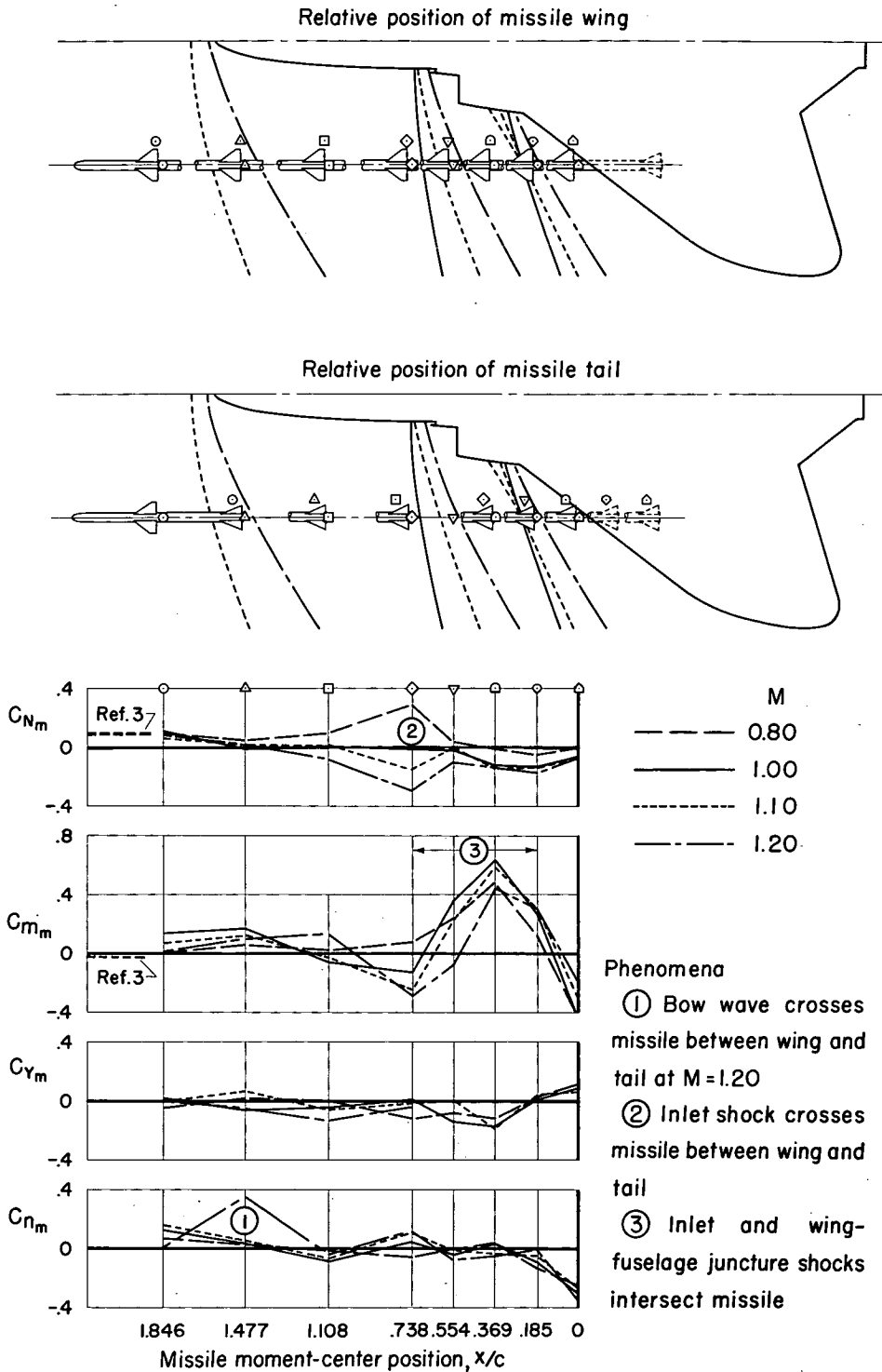
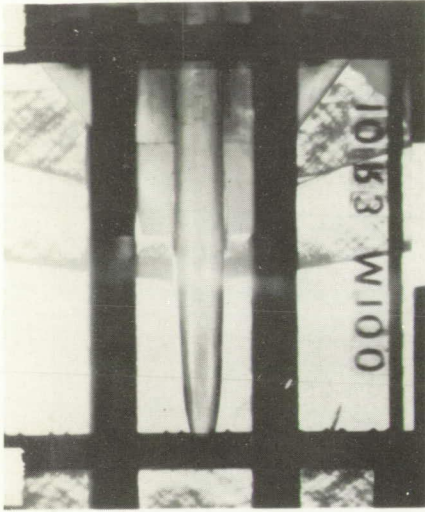
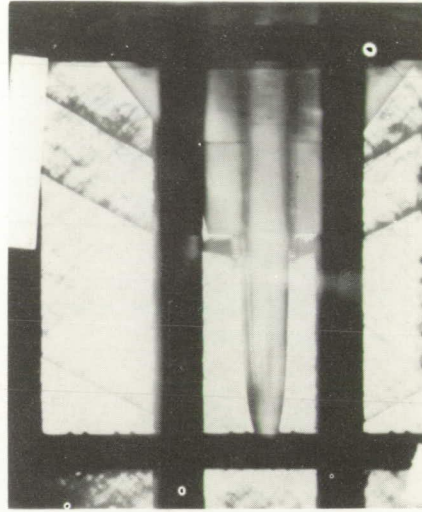


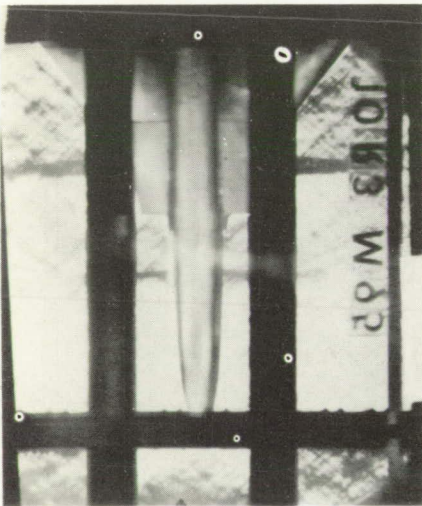
Figure 20.- Effect of Mach number on the aerodynamic coefficients of the missile; $\alpha = 0.7^\circ$.



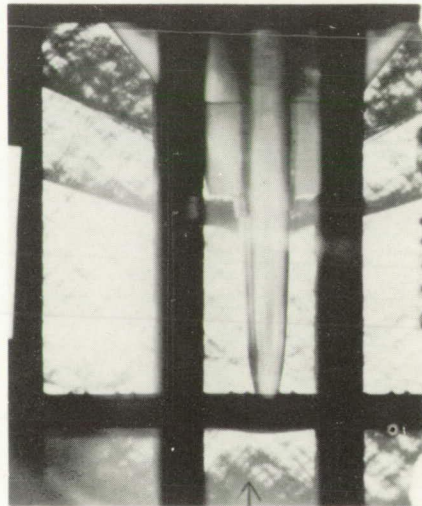
$\alpha = 0^\circ, M = 1.00$



$\alpha = 0^\circ, M = 1.20$
A-21470



$\alpha = 0^\circ, M = 0.95$



$\alpha = 0^\circ, M = 1.10$

(a) Plan.

Figure 21.- Schlieren photographs of the flow of the airplane model.



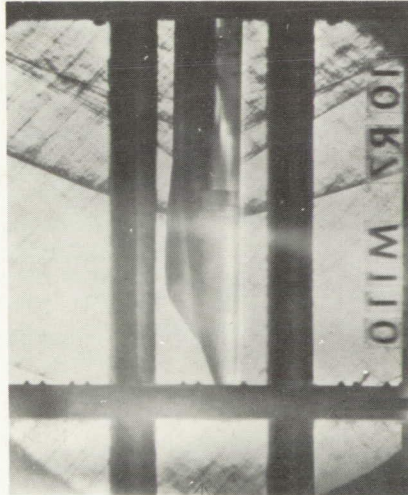
$\alpha = 0.6^\circ, M = 1.00$



$\alpha = 0.5^\circ, M = 1.20$



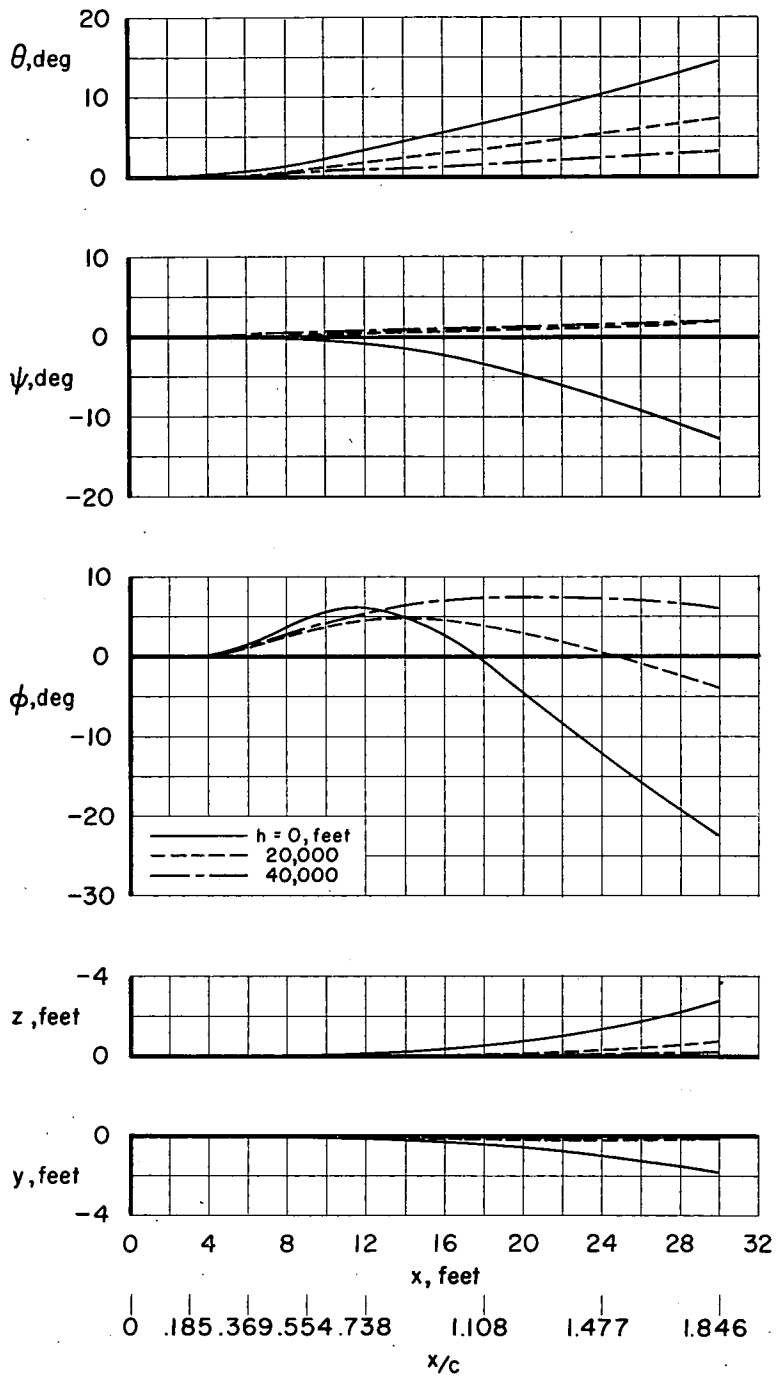
$\alpha = 0.6^\circ, M = 0.95$



$\alpha = 0.6^\circ, M = 1.10$

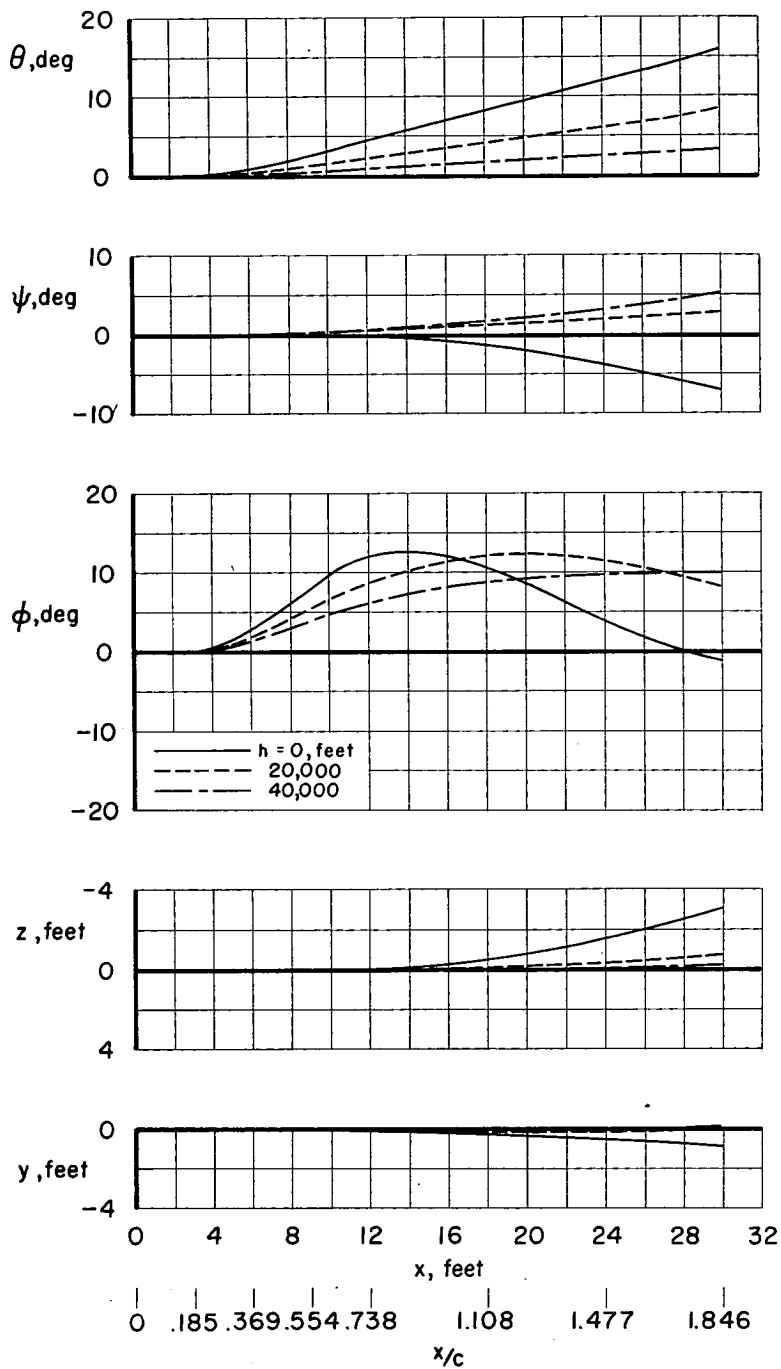
(b) Elevation.

Figure 21.- Concluded.



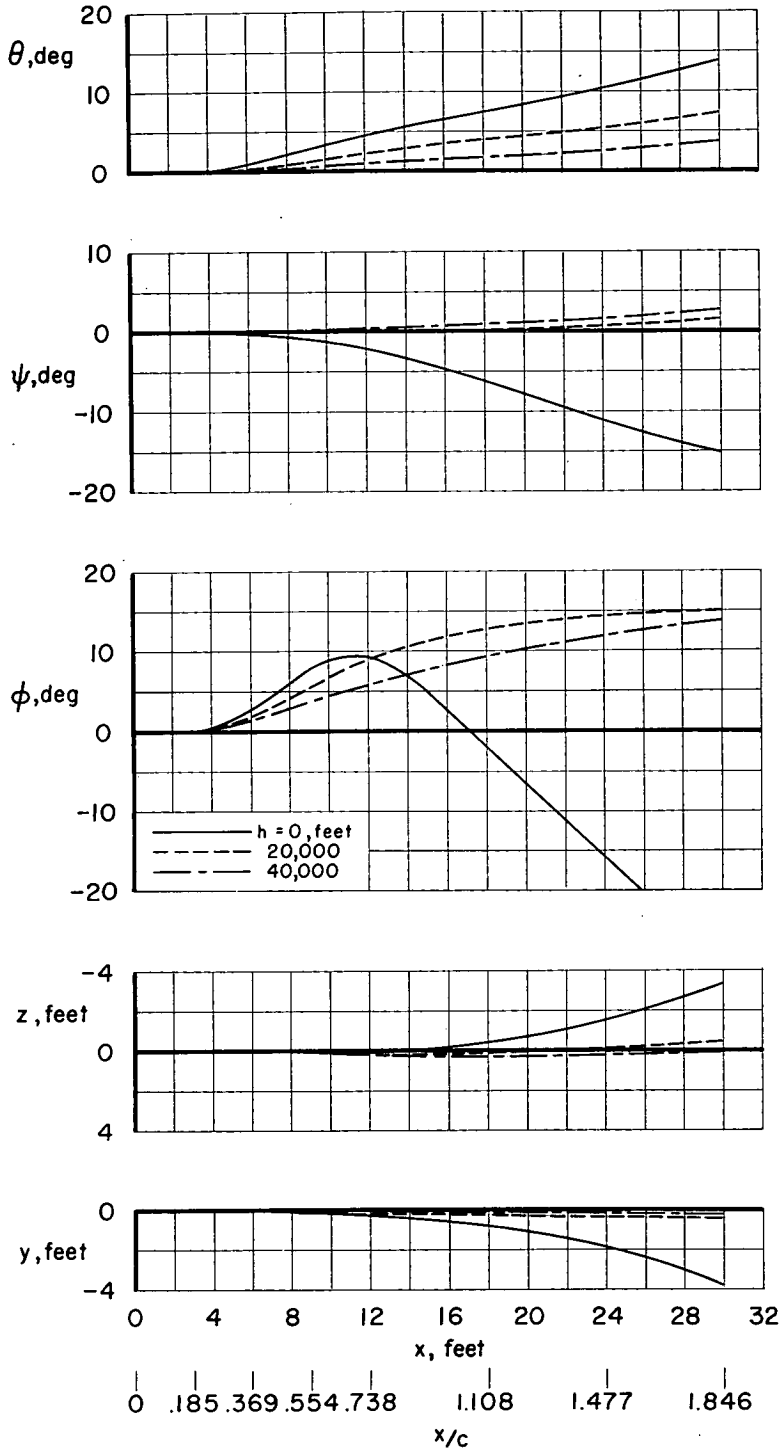
(a) $M = 0.90$.

Figure 22.- Attitude and position of the missile when launched from the airplane.



(b) $M = 1.00$.

Figure 22.- Continued.



(c) $M = 1.20$.

Figure 22.- Concluded.

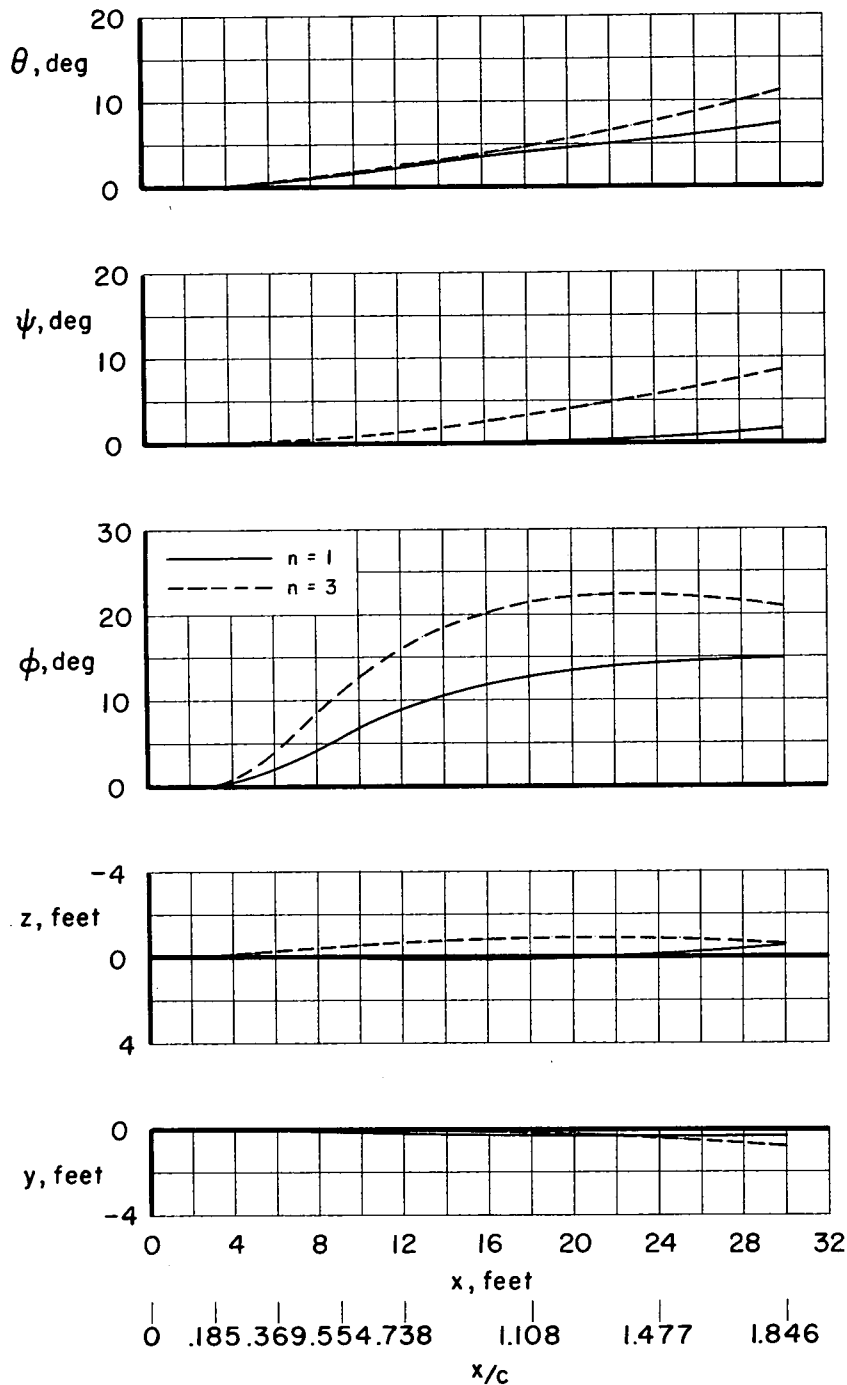
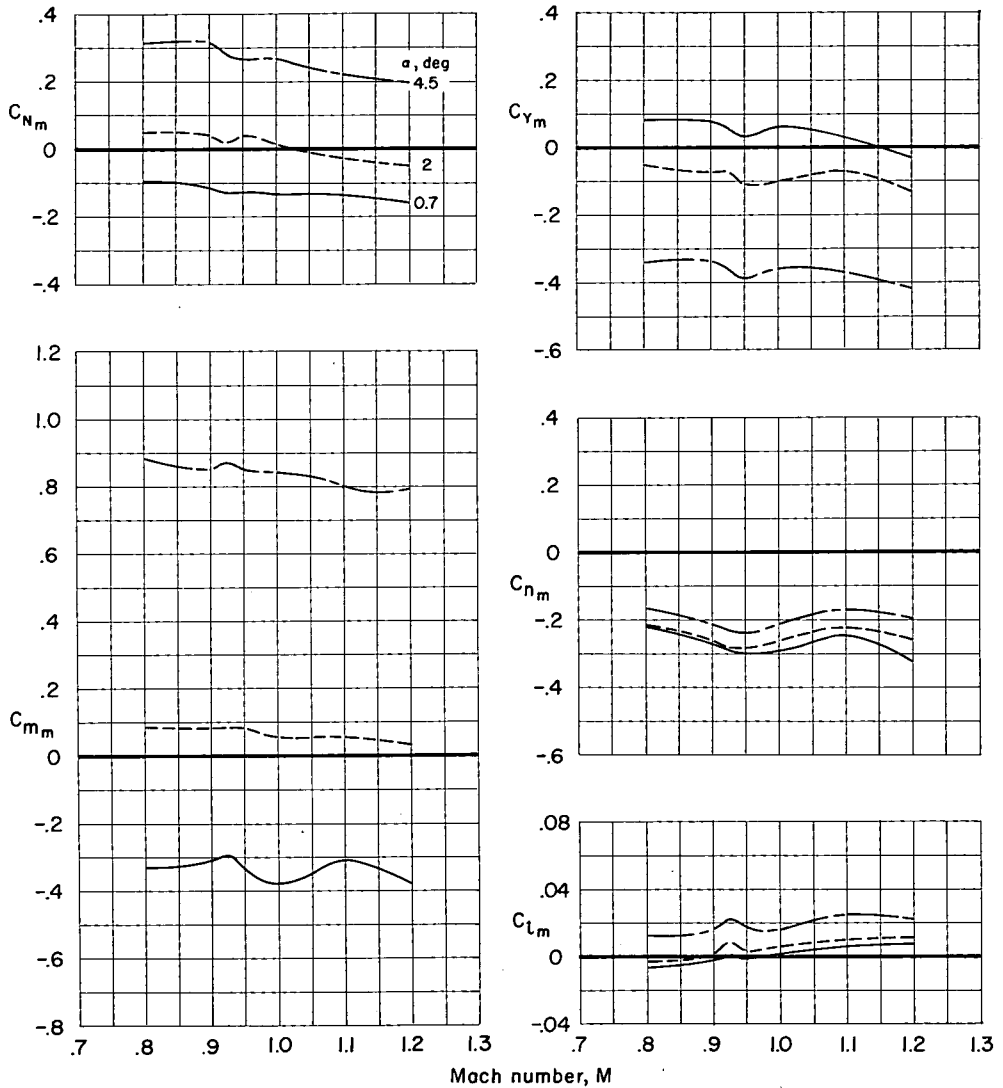
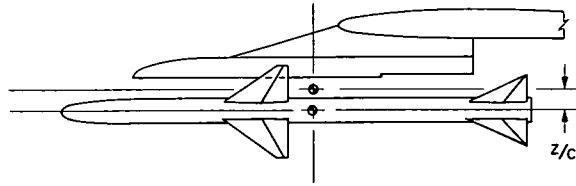
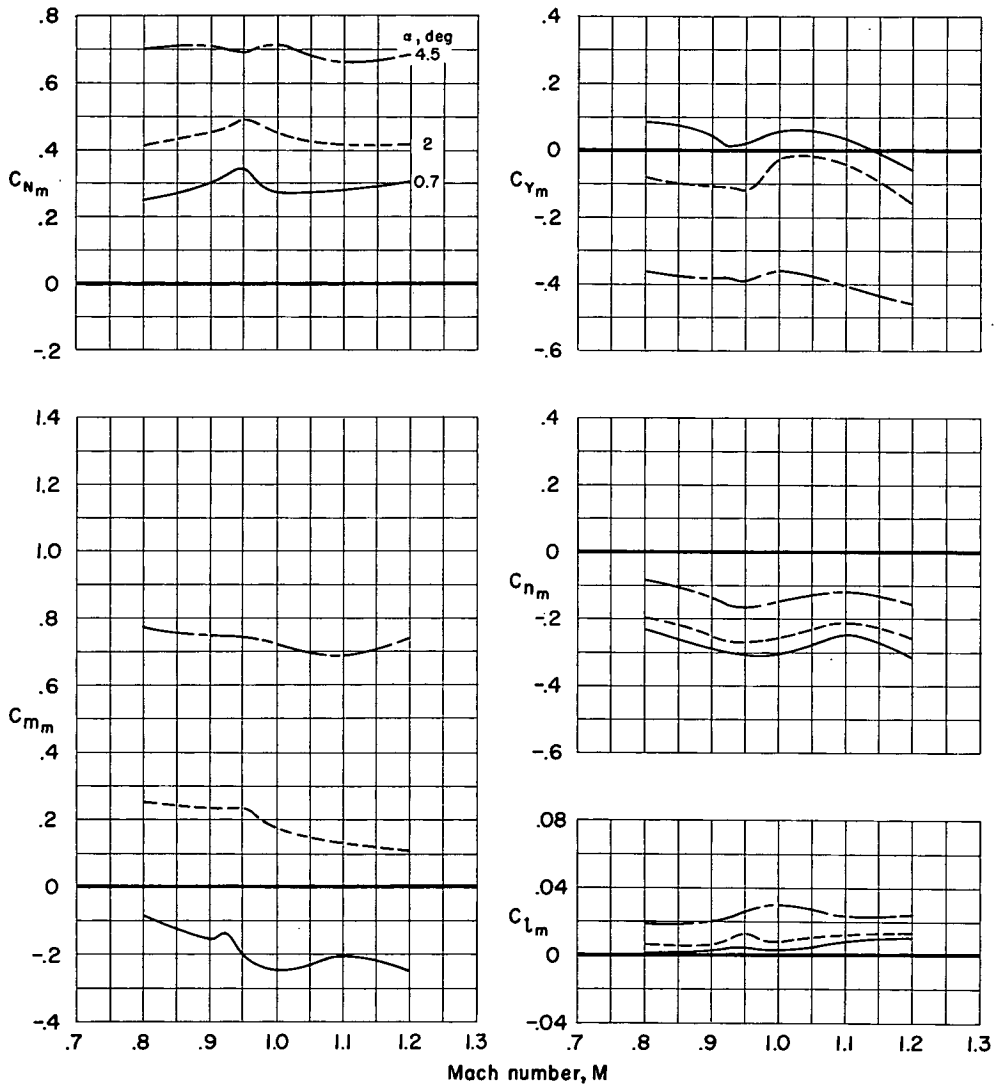
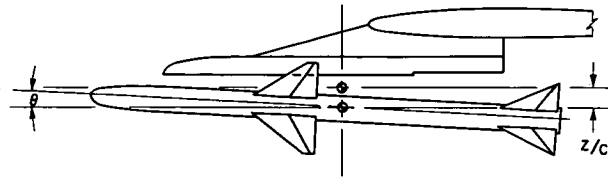


Figure 23.- Effect of load factor, with the airplane in a left turn, on the missile attitude and position; left missile launched at 20,000 feet altitude and a Mach number of 1.20.



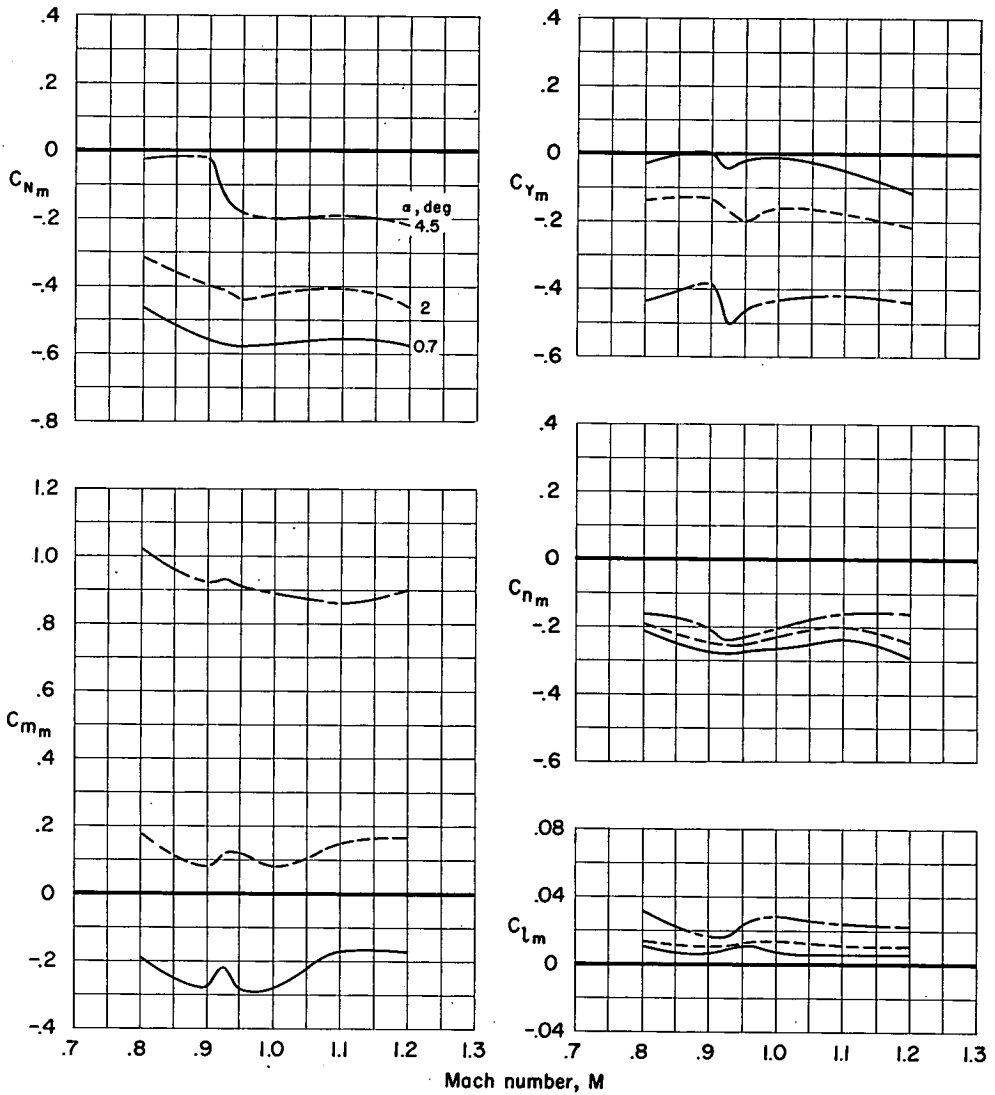
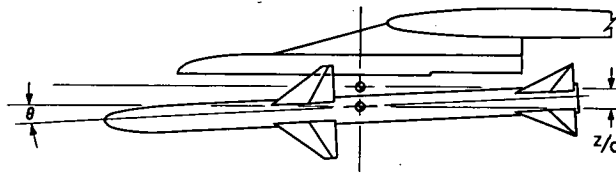
(a) $\theta = 0^\circ$.

Figure 24.- Force and moment characteristics of the missile in jettison position $z/c = 0.0308$; $\psi = \phi = 0^\circ$.



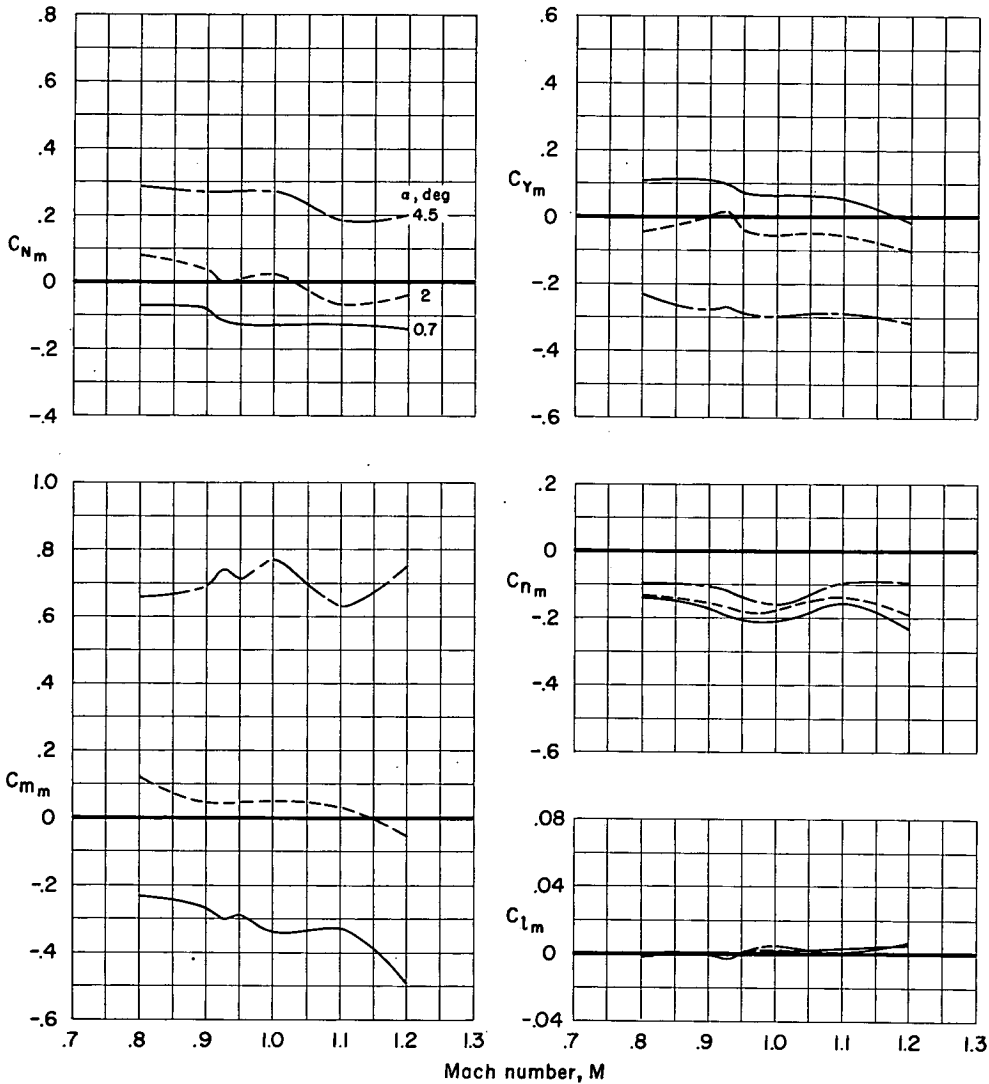
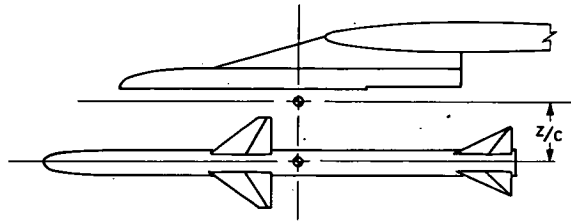
(b) $\theta = 3^\circ$.

Figure 24.- Continued.



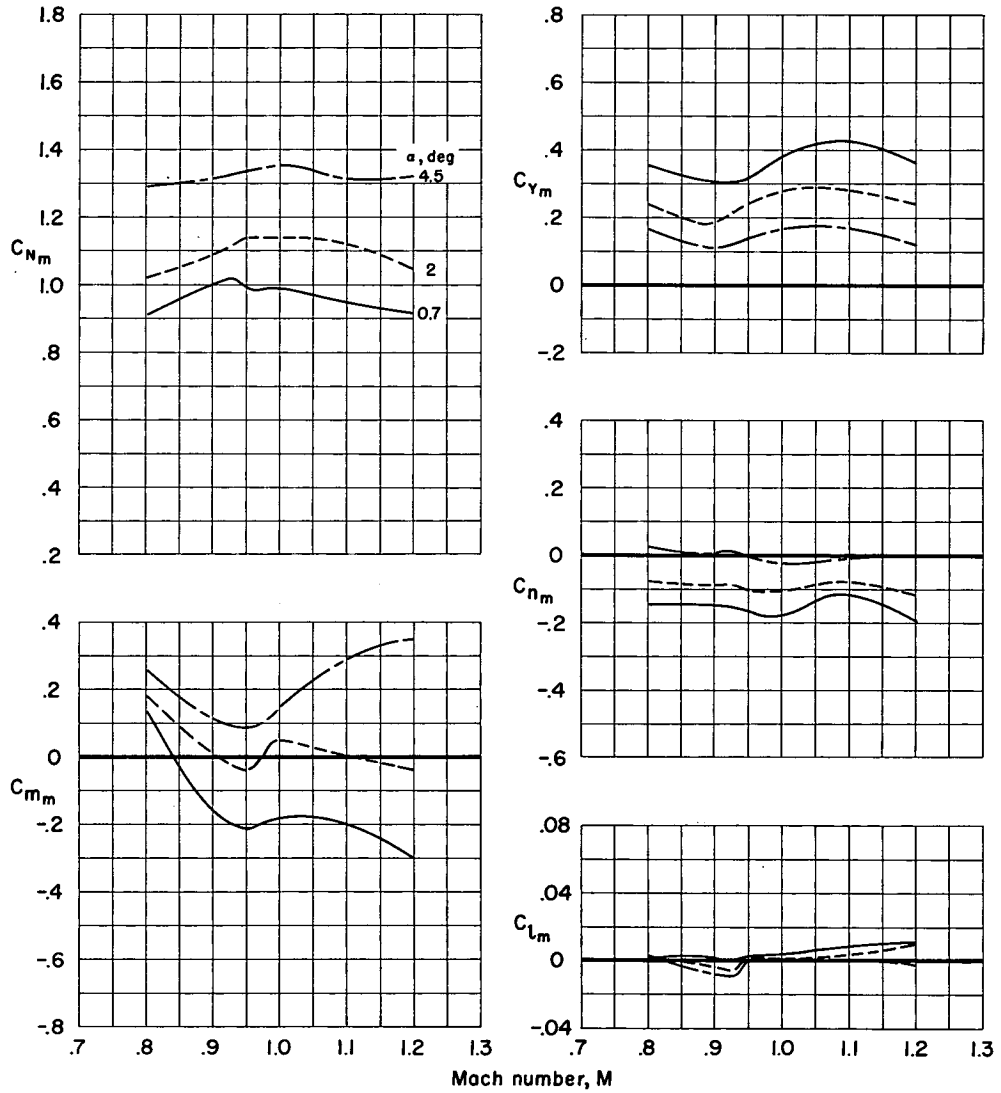
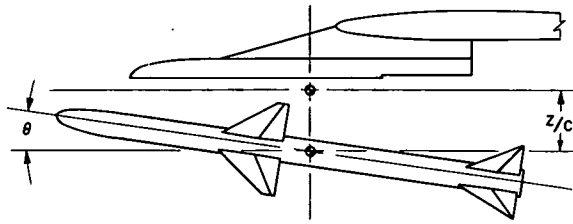
(c) $\theta = -3^\circ$.

Figure 24.- Concluded.



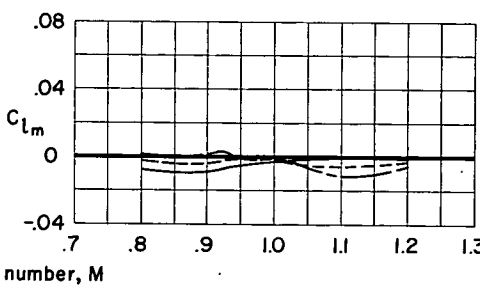
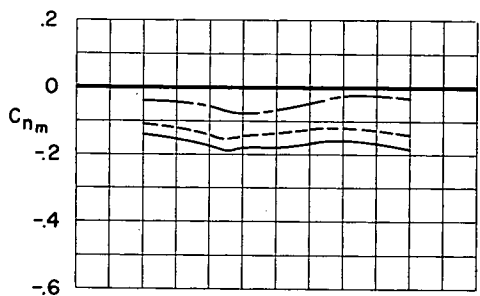
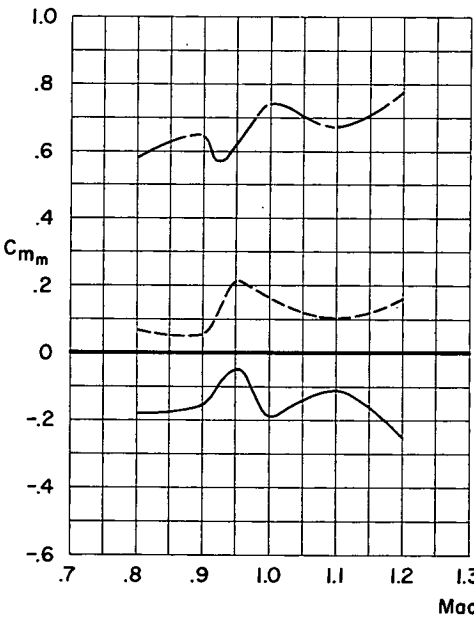
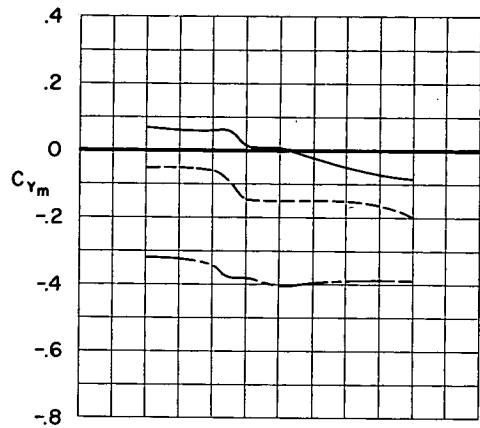
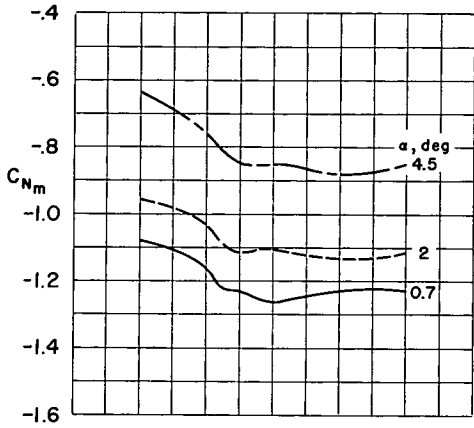
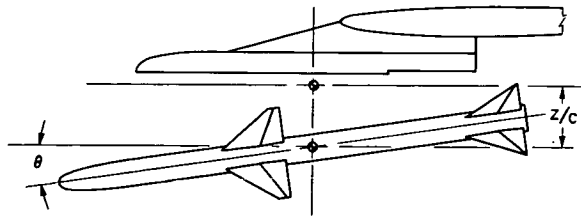
(a) $\theta = 0^\circ$.

Figure 25.- Force and moment characteristics of the missile in jettison position $z/c = 0.0923$; $\psi = \phi = 0^\circ$.



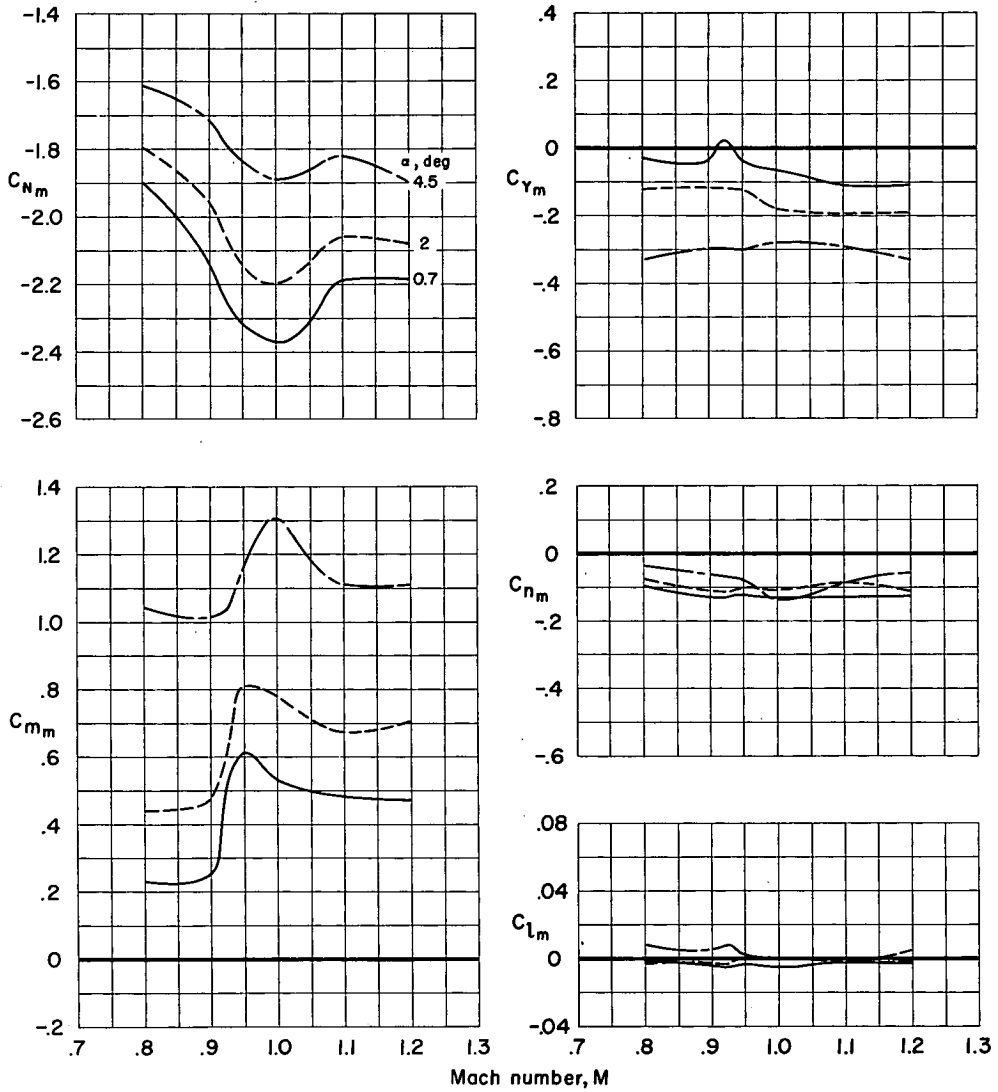
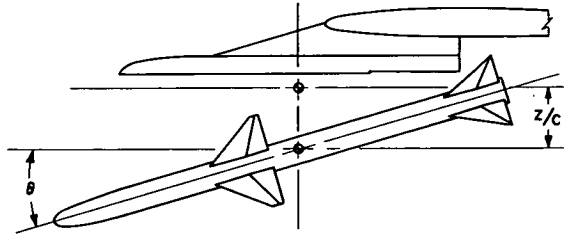
(b) $\theta = 8^\circ$.

Figure 25.- Continued.



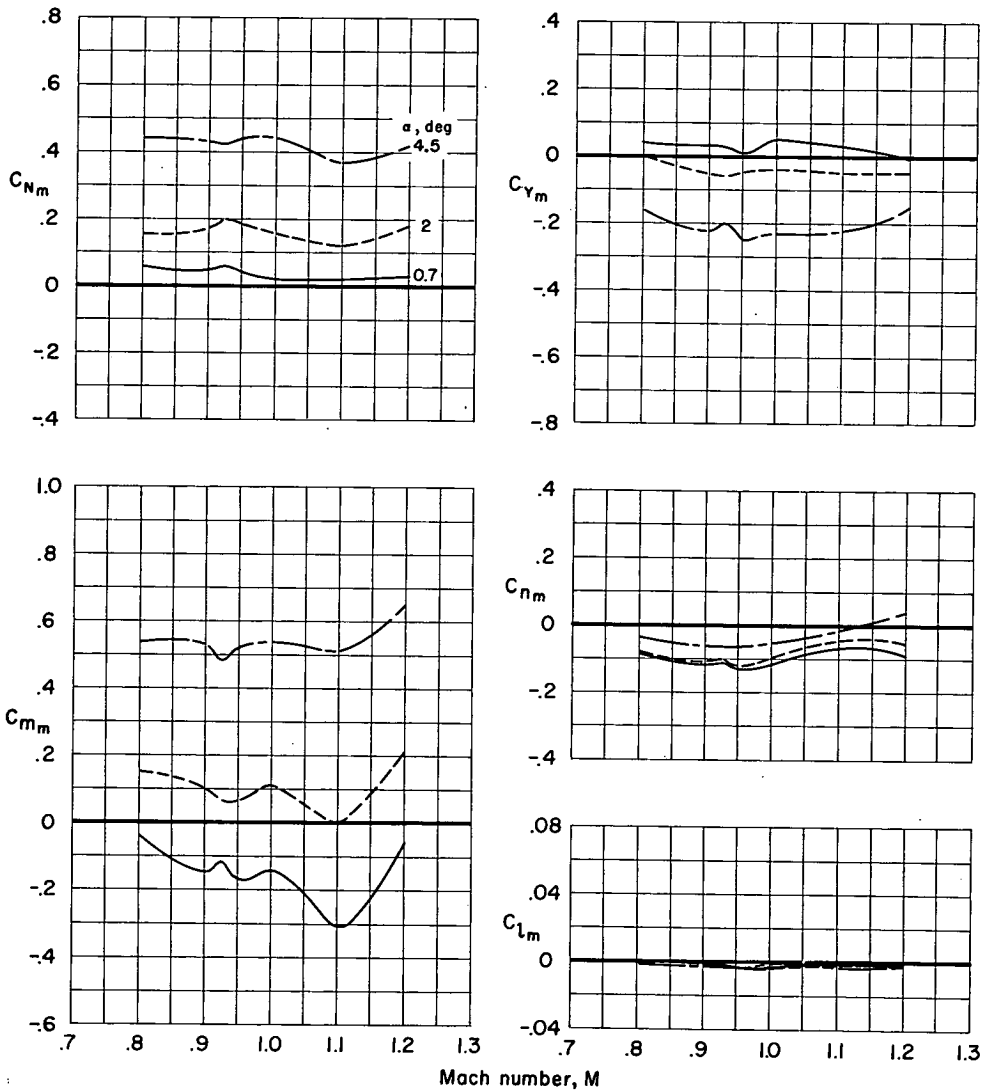
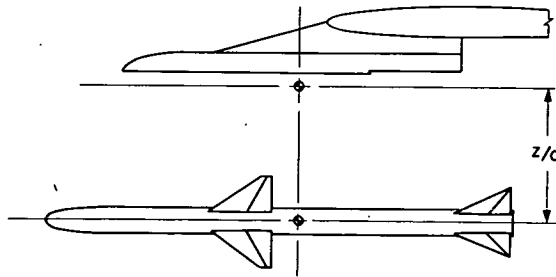
(c) $\theta = -8^\circ$.

Figure 25.- Continued.



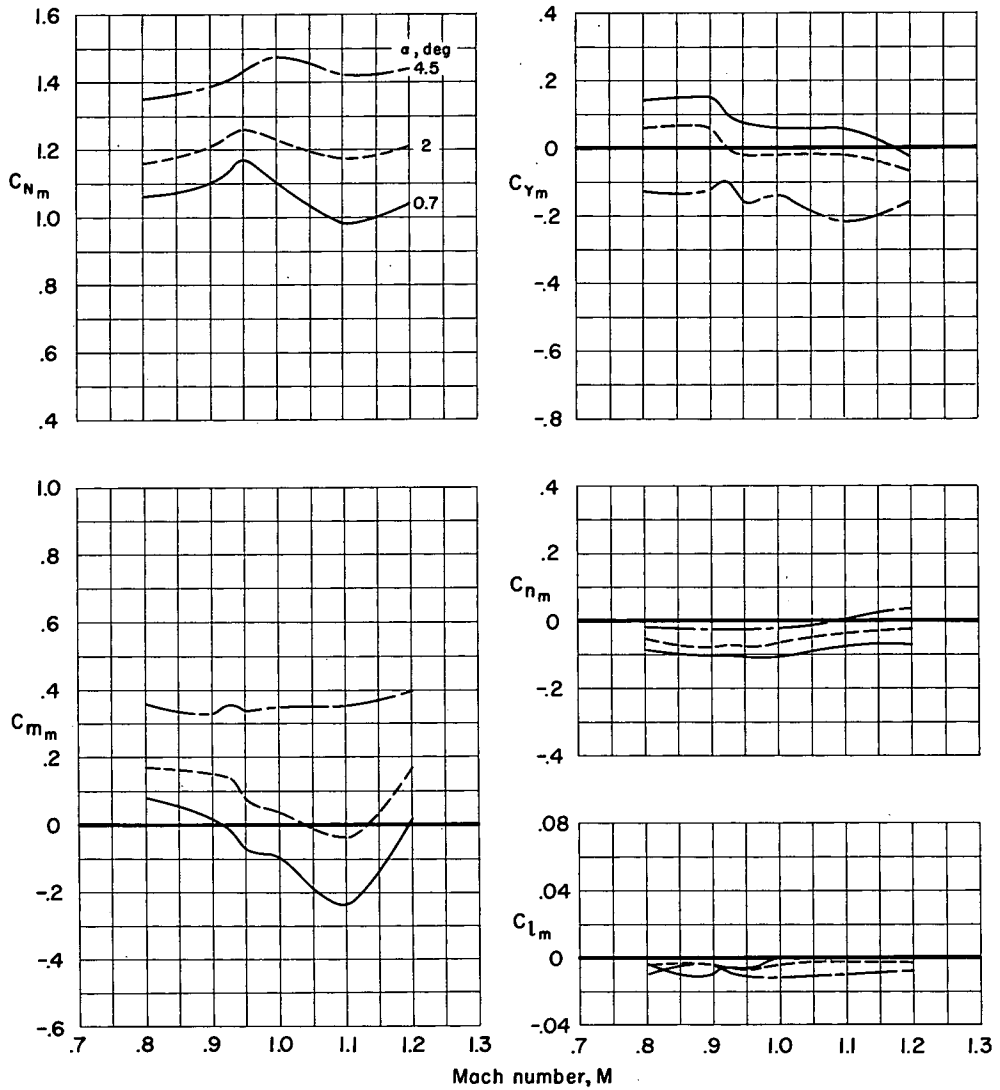
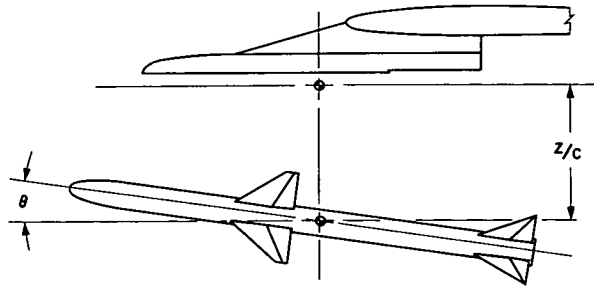
(d) $\theta = -16^\circ$.

Figure 25.- Concluded.



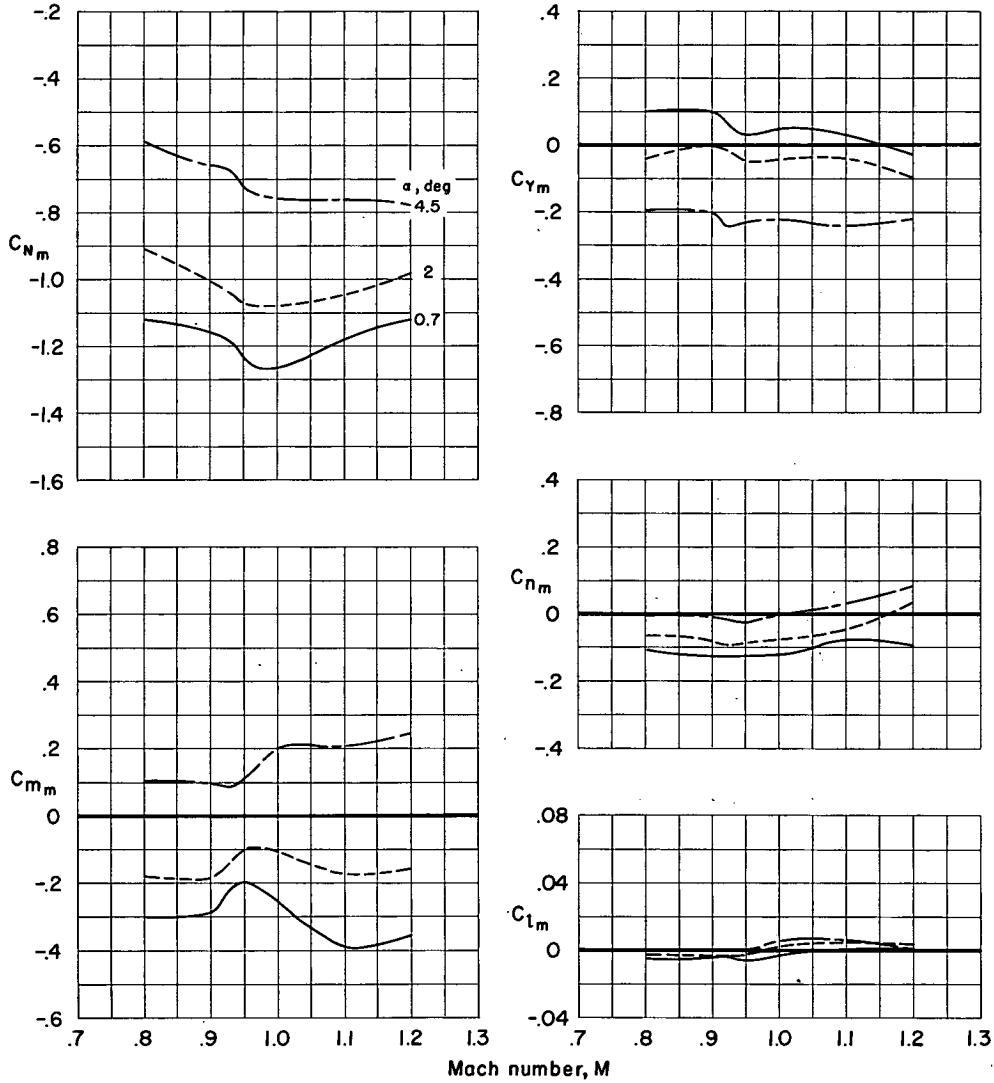
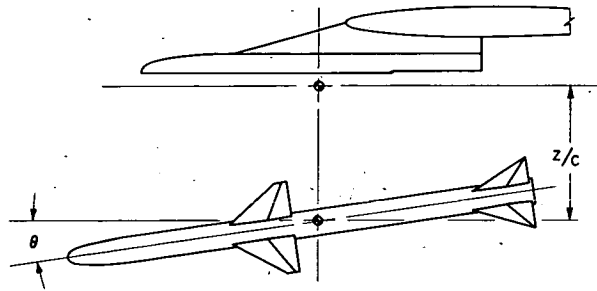
(a) $\theta = 0^\circ$.

Figure 26.- Force and moment characteristics of the missile in jettison position $z/c = 0.2051$; $\psi = \phi = 0^\circ$.



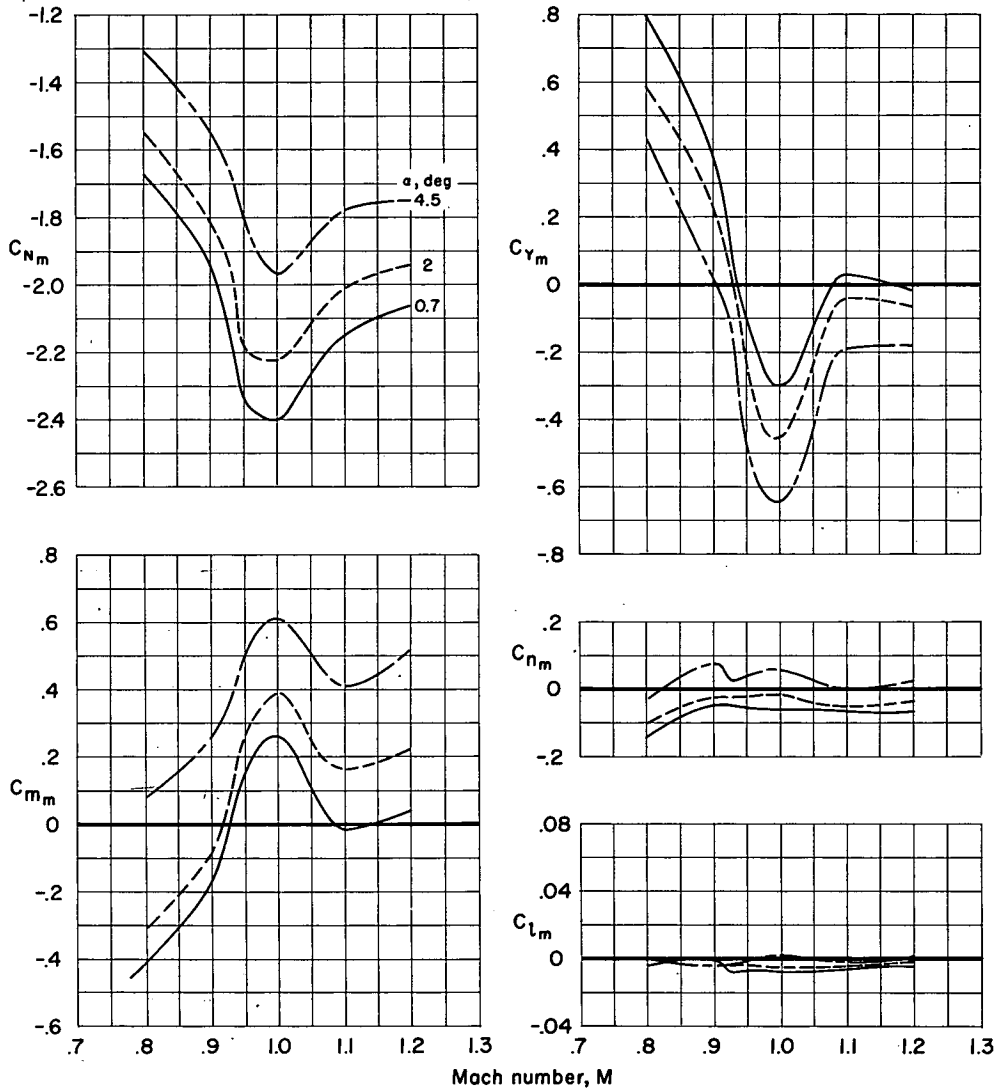
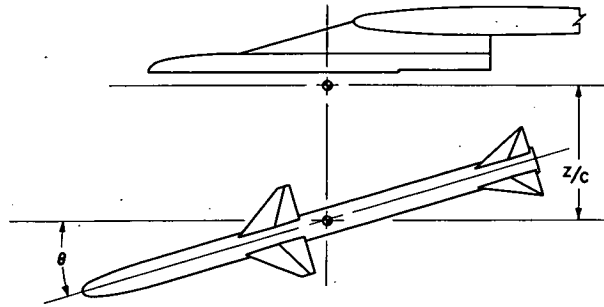
(b) $\theta = 8^\circ$.

Figure 26.- Continued.



(c) $\theta = -8^\circ$.

Figure 26.- Continued.



(d) $\theta = -16^\circ$.

Figure 26.- Concluded.

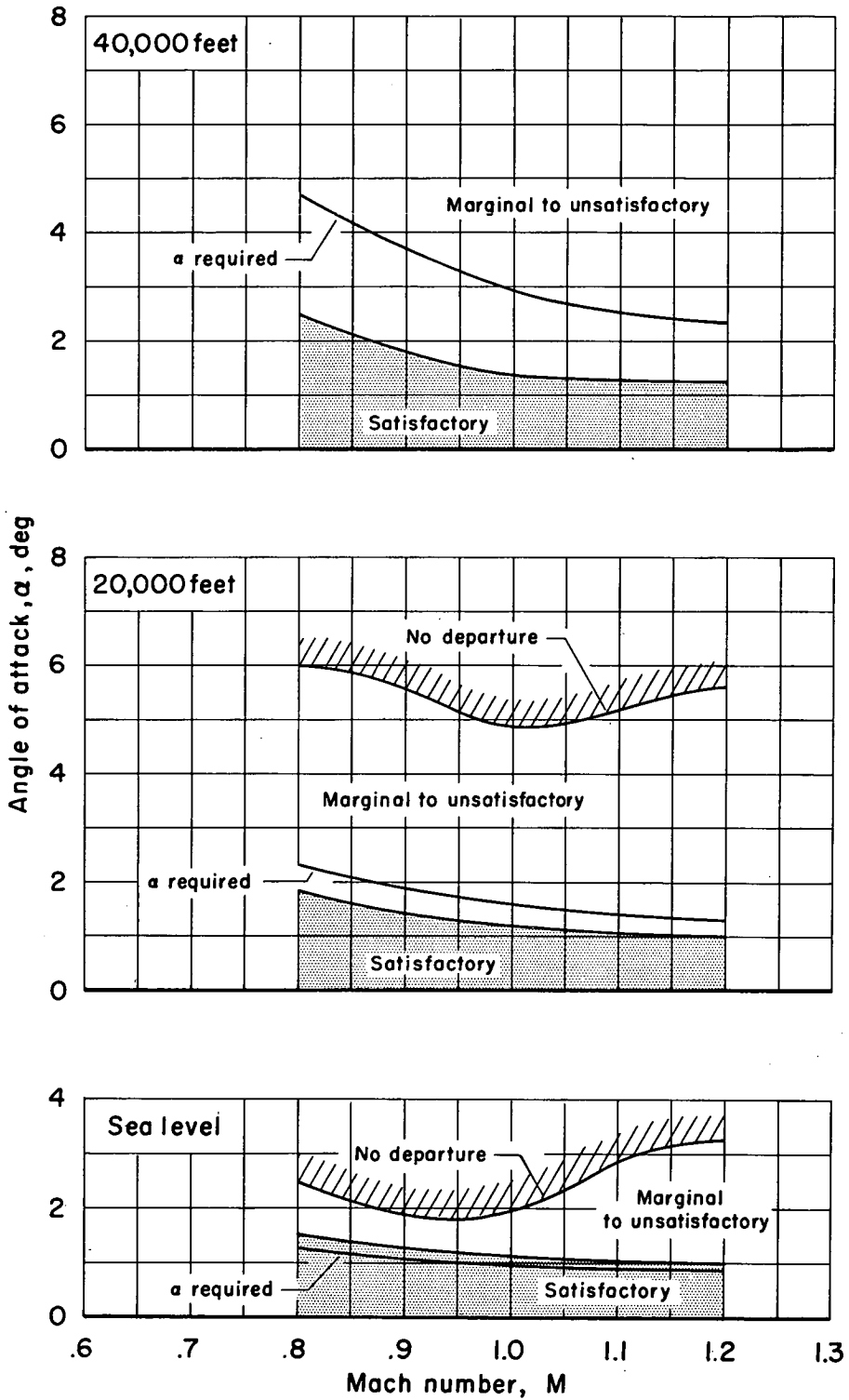


Figure 27.- Jettison boundaries of the airplane-missile combination.